ATOMIC AND PLASMA-MATERIAL INTERACTION DATA FOR FUSION

VOLUME 11

INTERNATIONAL ATOMIC ENERGY AGENCY, VIENNA, 2003

The volumes of ATOMIC AND PLASMA–MATERIAL INTERACTION DATA FOR FUSION are published by the International Atomic Energy normally once a year.

For these volumes, papers, letters and reviews are accepted which deal with the following topics:

- Elementary collision processes in fusion plasmas involving photons, electrons, ions, atoms and molecules;
- Collision processes of plasma particles with surfaces of fusion relevant materials;
- Plasma-material interaction phenomena, including the thermophysical response of materials.

Each submitted contribution should contain fusion relevant data and information in either of the above areas. Original contributions should provide new data, using well established methods. Review articles should give a critical analysis or evaluation of a wider range of data. They are normally prepared on the invitation by the Editor or on prior mutual consent. Each submitted contribution is assessed by two independent referees.

Every manuscript submitted must be accompanied by a *disclaimer* stating that the paper has not been published and is not being considered for publication elsewhere. If no copyright is claimed by the authors, the IAEA automatically owns the copyright of the paper.

Guidelines for the preparation of manuscripts are given on the inside back cover. Manuscripts and correspondence should be addressed to: The Editor, ATOMIC AND PLASMA–MATERIAL INTERACTION DATA FOR FUSION, International Atomic Energy Agency, Wagramer Strasse 5, P.O. Box 100, A-1400 Vienna, Austria.

Publisher: International Atomic Energy Agency, Wagramer Strasse 5, P.O. Box 100, A-1400 Vienna, Austria

Editor: R.E.H. Clark, Atomic and Molecular Data Unit, Division of Physical and Chemical Sciences

---

ATOMIC AND PLASMA–MATERIAL INTERACTION DATA FOR FUSION, VOLUME 11
IAEA, VIENNA, 2003
STI/PUB/023/APID/11

FOREWORD

In the conditions typical of plasmas found in nuclear fusion machines the temperatures are such that the light elements are completely stripped of their electrons. However, heavier impurity materials retain bound electrons. Such materials may exist in the plasma from contamination from the wall materials or may be introduced in the divertor region to dissipate energy from the plasma. These heavy elements can be very efficient radiators. This can be a problem in maintaining a high temperature in the plasma core. However, this process can be advantageous in the divertor region of the plasma where it is necessary to dissipate energy from the plasma with minimum disruption of the vessel walls. In either case it is important to have an accurate estimate of the total power radiated from heavy elements that are likely to be found in fusion machines. This was the focus of a recent IAEA Co-ordinated Research Project.

The calculation of total radiated power represents one of the more challenging tasks in plasma modelling. It is first necessary to construct a complete atomic database for all ionisation stages of the element under consideration. This includes all energy levels as well as excitation and ionisation processes and their inverse processes. In addition all radiative processes must be calculated. There can be large numbers of energy levels for each ionisation stage. The number of processes will increase roughly as the square of the number of levels. Furthermore, it is necessary to calculate cross sections for each transition over a range of energies for the calculation of rate coefficients, which require integration of cross section over the electron distribution for a range of electron velocities. Once all the atomic physics data have been gathered, it is necessary to solve the rate equations to arrive at a calculation of the total radiated power. These calculations are extremely time consuming and it is difficult to carry them out for heavy elements due to the large number of bound electrons resulting in a proliferation of energy levels.

The present volume of Atomic and Plasma-Material Interaction Data for Fusion represents the result of a co-ordinated effort of leading theoretical groups within the IAEA Co-ordinated Research Project (CRP) on Radiative Cooling Rates of Fusion Plasma Impurities. The contributions of the participants of this CRP, contained in the present volume, significantly enlarge information on radiative processes taking place in different regions of fusion plasmas. This information is an important ingredient in many modelling and diagnostic studies of fusion plasmas.

The IAEA is taking this opportunity to acknowledge the Co-ordinated Research Project participants for their dedicated effort and contribution to this volume.

EDITORIAL NOTE

This publication has been prepared from the original material as submitted by the authors. The views expressed do not necessarily reflect those of the IAEA, the governments of the nominating Member States or the nominating organizations.

The use of particular designations of countries or territories does not imply any judgement by the publisher, the IAEA, as to the legal status of such countries or territories, of their authorities and institutions or of the delimitation of their boundaries.

The mention of names of specific companies or products (whether or not indicated as registered) does not imply any intention to infringe proprietary rights, nor should it be construed as an endorsement or recommendation on the part of the IAEA.

The authors are responsible for having obtained the necessary permission for the IAEA to reproduce, translate or use material from sources already protected by copyrights.

CONTENTS

Comparison calculations of radiated power loss for silicon and iron

R.E.H. Clark[1], **J. Abdallah, Jr.**[2]
Los Alamos National Laboratory
Los Alamos, New Mexico,
United States of America

Abstract. An extensive comparison study of radiated power loss calculations for silicon and iron has been conducted. Several models with increasing amount of complexity are compared. The effect of fine structure level calculations compared to configuration average mode is examined. The difference due to using first order many body theory as compared to plane wave Born for electron impact excitation is examined. Examples are given of the effect of the various approximations for both radiated power and ionization balance. A recommended kinetics model is given.

1. Introduction

The calculation of radiated power from plasma impurities is of considerable importance in magnetic fusion devices [1]. The purpose of this work is to show a comparison of a variety of models for the calculation of radiated power from silicon and iron plasmas. A number of different data sets were calculated using the atomic physics codes developed at the Los Alamos National Laboratory. Different data sets were constructed using an increasing level of complexity in the types of electron configurations employed as well as in the method of calculating cross section data. Resulting data sets are compared to show the effects on the calculated radiated power. A recommended set of configurations is presented which will be used in a later paper [2] to calculate comprehensive results for a number of elements over a range of electron temperature and density.

In the next section we present a summary of the theoretical methods used in the calculation of the radiated power. In section 3 we discuss the various models used. In section 4 we present comparisons and discussion for the various model calculations. The final section summarizes the recommended model to be used in radiated power calculations.

2. Theoretical Methods

The basic atomic physics data for all models were calculated using the atomic physics codes developed at Los Alamos [3]. These codes have been developed over a number of years to provide atomic models for plasma modeling calculations. Since details of these codes are available elsewhere, we give a brief description of each here.

[1] email address: rehc@lanl.gov
[2] email address: abd@lanl.gov

The atomic structure calculations are carried out using the CATS [4] code. This is a modified version of the atomic structure codes of R. D. Cowan [5]. The atomic structure calculation is a Hartree-Fock calculation. It is essentially non relativistic, although the mass and Darwin terms are included in the radial wave function calculation. Spin-orbit interaction and configuration interaction can be included as a perturbation treatment. The CATS code is used to calculate0 radial wave functions, energy levels, bound-bound radiated transitions, and, if requested, plane wave Born (PWB) electron impact excitation cross sections. All calculated quantities are written to a computer file for use by other atomic physics codes as well as plasma modeling codes.

Calculation of distorted wave (DWA) or first order many body theory (FOMBT) electron impact excitation cross sections for selected transitions are carried out using the ACE code [6]. The ACE code reads in the atomic structure information from the data file produced by the CATS code and carries out cross section calculations for transitions selected by the user. Configuration interaction as well as spin-orbit mixing in the target state can be included. Unitarization is included following the method of Mann [7]. The resulting cross section information is stored on a data file for later use by a plasma modeling code.

The GIPPER code calculates cross sections for ionization processes including photoionization, electron impact ionization, and autoionization. The GIPPER code also reads in the structure data from the CATS data file and writes cross sections on a file for later use by a plasma modeling code.

Once all of the atomic physics data files have been produced, a plasma modeling code is run to calculate the required properties for a plasma. The modeling code used depends on the applicability of local thermodynamic equilibrium (LTE). For a plasma in LTE, only the energy levels and statistical weights are needed to find the ionization balance. Radiative absorption processes are needed if spectral information is desired. Collisional cross sections are not needed at all. However, for most magnetic fusion energy experiments, and for many other laboratory plasmas LTE does not hold. For these non LTE plasmas, the rate equations must be solved with inclusion of all processes linking all levels within an ion stage and connecting adjacent ions through ionization and recombination. The FINE code [8] is the Los Alamos non LTE plasma modeling code. The FINE code reads in all needed atomic data from the appropriate files and solves the coupled rate equations to determine the state populations for a given electron temperature and density. The FINE code can be run with an arbitrary radiation field present. For MFE applications it is appropriate to run with no radiation field present, which is the case in this paper. The user can request a variety of output calculations from the FINE code. In the present case we require the total radiated power from the plasma. This is calculated by summing all of the processes from the individual ions that give rise to radiation. The processes include radiative bound-bound, radiative recombination, and dielectronic recombination.

We note that in all of our models we use detailed balance to determine the cross sections for the inverse processes of transitions that are directly calculated by the codes listed above. For example, we use detailed balance to derive the cross sections for electron impact deexcitation from the electron impact excitation cross sections obtained from the ACE code. The GIPPER code calculates the cross sections for autoionization. We use detailed balance to obtain the dielectronic recombination cross sections. In this way we have a complete and consistent set of upward and downward transitions.

3. Summary of the models

We used the codes summarized in the preceding section to calculate radiated power for a variety of atomic physics models, differing in complexity. We briefly describe the models in this section.

The simplest model, called model A, uses configuration average quantities for a small number of configurations, all differing from the ground configuration by only one electron transition. In this case the set of configurations were of the form of (core-1)nl where core denotes the ground configuration of the ion. In this simple model an electron was removed from only each of the outer two electron shells. For example, in neutral silicon the core is $1s^2 2s^2 2p^6 3s^2 3p^2$. Our model would make one series of configurations moving one 3p electron to successive nl shells, then another series moving out one of the 3s electrons. The model called A moves each electron out through the 5g shell. To examine the dependence of radiated power on higher shells a second model, model B, increased the nl shell to 10m.

The next level of complexity was to construct a model based on fine structure levels. This means coupling the orbital angular momentum of the electrons to obtain a total angular momentum, L; coupling the electron spins to obtain a total spin, S and finally coupling the L and S to obtain a total angular momentum, J. In this case the effects of configuration mixing as well as intermediate coupling mixing due to the spin-orbit interaction are also included. This model used the small configuration set of model A, due to the rapid increase in the number of levels with increasing angular momentum of the higher shells. This fine structure model is designated as model L.

Finally, we investigated the effect of multiple electron permutations which greatly increase the possibility of dielectronic recombinations. In this model, model C, we allow two electron permutations involving the three outer occupied shells and going up through the next two higher shells, and then Rydberg series starting from each of those configurations. For the neutral silicon ground state listed above, we would allow permutations involving the 2p, 3s, 3p, 3d, and 4s shells. We would then allow each resulting configuration to have the outermost electron move out shell by shell to nl. Model C has the nl limit as 5g, similar to model A above. Model D has nl run through 10m, similar to model B above. No attempt was made to include fine structure levels because of the complexity of the resulting configurations.

For all of the models PWB cross sections were calculated for all possible transitions in each ion stage. In addition, FOMBT cross sections were calculated for all transitions from the ground state. This was done for each of the models summarized above. A final model, model P, used the same configuration set as model D above but used only PWB for all electron impact cross section, including those from the ground state. Since most of the ions exist in the ground state at the low densities typical of MFE plasmas, this is a good indication of sensitivity to detailed calculation of cross sections.

The models increase in complexity in the following manner. On average, model A has 20-30 configurations per ion stage. Model B has on the order of 100 configurations per ion stage. Model L has several hundred fine structure levels per ion stage. Model C has 100-200 configurations per ion stages. Model D has 800 to 1000 configurations per ion stage. A summary of the models is given in the accompanying table.

Table 1. Models used in calculations

Model	Types of configurations used	Upper limit on nl	Number of states for silicon	Number of states for iron
A	(core-1)nl	5g	360	687
B	(core-1)nl	10m	1368	3023
L	(core-1)nl	5g	4837	-
C	(core-2)$n_1l_1n_2l_2nl$	5g	2068	4087
D	(core-2)$n_1l_1n_2l_2nl$	10m	9148	19837
P	(core-2)$n_1l_1n_2l_2nl$ uses PWB for all transitions	10m	9148	19837

4. Comparison and discussion

For all of the comparisons we ran calculations of radiated power loss at an intermediate electron density of $10^{14}cm^2$ and a range of electron temperatures from 1 to 1000 eV. Calculations were performed with the FINE code using each of the models A, B, L, C, D, and P. In addition, calculations were performed with the widely used ADPAK code [9, 10]. We make comparisons among the various models for silicon first.

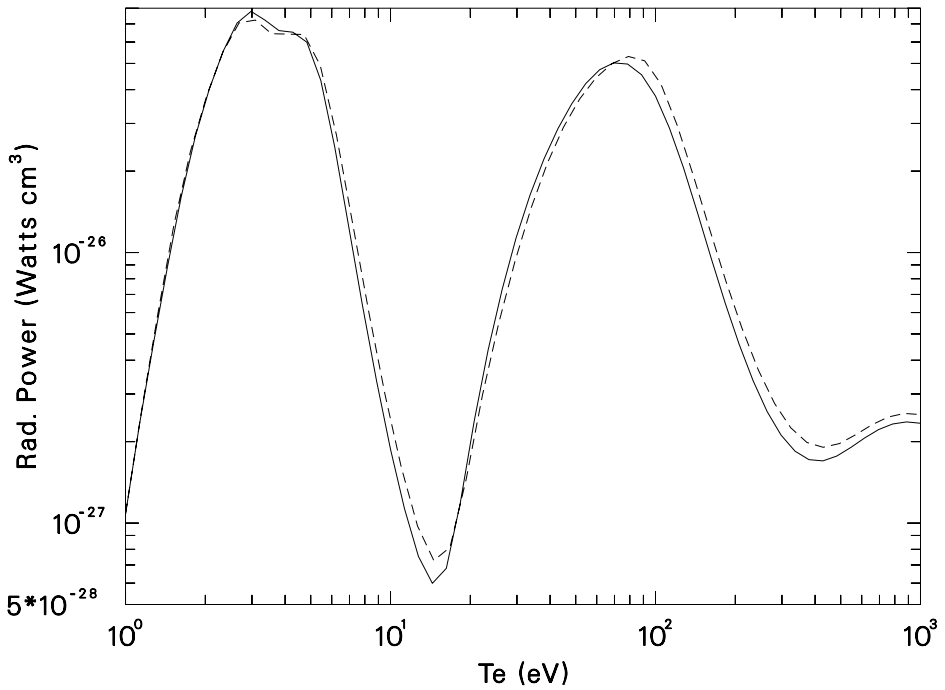

FIG. 1. Comparison of radiated power from model A (solid line) and model B (dashed line) for silicon.

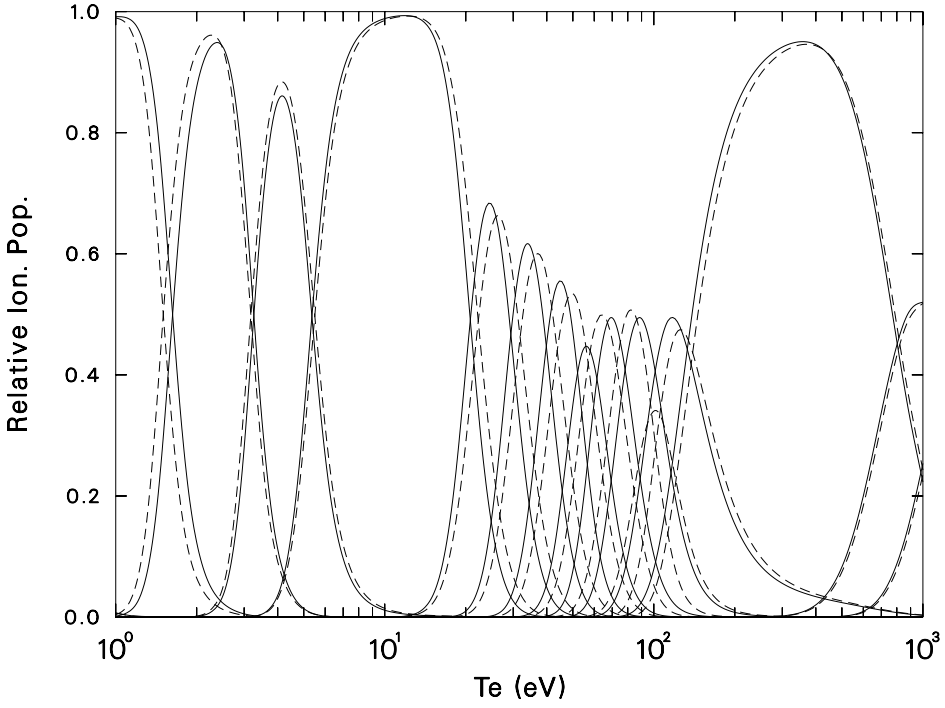

FIG. 2. Comparison of ionization balance from model A (solid line) and model B (dashed line) for silicon.

4.1. Calculations for silicon

We first present comparisons of radiated power and ionization balance from each of the models for silicon. Silicon is high enough in atomic number to give rise to a large number

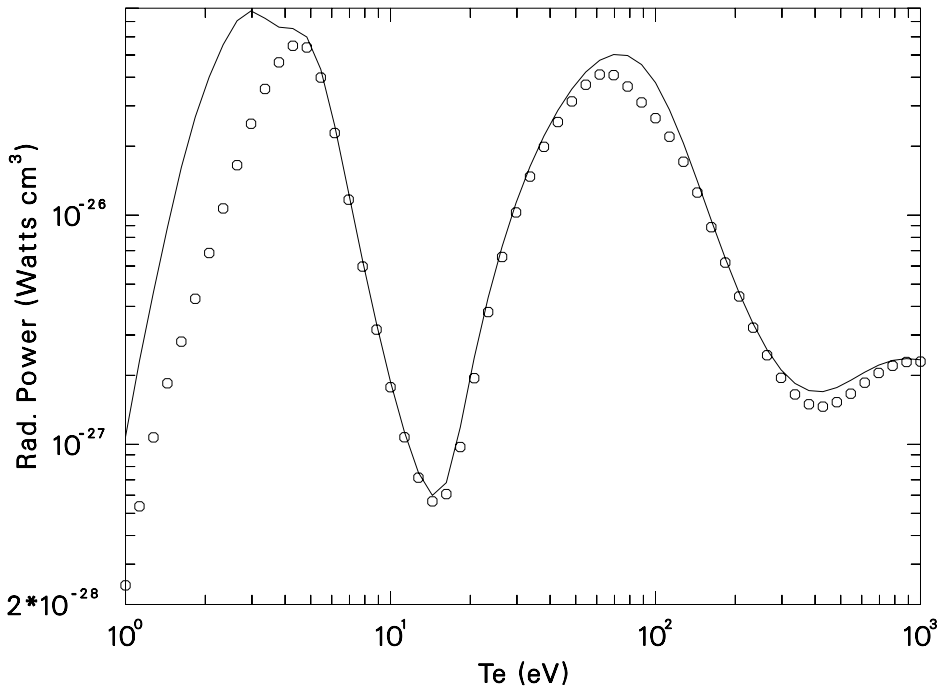

FIG. 3. Comparison of radiated power from model A (solid line) and model L (circles) for silicon.

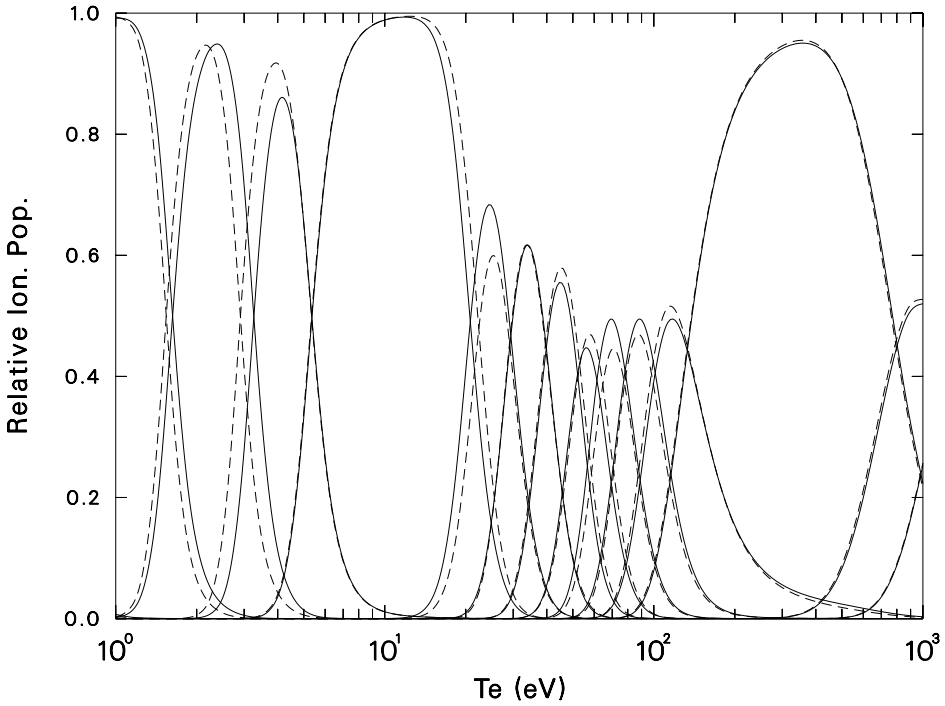

FIG. 4. Comparison of ionization balance from model A (solid line) and model L (dashed line) for silicon.

of ionization stages with complicated configurations so that the effects of different models should be interesting. At the same time it is still possible to run the fine structure model on all ionization stages of silicon.

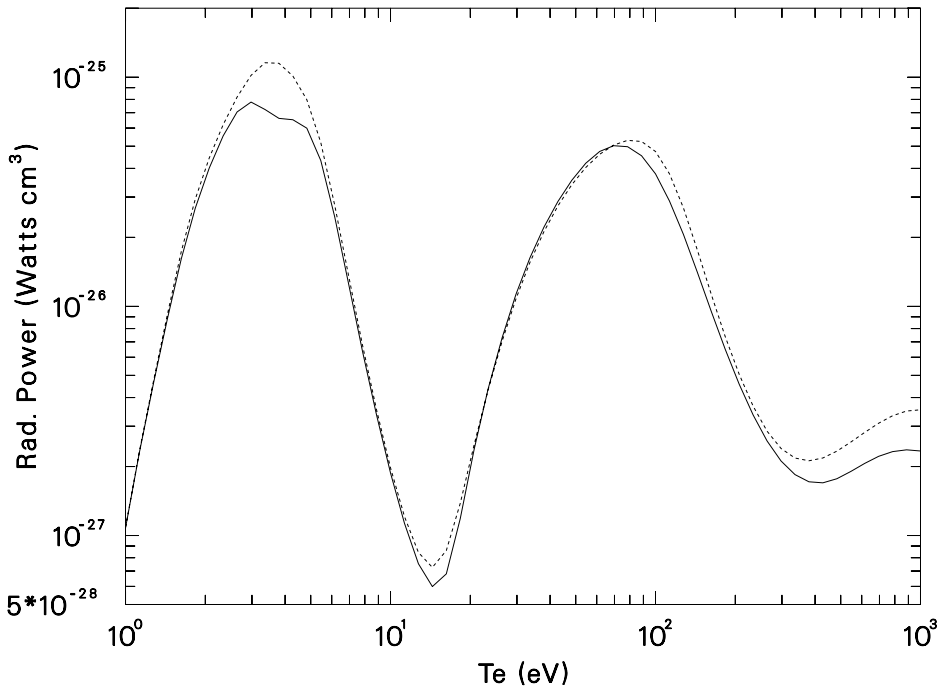

FIG. 5. Comparison of radiated power from model A (solid line) and model C (short dashes) for silicon.

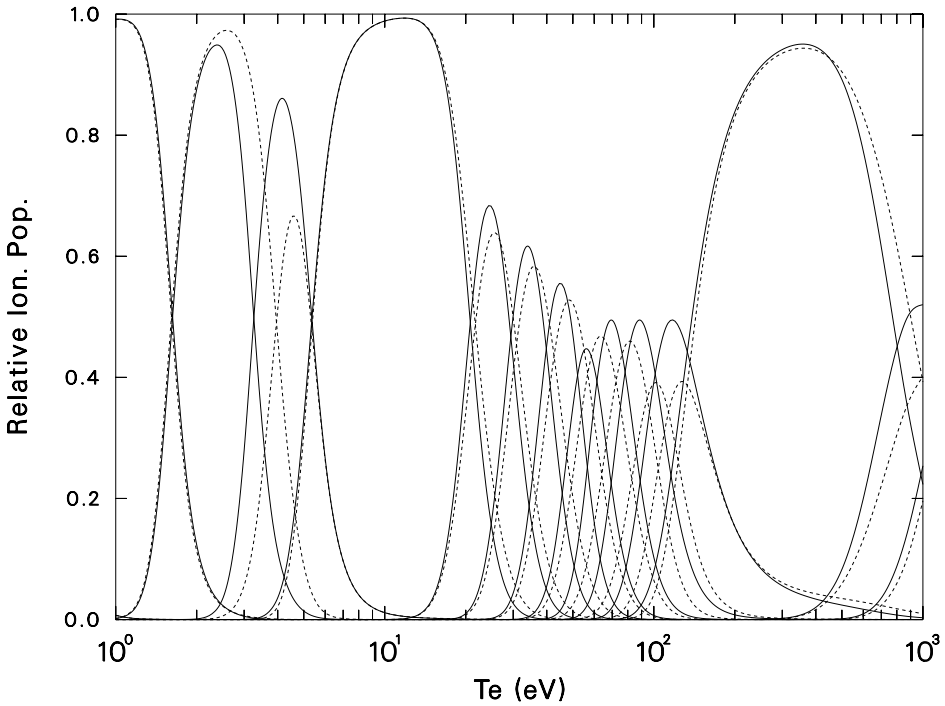

FIG. 6. Comparison of ionization balance from model A (solid line) and model C (short dashes) for silicon.

The first comparison is to see the effect of going to high lying shells in the simple model. Figure 1 shows the calculated radiated power for model A (solid line) compared to model B (dashed line). In this paper we give radiated power per electron per ion, so the units

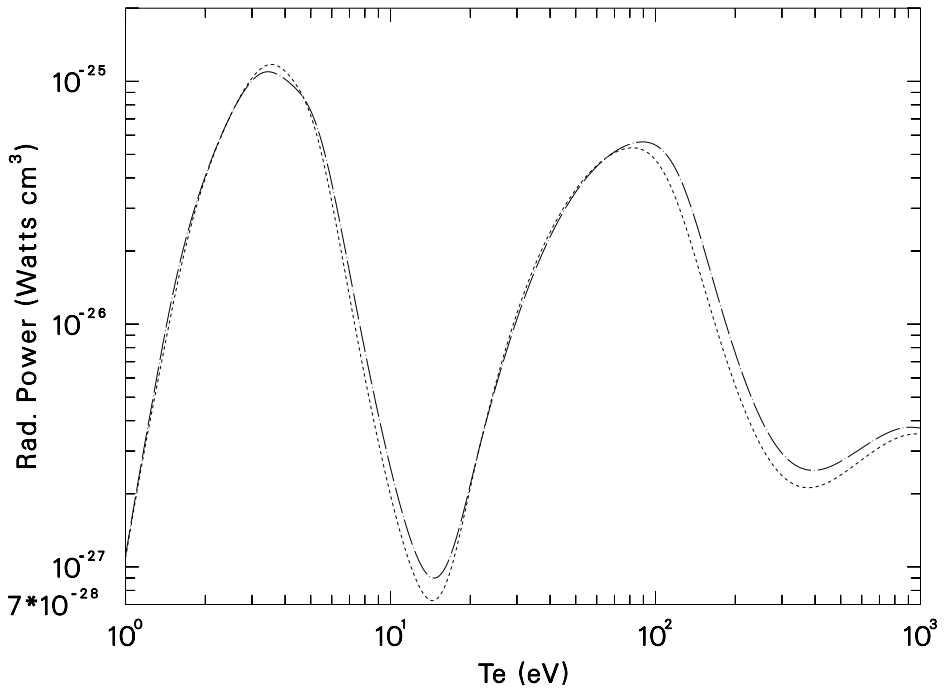

FIG. 7. Comparison of radiated power from model C (dashed line) and model D (chaindot) for silicon.

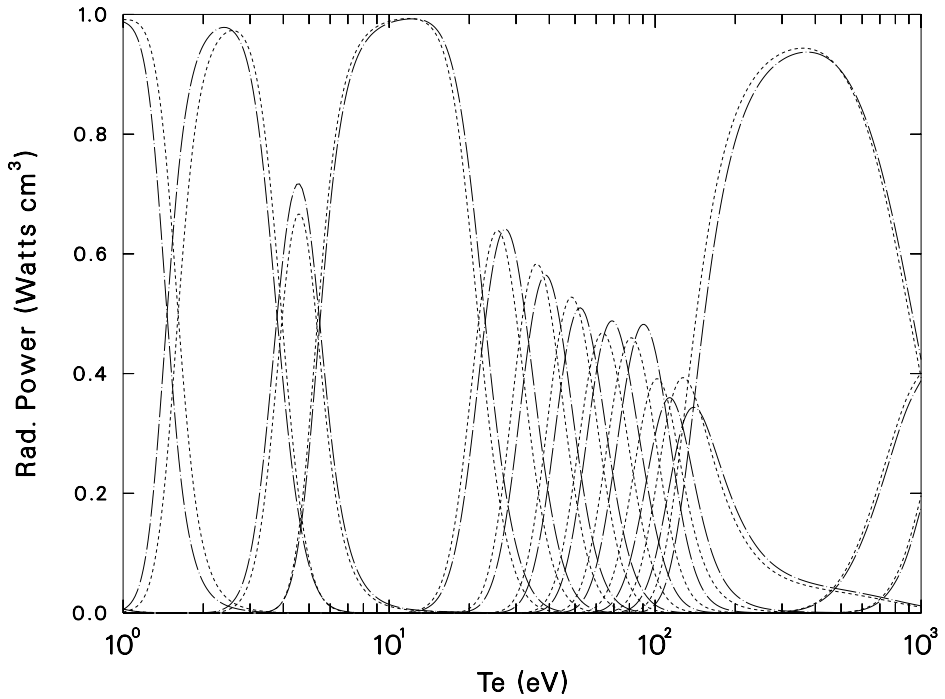

FIG. 8. Comparison of ionization balance from model C (dashed line) and model D (chaindot) for silicon.

for radiated power are watt cm^3. One sees that there is little difference between the two models for radiated power. Figure 2 shows the comparison of relative ion stage population for the two models. Again, one sees very little difference between the two models. Thus there appears to be little advantage in going to high lying shells in the simple, one-electron jump model.

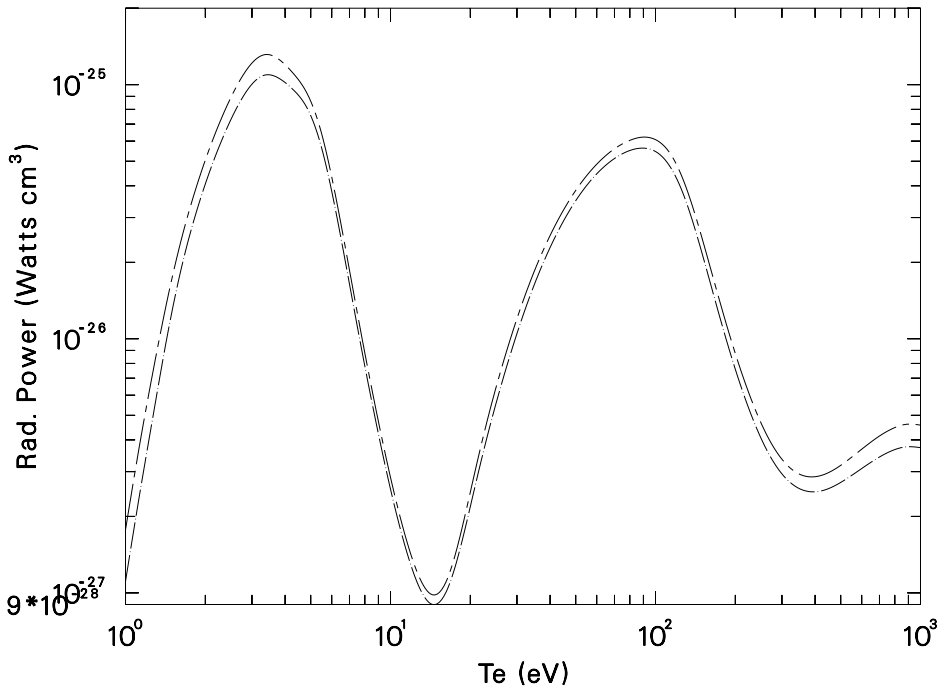

FIG. 9. Comparison of radiated power from model D (chaindot) and model P (chaindash) for silicon.

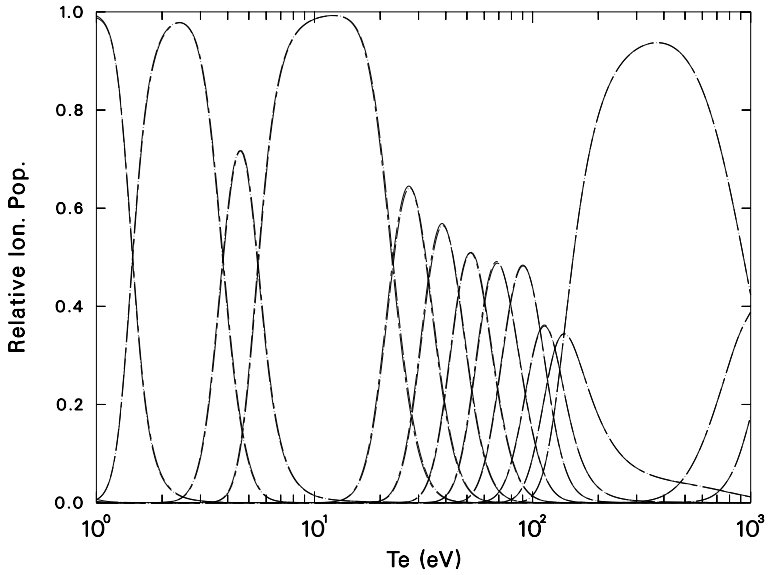

FIG. 10. Comparison of ionization balance from model D (chaindot) and model P (chaindash) for silicon.

The next comparison is to see the effect of fine structure on the calculation. Figure 3 shows a comparison between model A (solid line) and model L (circles). Here one sees a noticeable difference at the low temperatures. This is due to the splitting of the spin states in the fine structure model. In the configuration average mode, all collisional excitations to a dipole allowed level will result in radiation. In the fine structure level model, the spin forbidden states will have a high probability of being collisionally deexcited, thus decreasing the amount of radiation. This effect decreases with higher atomic number due to the spin-orbit mixing of the spin forbidden with spin allowed. This spin-orbit mixing

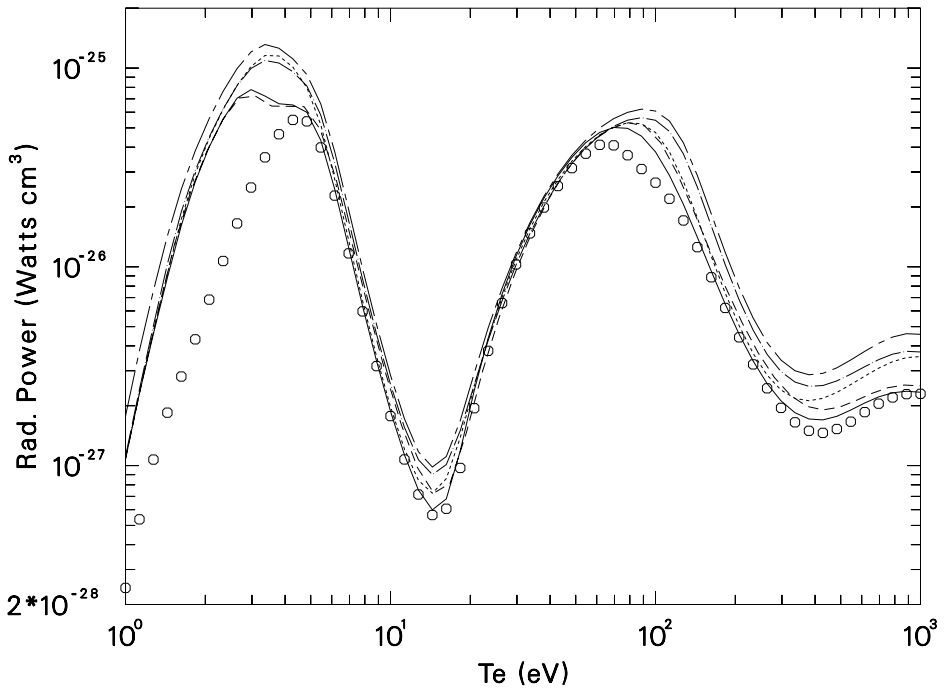

FIG. 11. Comparison of radiated power from models A, B, L, C, D, and P (plot symbols as in figures 1, 3, 5, 6, and 9) for silicon.

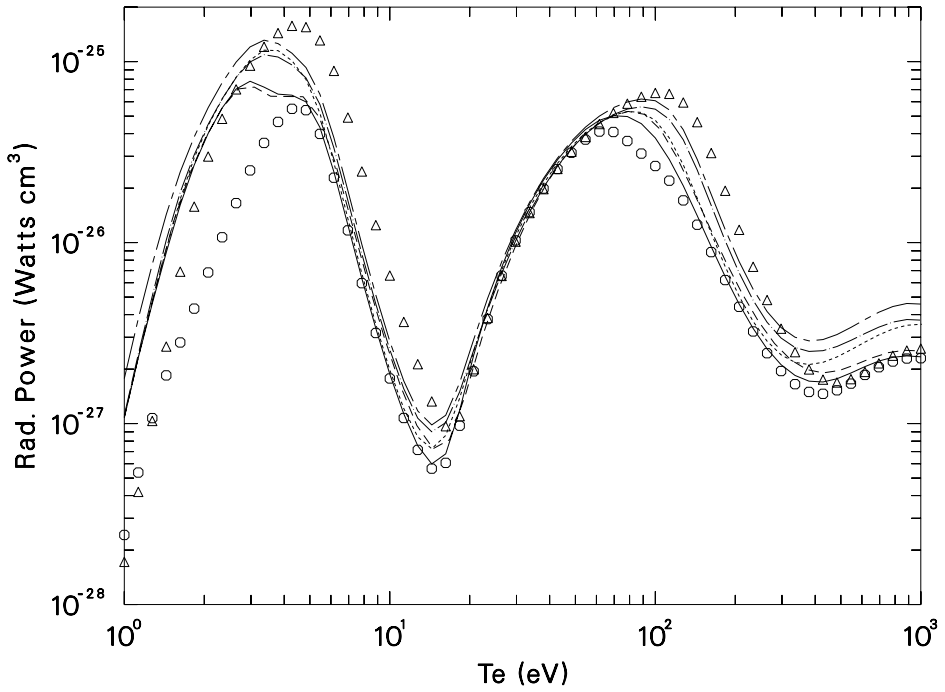

FIG. 12. Same as figure 11, but with addition of radiated power calculation from ADPAK (triangles) for silicon.

allows an apparently spin-forbidden transition to have a spin-allowed component which allows radiative decay to occur. Also, since the spin-orbit mixing depends on the effective charge seen by a shell, the mixing is higher for more highly stripped shells. Thus, in Be-like Si, Si XI, there is sufficient mixing of the $2s2p^1P_1$ level with the $2s2p^3P_1$ that the apparently spin forbidden transition does actually radiate. Similarly, the 1s2p singlet and

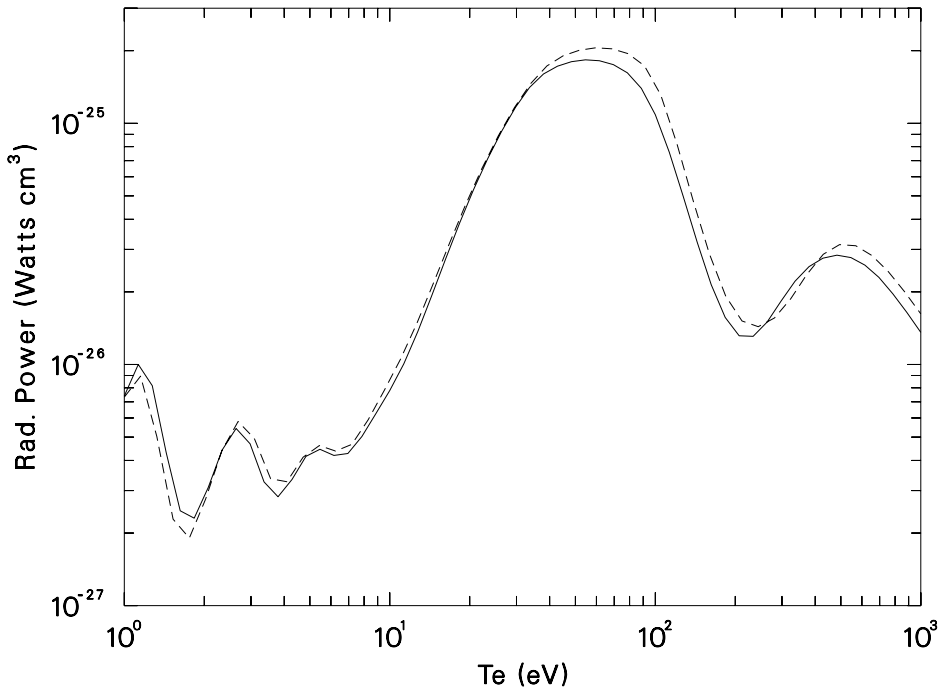

FIG. 13. Comparison of radiated power from model A (solid line) and model B (dashed line) for iron.

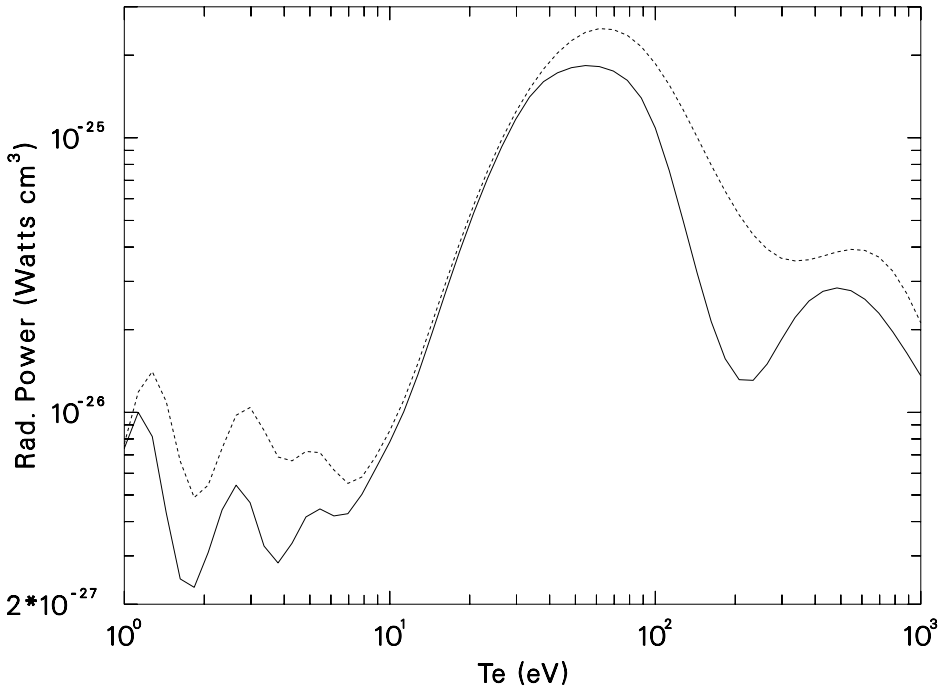

FIG. 14. Comparison of radiated power from model A (solid line) and model C (short dashes) for iron.

triplet levels in He-like Si, Si XIII, show sufficient mixing that the helium-like ion radiates nearly as much in the fine structure mode as in the configuration mode. However, the 3s3p levels of Mg-like Si, Si II, do not mix and the triplet state is nearly completely forbidden. Thus, at the low temperatures where the n = 3 shells are dominant, the fine structure calculation goes well below the configuration average model, while at higher temperatures,

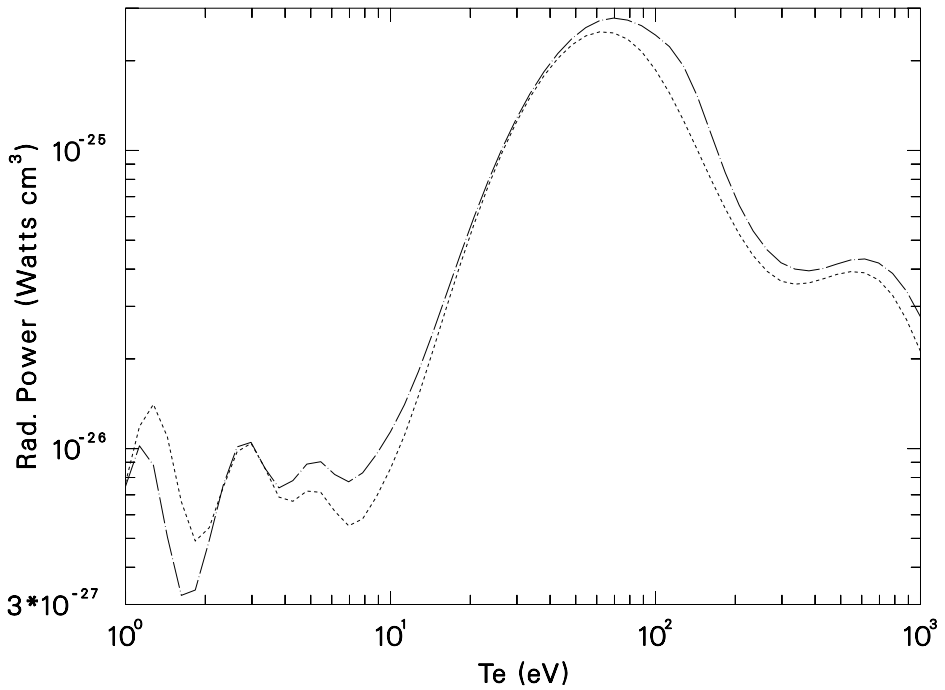

FIG. 15. Comparison of radiated power from model C (short dashes) and model D (chain-dot) for iron.

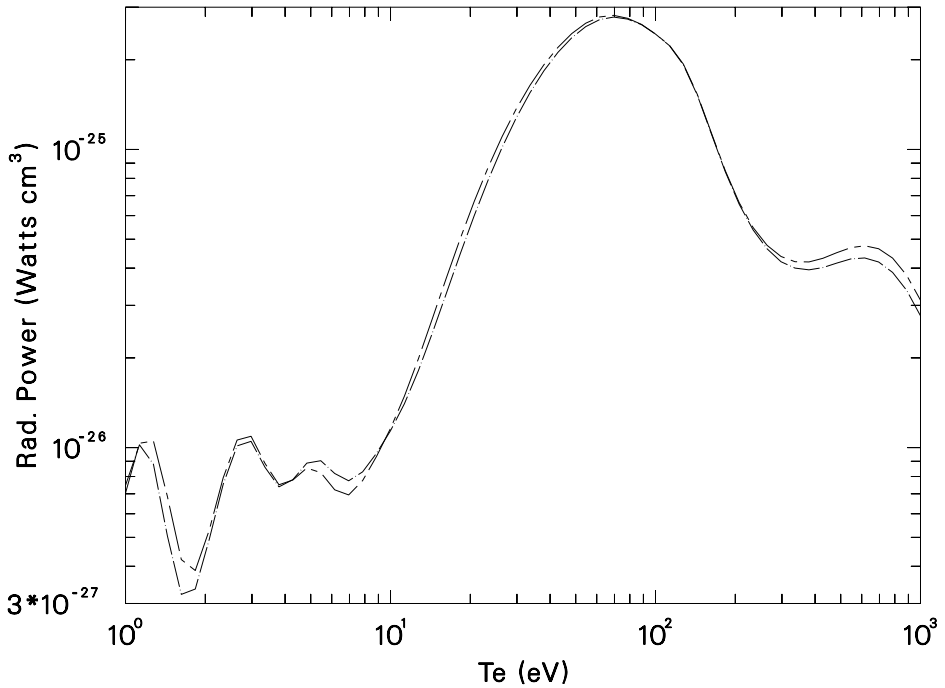

FIG. 16. Comparison of radiated power from model D (chaindot) and model P (chaindash) for iron.

where there is significant mixing of the spin states, the fine structure calculation is very close to the configuration average calculation.

Figure 4 shows a comparison of the ion stage populations as a function of temperature for models A and L. One sees that the fine structure and configuration average models

agree quite well in ion stage populations. There appears to be some possible advantage to going to the extra detail required for the fine structure level calculation, but the advantage largely disappears for temperatures above a few eV. We emphasize that these observations apply to ionization balance and total radiated power. For more detailed quantities such as spectra, the configuration model would be expected to be much worse compared to a fine structure model using the same configurations.

The next comparison is between models A and C. This compares the effect of including a number of two electron permutations in the model calculation, thus greatly increasing the number of autoionization/dielectronic recombination possibilities. Figure 5 shows the comparison of radiated power from model A (solid line), the simple model, with model C (short dashes), the model using two electron permutations through n=5. There is some enhancement of radiated power from using the two electron permutations near the peaks of the curve, but again the overall effect is not large. In Figure 6 we show a comparison of the relative ionization stage populations. Again, the difference is not exteremely large, but is more significant than the differences seen in either figure 2 or figure 4. This shows that the effect of two electron permutations has more impact

We next show comparisons between model C (short dashes) and model D (chaindot), the two electron permutation models, model D having Rydberg levels through the n=10 shell versus n=5 for model C. Figure 7 shows the comparison for radiated power and figure 8 shows the comparison for relative ionization stage population. One sees from figure 7 that going to high n in the two electron permutation model has a similar effect on the radiated power as going to high n in the one electron jump model as shown in figure 1.

The next set of comparisons shows the effect of the FOMBT cross sections compared to the PWB cross sections for excitations from the ground state. In figure 9 the comparison of model D with FOMBT from the ground states (chaindot) is made with model D with PWB from the ground state (chaindash). In both cases PWB was used in calculating cross sections from all other states. We note here that the PWB calculation includes Cowan's [5] modification for low energy behavior of the PWB cross sections, which keeps the cross section finite at low energy. One sees very little difference in the radiated power between the two cases. In figure 10 it is nearly impossible to distinguish between the two sets of curves showing relative ionization stage populations, indicating that the amount of detail in the calculation of the electron impact excitation cross sections has little impact on the ionization balance in the low density case considered here.

We now combine the plots of radiated power from all of the models into one graph, figure 11. This shows the spread from the various approximations and serves as an indicator of the sensitivity of radiated power to the various models. Although there are some areas with as much as a factor of two difference between the highest and lowest curves, the overall agreement among the wide variety of models is quite good. This gives us confidence that the radiated power calculations should be reliable. It also points out that for a relatively simple system at low density even the simplest models give good agreement with the more complex models.

As a final comparison, the same curves from figure 11 are repeated in figure 12, with the addition of results from the popular ADPAK code (triangles). Figure 12 shows that the

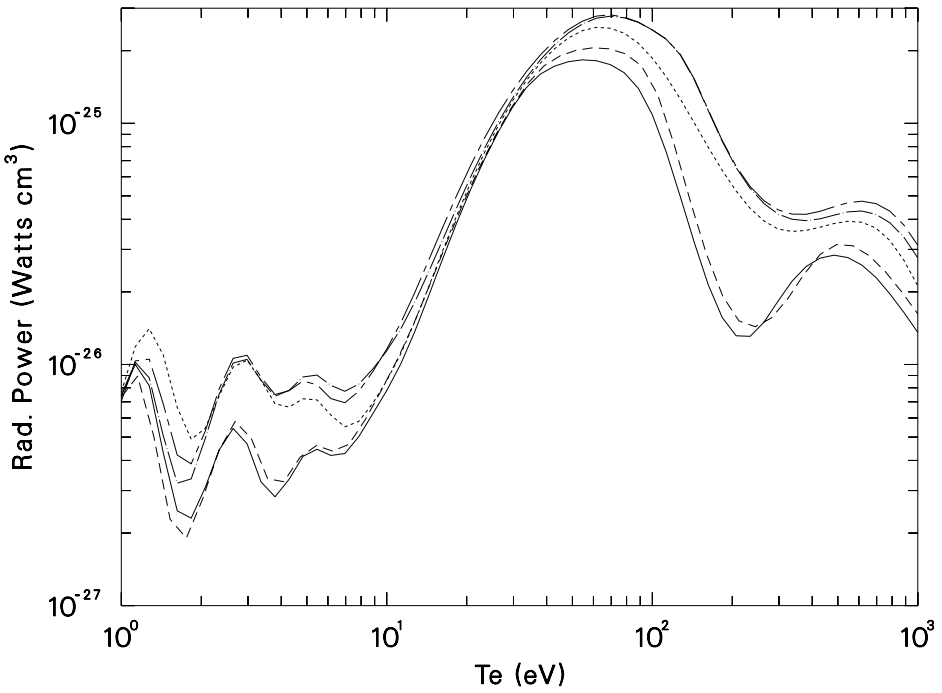

FIG. 17. Comparison of radiated power from models A, B, C, D, and P (plot symbols as in figures 13-16) for iron.

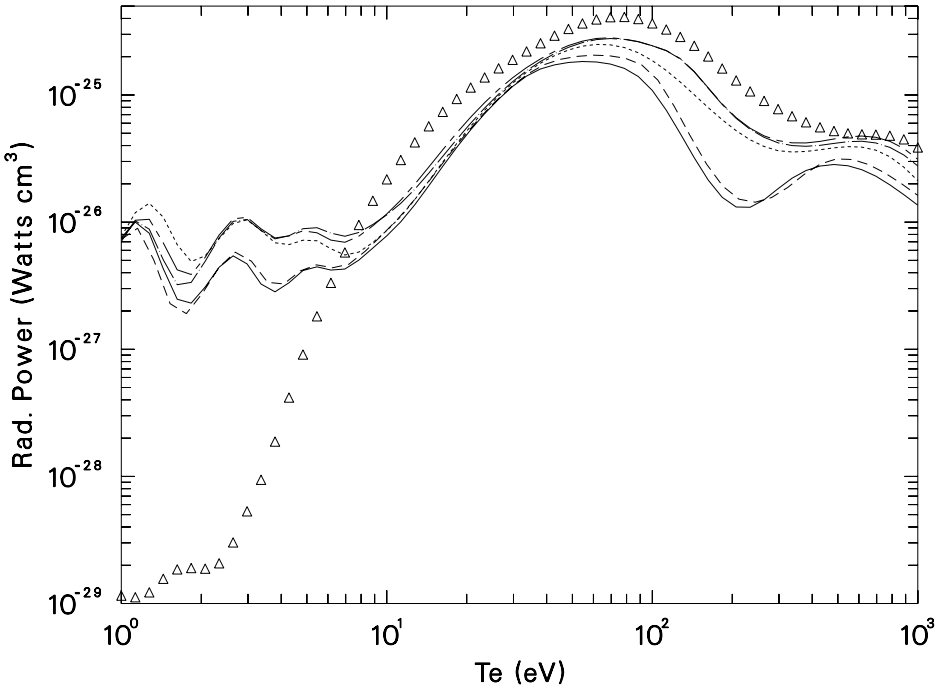

FIG. 18. Same as figure 17 with addition of radiated power calculation from ADPAK (triangles) for iron.

ADPAK results lie close to most of the detailed calculations. As the ADPAK model is quite simple, an average ion type approximation using fits to atomic data and screening parameters, the agreement between ADPAK and the detailed models is impressive.

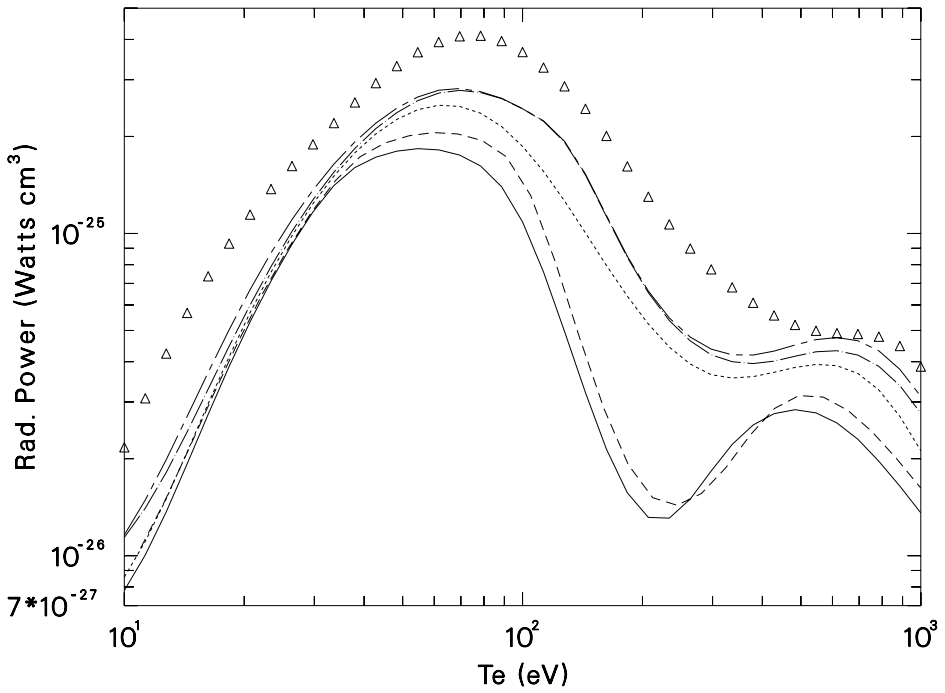

FIG. 19. Same as figure 18, but for electron temperatures above 10 eV.

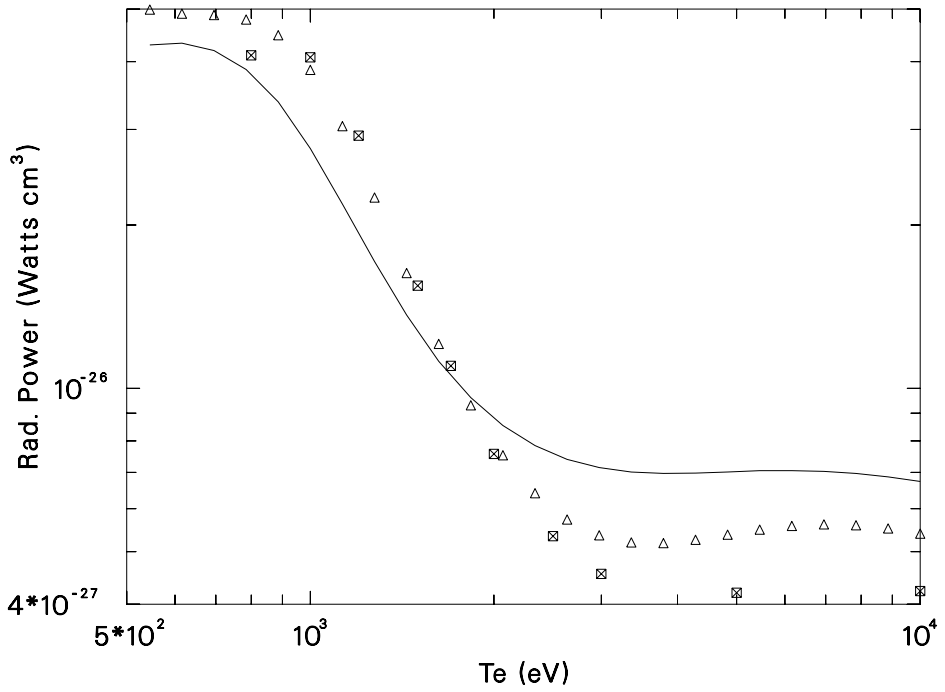

FIG. 20. Comparison of radiated power for iron calculated with model D (solid line), with ADPAK (triangles), and Merts et al. (squares).

4.2. Calculations for iron

The same type models were used in modeling iron as were used in silicon, with the exception that no fine structure calculations were performed because the number of fine structure levels increases dramatically with more complex ions. Thus for iron the models

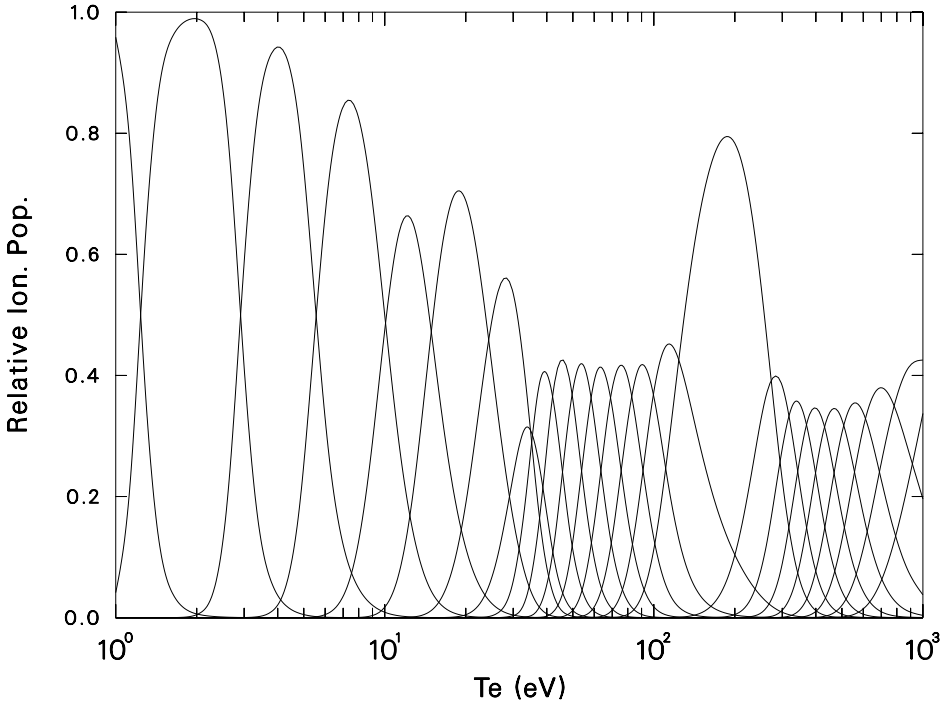

FIG. 21. Ionization balance from model A for iron.

labeled A, B, C, D, and P were used, of course being extended over all of the ion stages of iron. We also include comparisons with the ADPAK code.

In figure 13 we show a comparison of model A (solid line) with model B (dashed line) for radiated power. This is a comparison of the simple models going to the n=5 and n=10 shells, respectively. As in the silicon there is not a large difference between the two calculations. However, there is a noticeable difference in the shape of the radiated power for iron compared to the results for silicon. This reflects the more complex nature of the iron ions.

We next compare the simple model with one electron jumps, model A, with the model using two electron permutations, model C, both going to nl = 5g. Figure 14 shows a comparison of radiated power from these two calculations for iron with the solid line representing model A and the short dashes model C. There is obviously a large difference between these two models. It is apparent that the two electron permutations are of much more importance in iron over this temperature region than for the silicon.

The effect of increasing the upper limit on n in the two electron permutation model is shown in figure 15. The calculated radiated power from model C (short dashed lint), the model going to nl = 5g, is compared to model D (chaindot), the model going to nl = 10m. The difference is not as great as between models A and C, but is greater than the corresponding comparison in silicon.

Next we compare the effect of using PWB versus FOMBT for excitations from the ground state. Figure 16 shows this comparison for radiated power using FOMBT (chaindot) from the ground state with using PWB from the ground state (chaindash). As in silicon, the difference between the two is small.

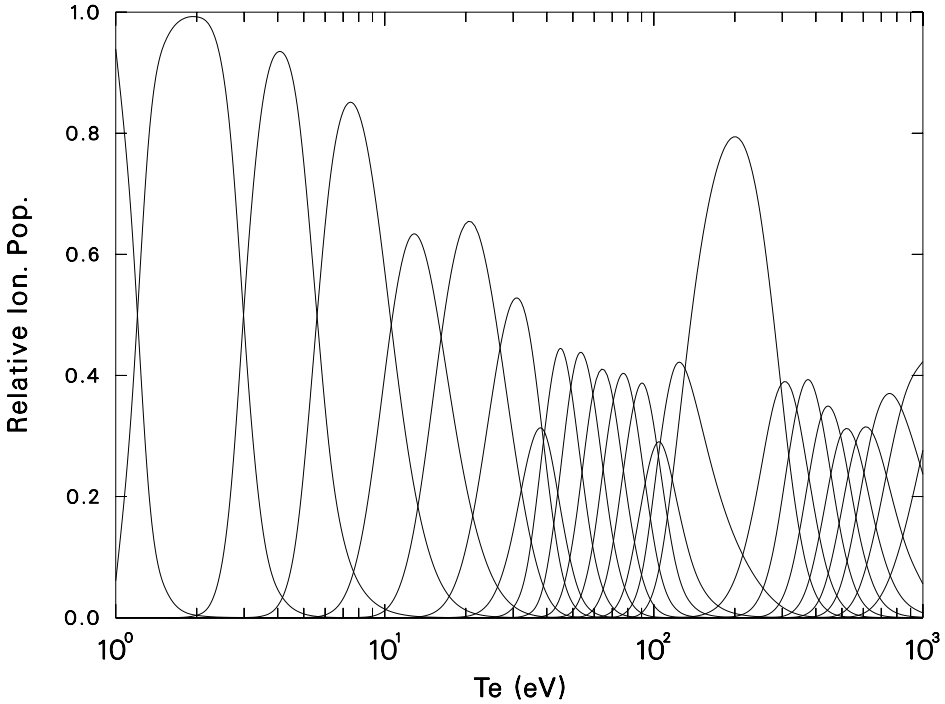

FIG. 22. Ionization balance from model B for iron.

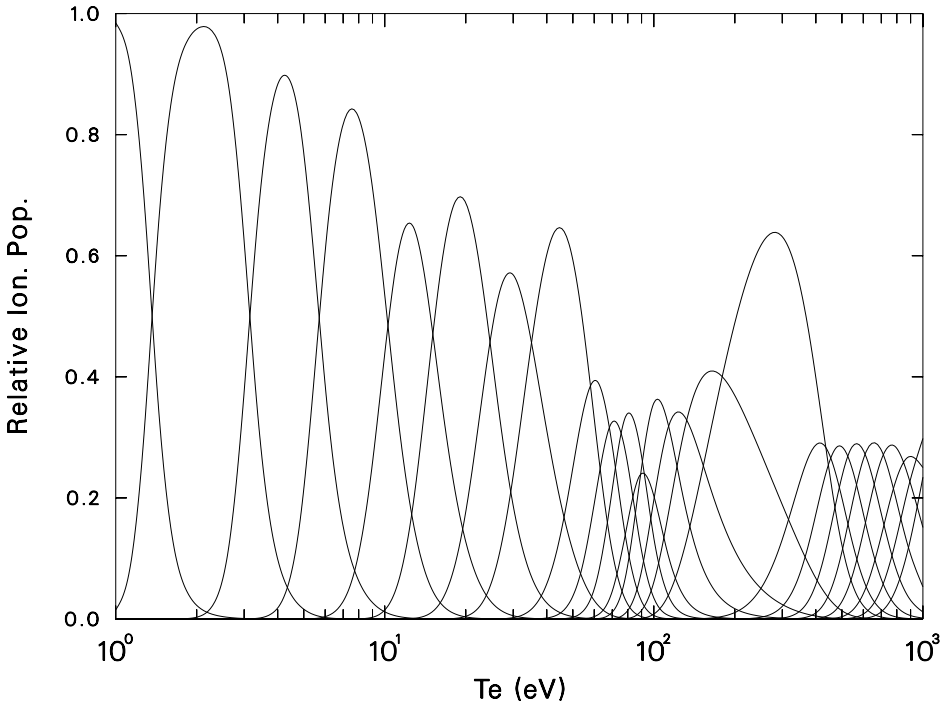

FIG. 23. Ionization balance from model C for iron.

In figure 17 we show the radiated power from all five models on the same plot. This figure shows clearly the larger spread among the various models. It also shows a rather distinct difference between the single electron excitation models, models A and B, as opposed to the two electron permutation models.

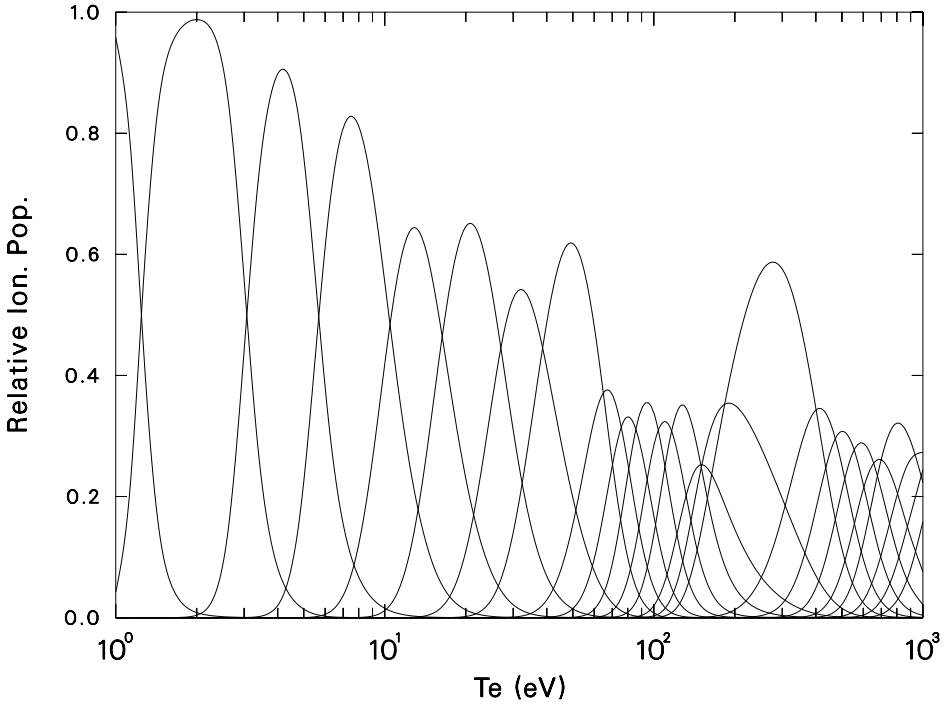

FIG. 24. Ionization balance from model D for iron.

In figure 18 we add the ADPAK results to the plot from figure 17. Here, one sees large differences between the ADPAK and detailed model at both low and high temperatures, although the differences are more dramatic at the low temperatures. We note that the large difference between ADPAK and the detailed models at low temperature is due to transitions within the n=3 configurations. When we omit those transitions from our simple model, we obtain reasonable agreement with ADPAK at low temperatures. Figure 19 shows the same comparison, but at temperatures from 10 eV and higher. Even at these higher temperatures the ADPAK results are significantly different from the detailed models.

Next we compare our current results and the ADPAK results with those of Merts et. al. [11] from 1976. The Merts calculations were carried out for an electron temperature range of 800 to 10000 eV, so we change the temperature scale of the graph. The comparison is shown in figure 20. The square symbols are those of Merts et. al., the triangles are from ADPAK, and the line represents our model D results. One see the ADPAK and Merts results in good agreement up to a few keV where the Merts results are significantly lower. The ADPAK results generally agree with the model D results to approximately 20

We now look at comparisons of ionization balance calculations for iron. Because of the larger number of ionization stages we show each ionization balance calculation as a separate graph. Figure 21 shows the ionization balance calculation from model A, figure 22 from model B, figure 23 from model C, and figure 24 from model D.

In general we note that there is a smooth progression from one ion stage to the next with increasing temperature. We also note that there are noticeable differences in the ionization balance calculations for the different models. Most of the differences are attributable to differences in the number of autoionization/dielectronic recombination (AI/DR) channels

included in each different model. For model A, the simplest model, (shown in figure 21) there are very few AI/DR channels. Going to model B (shown in figure 22), with nl = 10m, the number of AI/DR channels increases substantially. This causes the differences seen in the ion stages at temperatures near 100 eV. These are ion stages with 11 and 12 bound electrons and are greatly impacted by the AI/DR channels. Progressing to model C (figure 23) there is more change evident in the ion stages between 30 end 100 eV. In fact, the ion stage that was the lowest in population in models A and B now has substantial population. This is the argon-like stage centered around 45 eV. The simplest models only allowed electron excitations from the 3p and 3s shells of this ion stage. These models also did not allow permutations of the type (core-1)3dnl, with core-1 representing removal of one electron from the argon-like core. This choice of configurations causes the argon-like to be underpopulated. Models C and D allow permutations of the type (core-2)$n_1l_1n_2l_2nl$, with n_1l_1 and n_2l_2 allowed to run through the 4s shell. This choice gives sufficient numbers of configurations to populate the argon-like stage correctly. One sees from figure 24 that increasing nl from 5g to 10m further changes the ionization balance, indicating that high lying AI/DR channels are important in achieving the correct ionization balance.

5. Summary and Conclusions

From the above extensive comparisons of radiated power loss for silicon and iron we note that for the lighter elements the simple models produce results that are in good agreement with the more complex models. However this changes for the more complex elements. In that case it appears that it is necessary to go into considerable detail in the model in order to produce radiated power estimates that have even a factor of two reliability. Furthermore, for increasingly high atomic number relativistic effects will be more important, so that the calculations would need to use fully relativistic atomic physics data throughout. In the present case our recommendation is to use the model D type of configuration sets for all calculations and to use the FOMBT cross sections for excitations from the ground states. For most elements it is not feasible to make fine structure level calculations with this large a set of configurations, but the effect on radiated power should be smaller for the higher atomic number elements.

This work was supported under the auspices of the United States Department of Energy.

REFERENCES

[1] D. Post, J. Abdallah, R. E. H. Clark, and N. Putvinskaya, Phys. Plasmas, **2**, 2328, (1995).

[2] J. Abdallah, Jr. and R. E. H. Clark, Next paper in this journal.

[3] J. Abdallah, Jr., R. E. H. Clark, D. P. Kilcrease, G. Csanak, and C. J. Fontes, Proceedings of the 10^{th} APS Topical Conference on Atomic Processes in Plasmas, AIP Proceedings, **381**, 131, (1996).

[4] J. Abdallah, Jr., R. E. H. Clark, and R. D. Cowan, Los Alamos Manual No. LA-11436-M I, 1988

[5] R. D. Cowan, *Theory of Atomic Spectra*, (University of California Press, Berkely, 1981).

[6] R. E. H. Clark, J. Abdallah, Jr., G. Csanak, J. B. Mann, and R. D. Cowan, Los Alamos Manual No. LA-11436-M II, 1988

[7] J. B. Mann, At. Data Nuc. Data Tables, **29**, 407, (1983).

[8] J. Abdallah, Jr. and R. E. H. Clark, Los Alamos Manual No. LA-11926, (1990).

[9] R. Hulse, Nucl. Technol. Fusion, **3**, 259, (1983).

[10] D. E. Post, R. V. Jensen, C. B. Tarter, W. H. Grasberger, and W. A. Lokke, At. Nuc. Data Tables, **20**, 397, (1977).

[11] A. L. Merts, R. D. Cowan, and N. H. Magee, Los Alamos Report LA-6220-MS, 1976.

Calculated radiated power loss for neon, silicon, argon, titanium, and iron

J. Abdallah, Jr.[1], **R.E.H. Clark**[2]
Los Alamos National Laboratory
Los Alamos, New Mexico,
United States of America

Abstract. Calculations for radiated power loss for five elements of interest in magnetic fusion energy research have been carried out. The power loss calculations have been made for a wide range of electron temperature and density. Similarities and differences in the radiated power as functions of temperature and density are noted. Comparisons are made with the widely used ADPAK code.

1. Introduction

The recommended method of the previous paper [1] has been used to calculate the radiated power for a number of elements over a wide range of electron temperature and density. The radiated power from plasma impurities is of considerable importance in magnetic fusion devices [2]. The calculations were carried out using the atomic physics codes developed at the Los Alamos National Laboratory [3]. Comparisons are shown for the radiated power from the various elements. Differences and similarities among the various element are noted. Comparisons are also made with the widely used ADPAK code [4, 5].

In the next section we present a summary of the theoretical methods used in the calculation of the radiated power. In section 3 we present the radiated power in both tabular and graphical form for five elements for a range of electron temperatures and densities. We also show the ionization balance calculations in graphical form. In the final section we summarize the results.

2. Theoretical methods

The basic atomic physics data for all plasma simulations presented here were carried out using the set of atomic physics codes developed at Los Alamos National Laboratory [3]. These codes were developed over a number of years to provide a general plasma modeling capability. Since these codes have been described in detail elsewhere [6–10] and have been summarized in the previous paper [1], we give only a brief review of them here.

The atomic structure calculations are carried out using the CATS [6] code. This is a modified version of the atomic structure codes of R. D. Cowan [7]. All quantities are

[1] email address: abd@lanl.gov
[2] email address: rehc@lanl.gov

written to a computer file for use by other atomic physics codes as well as plasma modeling codes.

Calculation of distorted wave or first order many body theory electron impact excitation cross sections is carried out using the ACE code [8]. The ACE code reads in the atomic structure information from the data file generated by the CATS code and carries out cross section calculations for transitions and impact electron energies selected by the user. The resulting cross section information is stored on a data file for later use by a plasma modeling code.

The GIPPER code calculates cross sections for ionization processes including photoionization, electron impact ionization, and autoionization. The GIPPER code also reads in the atomic structure information from the file generated by the CATS code and writes out the cross section information to a file for later use by a plasma modeling code.

Once all the atomic physics data files have been generated, a plasma modeling code, FINE [10], is run to calculate the required properties of the plasma. The FINE code reads in all needed atomic data from the appropriate files and solves the coupled rate equations to determine the state populations for a given electron temperature and density. Any other properties of the plasma, such as radiated power, can then be calculated using the state populations and relevant atomic physics quantities. The radiated power is calculated by summing all of the processes from the individual ionization stages that give rise to radiation; this includes radiative bound-bound, radiative recombination, and dielectronic recombination.

In the previous paper [1] we compared the effect of various approximations in the modeling process on the radiated power. In that paper we concluded that the method called model D was the best model for our calculations. Therefore, we use that method for all the calculations presented here. In this method permutations of two electrons are permitted in each ionization stage. The permutations are permitted among the outer three occupied shells of the ground configuration and among the next two higher shells with the addition of Rydberg configurations through the 10m shell. Calculations are carried out in the configuration average mode, not in fine structure mode. However, this does not imply an average atom method; individual configurations for all ionization stages are followed in the calculation, we simply do not do the angular coupling over the electron shells to form fine structure levels. Electron impact excitation cross sections for all transitions among all levels of each ionization stage are calculated using the plane wave Born approximation. For excitations from the ground configuration the cross sections are calculated using the first order many body theory.

We have used the method outlined above to calculate the radiated power from plasmas of neon, silicon, argon, titanium, and iron. The calculations were carried out for electron densities of 10^{13}, 10^{14}, 10^{15}, and 10^{16} cm^{-3}. For each electron density calculations were carried out for 96 temperatures on a logarithmic grid from 1 to 100000eV. The radiated power is the radiated power per electron per ion so that the unit for radiated power in this paper is watts cm^3.

3. Results

We present the tabulated results for radiated power for neon, silicon, argon, titanium, and iron in tables 1-5 respectively. Each table gives the radiated power as a function of electron temperature for each of the four electron densities.

We show the radiated power graphically in figures 1-5 for these five elements. Each figure shows the radiated power as a function of electron temperature. In each graph the solid line represents the electron density of 10^{13} cm^{-3}, the long dashes represents 10^{14} cm^{-3}, the short dashes represents 10^{15} cm^{-3}, and the dotted line represents 10^{16} cm^{-3}.

Figures 1-5 show a clear trend in the dependence of the radiated power on electron density for the different elements. For the noble gases, neon and argon, the dependence on electron density is quite small over all temperatures. For the other elements there is considerable spread in the curves for different densities at the lower temperatures. At the higher temperatures this density dependency disappears; the four curves come together at the higher temperatures for all four elements. One also sees a pronounced difference in the temperature behavior of the different elements. The noble gases show a large drop in radiated power at the low temperatures. The other elements show a much less significant drop at the lower temperatures.

Table 1. Radiated power for neon

	Electron Density			
Temperature	$1.0000 \times 10^{+13}$	$1.0000 \times 10^{+14}$	$1.0000 \times 10^{+15}$	$1.0000 \times 10^{+16}$
$1.0000 \times 10^{+0}$	1.2770×10^{-33}	1.2629×10^{-33}	1.2509×10^{-33}	1.2268×10^{-33}
$1.1288 \times 10^{+0}$	9.2725×10^{-33}	9.1395×10^{-33}	9.0248×10^{-33}	8.8224×10^{-33}
$1.2743 \times 10^{+0}$	5.6179×10^{-32}	5.5395×10^{-32}	5.4626×10^{-32}	5.3197×10^{-32}
$1.4384 \times 10^{+0}$	2.6105×10^{-31}	2.6203×10^{-31}	2.6115×10^{-31}	2.5424×10^{-31}
$1.6238 \times 10^{+0}$	6.6568×10^{-31}	6.9533×10^{-31}	7.1676×10^{-31}	7.0759×10^{-31}
$1.8330 \times 10^{+0}$	8.0348×10^{-31}	8.3675×10^{-31}	8.7017×10^{-31}	8.7325×10^{-31}
$2.0691 \times 10^{+0}$	7.7390×10^{-31}	7.7660×10^{-31}	7.9221×10^{-31}	8.0407×10^{-31}
$2.3357 \times 10^{+0}$	1.0318×10^{-30}	1.0161×10^{-30}	1.0295×10^{-30}	1.0707×10^{-30}
$2.6367 \times 10^{+0}$	2.4337×10^{-30}	2.4192×10^{-30}	2.4802×10^{-30}	2.6318×10^{-30}
$2.9764 \times 10^{+0}$	7.4474×10^{-30}	7.4762×10^{-30}	7.8286×10^{-30}	8.4257×10^{-30}
$3.3598 \times 10^{+0}$	2.3300×10^{-29}	2.3583×10^{-29}	2.5624×10^{-29}	2.7885×10^{-29}
$3.7927 \times 10^{+0}$	6.9907×10^{-29}	7.1253×10^{-29}	7.7595×10^{-29}	8.1530×10^{-29}
$4.2813 \times 10^{+0}$	1.8370×10^{-28}	1.8647×10^{-28}	1.9423×10^{-28}	1.9639×10^{-28}
$4.8329 \times 10^{+0}$	4.0329×10^{-28}	4.0682×10^{-28}	4.1467×10^{-28}	4.2002×10^{-28}
$5.4556 \times 10^{+0}$	7.9390×10^{-28}	8.0130×10^{-28}	8.2618×10^{-28}	8.8100×10^{-28}
$6.1585 \times 10^{+0}$	1.4965×10^{-27}	1.5270×10^{-27}	1.6462×10^{-27}	1.8977×10^{-27}
$6.9519 \times 10^{+0}$	2.8073×10^{-27}	2.9127×10^{-27}	3.2753×10^{-27}	3.7760×10^{-27}
$7.8476 \times 10^{+0}$	5.1079×10^{-27}	5.3198×10^{-27}	5.9021×10^{-27}	6.3781×10^{-27}
$8.8587 \times 10^{+0}$	8.4760×10^{-27}	8.7236×10^{-27}	9.3129×10^{-27}	9.7154×10^{-27}
$1.0000 \times 10^{+1}$	1.2763×10^{-26}	1.2981×10^{-26}	1.3593×10^{-26}	1.4318×10^{-26}
$1.1288 \times 10^{+1}$	1.8216×10^{-26}	1.8420×10^{-26}	1.9299×10^{-26}	2.0566×10^{-26}
$1.2743 \times 10^{+1}$	2.5301×10^{-26}	2.5515×10^{-26}	2.6695×10^{-26}	2.7769×10^{-26}
$1.4384 \times 10^{+1}$	3.3811×10^{-26}	3.4001×10^{-26}	3.5098×10^{-26}	3.5122×10^{-26}
$1.6238 \times 10^{+1}$	4.3029×10^{-26}	4.3156×10^{-26}	4.3913×10^{-26}	4.2555×10^{-26}
$1.8330 \times 10^{+1}$	5.2678×10^{-26}	5.2740×10^{-26}	5.3116×10^{-26}	4.9645×10^{-26}
$2.0691 \times 10^{+1}$	6.2331×10^{-26}	6.2323×10^{-26}	6.2148×10^{-26}	5.5215×10^{-26}
$2.3357 \times 10^{+1}$	7.0985×10^{-26}	7.0888×10^{-26}	6.9876×10^{-26}	5.8172×10^{-26}
$2.6367 \times 10^{+1}$	7.7800×10^{-26}	7.7578×10^{-26}	7.5364×10^{-26}	5.7977×10^{-26}
$2.9764 \times 10^{+1}$	8.1728×10^{-26}	8.1328×10^{-26}	7.7511×10^{-26}	5.4757×10^{-26}
$3.3598 \times 10^{+1}$	8.0124×10^{-26}	7.9533×10^{-26}	7.4173×10^{-26}	4.8534×10^{-26}
$3.7927 \times 10^{+1}$	7.0253×10^{-26}	6.9572×10^{-26}	6.3667×10^{-26}	3.9347×10^{-26}
$4.2813 \times 10^{+1}$	5.2691×10^{-26}	5.2120×10^{-26}	4.7280×10^{-26}	2.8455×10^{-26}

Table 1 Continued

Temperature	$1.0000 \times 10^{+13}$	$1.0000 \times 10^{+14}$	$1.0000 \times 10^{+15}$	$1.0000 \times 10^{+16}$
$4.8329 \times 10^{+1}$	3.3688×10^{-26}	3.3342×10^{-26}	3.0391×10^{-26}	1.8467×10^{-26}
$5.4556 \times 10^{+1}$	1.9637×10^{-26}	1.9465×10^{-26}	1.7961×10^{-26}	1.1289×10^{-26}
$6.1585 \times 10^{+1}$	1.1204×10^{-26}	1.1124×10^{-26}	1.0404×10^{-26}	6.8400×10^{-27}
$6.9519 \times 10^{+1}$	6.5638×10^{-27}	6.5255×10^{-27}	6.1704×10^{-27}	4.2420×10^{-27}
$7.8476 \times 10^{+1}$	4.0559×10^{-27}	4.0361×10^{-27}	3.8488×10^{-27}	2.7522×10^{-27}
$8.8587 \times 10^{+1}$	2.6351×10^{-27}	2.6242×10^{-27}	2.5194×10^{-27}	1.8695×10^{-27}
$1.0000 \times 10^{+2}$	1.8224×10^{-27}	1.8159×10^{-27}	1.7531×10^{-27}	1.3456×10^{-27}
$1.1288 \times 10^{+2}$	1.3536×10^{-27}	1.3495×10^{-27}	1.3091×10^{-27}	1.0381×10^{-27}
$1.2743 \times 10^{+2}$	1.1054×10^{-27}	1.1026×10^{-27}	1.0745×10^{-27}	8.8023×10^{-28}
$1.4384 \times 10^{+2}$	1.0057×10^{-27}	1.0035×10^{-27}	9.8241×10^{-28}	8.3240×10^{-28}
$1.6238 \times 10^{+2}$	1.0201×10^{-27}	1.0183×10^{-27}	1.0013×10^{-27}	8.7775×10^{-28}
$1.8330 \times 10^{+2}$	1.1288×10^{-27}	1.1273×10^{-27}	1.1131×10^{-27}	1.0071×10^{-27}
$2.0691 \times 10^{+2}$	1.3215×10^{-27}	1.3202×10^{-27}	1.3080×10^{-27}	1.2156×10^{-27}
$2.3357 \times 10^{+2}$	1.5768×10^{-27}	1.5758×10^{-27}	1.5655×10^{-27}	1.4862×10^{-27}
$2.6367 \times 10^{+2}$	1.8668×10^{-27}	1.8660×10^{-27}	1.8576×10^{-27}	1.7914×10^{-27}
$2.9764 \times 10^{+2}$	2.1444×10^{-27}	2.1438×10^{-27}	2.1374×10^{-27}	2.0853×10^{-27}
$3.3598 \times 10^{+2}$	2.3349×10^{-27}	2.3346×10^{-27}	2.3306×10^{-27}	2.2958×10^{-27}
$3.7927 \times 10^{+2}$	2.4015×10^{-27}	2.4012×10^{-27}	2.3983×10^{-27}	2.3721×10^{-27}
$4.2813 \times 10^{+2}$	2.2849×10^{-27}	2.2847×10^{-27}	2.2830×10^{-27}	2.2664×10^{-27}
$4.8329 \times 10^{+2}$	2.0363×10^{-27}	2.0362×10^{-27}	2.0353×10^{-27}	2.0255×10^{-27}
$5.4556 \times 10^{+2}$	1.7329×10^{-27}	1.7328×10^{-27}	1.7324×10^{-27}	1.7269×10^{-27}
$6.1585 \times 10^{+2}$	1.4481×10^{-27}	1.4481×10^{-27}	1.4479×10^{-27}	1.4448×10^{-27}
$6.9519 \times 10^{+2}$	1.2056×10^{-27}	1.2056×10^{-27}	1.2055×10^{-27}	1.2038×10^{-27}
$7.8476 \times 10^{+2}$	1.0112×10^{-27}	1.0112×10^{-27}	1.0112×10^{-27}	1.0102×10^{-27}
$8.8587 \times 10^{+2}$	8.6142×10^{-28}	8.6142×10^{-28}	8.6139×10^{-28}	8.6086×10^{-28}
$1.0000 \times 10^{+3}$	7.4533×10^{-28}	7.4532×10^{-28}	7.4531×10^{-28}	7.4500×10^{-28}
$1.1288 \times 10^{+3}$	6.5521×10^{-28}	6.5521×10^{-28}	6.5520×10^{-28}	6.5501×10^{-28}
$1.2743 \times 10^{+3}$	5.8515×10^{-28}	5.8515×10^{-28}	5.8514×10^{-28}	5.8502×10^{-28}
$1.4384 \times 10^{+3}$	5.2949×10^{-28}	5.2949×10^{-28}	5.2949×10^{-28}	5.2941×10^{-28}
$1.6238 \times 10^{+3}$	4.8529×10^{-28}	4.8529×10^{-28}	4.8529×10^{-28}	4.8523×10^{-28}
$1.8330 \times 10^{+3}$	4.4985×10^{-28}	4.4985×10^{-28}	4.4985×10^{-28}	4.4982×10^{-28}
$2.0691 \times 10^{+3}$	4.1450×10^{-28}	4.1450×10^{-28}	4.1450×10^{-28}	4.1447×10^{-28}
$2.3357 \times 10^{+3}$	3.9894×10^{-28}	3.9894×10^{-28}	3.9894×10^{-28}	3.9892×10^{-28}

Table 1 Continued

Temperature	$1.0000 \times 10^{+13}$	$1.0000 \times 10^{+14}$	$1.0000 \times 10^{+15}$	$1.0000 \times 10^{+16}$
$2.6367 \times 10^{+3}$	3.8064×10^{-28}	3.8064×10^{-28}	3.8064×10^{-28}	3.8063×10^{-28}
$2.9764 \times 10^{+3}$	3.6599×10^{-28}	3.6599×10^{-28}	3.6599×10^{-28}	3.6598×10^{-28}
$3.3598 \times 10^{+3}$	3.5437×10^{-28}	3.5437×10^{-28}	3.5437×10^{-28}	3.5436×10^{-28}
$3.7927 \times 10^{+3}$	3.4530×10^{-28}	3.4530×10^{-28}	3.4530×10^{-28}	3.4529×10^{-28}
$4.2813 \times 10^{+3}$	3.3831×10^{-28}	3.3831×10^{-28}	3.3831×10^{-28}	3.3830×10^{-28}
$4.8329 \times 10^{+3}$	3.3325×10^{-28}	3.3325×10^{-28}	3.3325×10^{-28}	3.3324×10^{-28}
$5.4556 \times 10^{+3}$	3.2972×10^{-28}	3.2972×10^{-28}	3.2972×10^{-28}	3.2972×10^{-28}
$6.1585 \times 10^{+3}$	3.2769×10^{-28}	3.2769×10^{-28}	3.2769×10^{-28}	3.2768×10^{-28}
$6.9519 \times 10^{+3}$	3.2694×10^{-28}	3.2694×10^{-28}	3.2694×10^{-28}	3.2694×10^{-28}
$7.8476 \times 10^{+3}$	3.2726×10^{-28}	3.2726×10^{-28}	3.2726×10^{-28}	3.2726×10^{-28}
$8.8587 \times 10^{+3}$	3.2865×10^{-28}	3.2865×10^{-28}	3.2865×10^{-28}	3.2865×10^{-28}
$1.0000 \times 10^{+4}$	3.3105×10^{-28}	3.3105×10^{-28}	3.3105×10^{-28}	3.3105×10^{-28}
$1.1288 \times 10^{+4}$	3.3441×10^{-28}	3.3441×10^{-28}	3.3441×10^{-28}	3.3441×10^{-28}
$1.2743 \times 10^{+4}$	3.3870×10^{-28}	3.3870×10^{-28}	3.3870×10^{-28}	3.3870×10^{-28}
$1.4384 \times 10^{+4}$	3.4390×10^{-28}	3.4390×10^{-28}	3.4390×10^{-28}	3.4390×10^{-28}
$1.6238 \times 10^{+4}$	3.5001×10^{-28}	3.5001×10^{-28}	3.5001×10^{-28}	3.5001×10^{-28}
$1.8330 \times 10^{+4}$	3.5705×10^{-28}	3.5705×10^{-28}	3.5705×10^{-28}	3.5705×10^{-28}
$2.0691 \times 10^{+4}$	3.6502×10^{-28}	3.6502×10^{-28}	3.6502×10^{-28}	3.6501×10^{-28}
$2.3357 \times 10^{+4}$	3.7393×10^{-28}	3.7393×10^{-28}	3.7393×10^{-28}	3.7393×10^{-28}
$2.6367 \times 10^{+4}$	3.8383×10^{-28}	3.8383×10^{-28}	3.8383×10^{-28}	3.8383×10^{-28}
$2.9764 \times 10^{+4}$	3.9476×10^{-28}	3.9476×10^{-28}	3.9476×10^{-28}	3.9476×10^{-28}
$3.3598 \times 10^{+4}$	4.0676×10^{-28}	4.0676×10^{-28}	4.0676×10^{-28}	4.0676×10^{-28}
$3.7927 \times 10^{+4}$	4.1989×10^{-28}	4.1989×10^{-28}	4.1989×10^{-28}	4.1989×10^{-28}
$4.2813 \times 10^{+4}$	4.3420×10^{-28}	4.3420×10^{-28}	4.3420×10^{-28}	4.3420×10^{-28}
$4.8329 \times 10^{+4}$	4.4977×10^{-28}	4.4977×10^{-28}	4.4977×10^{-28}	4.4977×10^{-28}
$5.4556 \times 10^{+4}$	4.6666×10^{-28}	4.6666×10^{-28}	4.6666×10^{-28}	4.6666×10^{-28}
$6.1585 \times 10^{+4}$	4.8495×10^{-28}	4.8495×10^{-28}	4.8495×10^{-28}	4.8495×10^{-28}
$6.9519 \times 10^{+4}$	5.0472×10^{-28}	5.0472×10^{-28}	5.0472×10^{-28}	5.0472×10^{-28}
$7.8476 \times 10^{+4}$	5.2606×10^{-28}	5.2606×10^{-28}	5.2606×10^{-28}	5.2606×10^{-28}
$8.8587 \times 10^{+4}$	5.4905×10^{-28}	5.4905×10^{-28}	5.4905×10^{-28}	5.4905×10^{-28}
$1.0000 \times 10^{+5}$	5.7381×10^{-28}	5.7381×10^{-28}	5.7381×10^{-28}	5.7381×10^{-28}

Table 2. Radiated power for silicon

	Electron Density			
Temperature	$1.0000 \times 10^{+13}$	$1.0000 \times 10^{+14}$	$1.0000 \times 10^{+15}$	$1.0000 \times 10^{+16}$
$1.0000 \times 10^{+0}$	1.1401×10^{-27}	1.1115×10^{-27}	8.7559×10^{-28}	2.8650×10^{-28}
$1.1288 \times 10^{+0}$	2.4498×10^{-27}	2.4202×10^{-27}	1.9319×10^{-27}	6.4096×10^{-28}
$1.2743 \times 10^{+0}$	4.9151×10^{-27}	5.0627×10^{-27}	4.0756×10^{-27}	1.3055×10^{-27}
$1.4384 \times 10^{+0}$	9.4998×10^{-27}	1.0324×10^{-26}	8.0564×10^{-27}	2.3443×10^{-27}
$1.6238 \times 10^{+0}$	1.7654×10^{-26}	1.8944×10^{-26}	1.3937×10^{-26}	3.7610×10^{-27}
$1.8330 \times 10^{+0}$	2.9995×10^{-26}	3.0530×10^{-26}	2.1621×10^{-26}	5.7024×10^{-27}
$2.0691 \times 10^{+0}$	4.5896×10^{-26}	4.5002×10^{-26}	3.0986×10^{-26}	8.0753×10^{-27}
$2.3357 \times 10^{+0}$	6.4879×10^{-26}	6.2326×10^{-26}	4.0309×10^{-26}	9.8205×10^{-27}
$2.6367 \times 10^{+0}$	8.6599×10^{-26}	8.1597×10^{-26}	4.4606×10^{-26}	1.0740×10^{-26}
$2.9764 \times 10^{+0}$	1.1008×10^{-25}	9.9545×10^{-26}	4.3270×10^{-26}	1.2774×10^{-26}
$3.3598 \times 10^{+0}$	1.3243×10^{-25}	1.0920×10^{-25}	4.4333×10^{-26}	1.4629×10^{-26}
$3.7927 \times 10^{+0}$	1.4717×10^{-25}	1.0601×10^{-25}	4.8269×10^{-26}	1.2106×10^{-26}
$4.2813 \times 10^{+0}$	1.4569×10^{-25}	9.5839×10^{-26}	4.7096×10^{-26}	6.4423×10^{-27}
$4.8329 \times 10^{+0}$	1.2388×10^{-25}	8.1290×10^{-26}	3.4699×10^{-26}	2.7929×10^{-27}
$5.4556 \times 10^{+0}$	8.5451×10^{-26}	5.7965×10^{-26}	1.9425×10^{-26}	1.2152×10^{-27}
$6.1585 \times 10^{+0}$	4.6957×10^{-26}	3.3316×10^{-26}	9.6596×10^{-27}	5.6894×10^{-28}
$6.9519 \times 10^{+0}$	2.2892×10^{-26}	1.7079×10^{-26}	4.8031×10^{-27}	2.9034×10^{-28}
$7.8476 \times 10^{+0}$	1.1130×10^{-26}	8.6592×10^{-27}	2.5027×10^{-27}	1.6147×10^{-28}
$8.8587 \times 10^{+0}$	5.7036×10^{-27}	4.5765×10^{-27}	1.3871×10^{-27}	9.8793×10^{-29}
$1.0000 \times 10^{+1}$	3.1160×10^{-27}	2.5589×10^{-27}	8.2493×10^{-28}	7.0998×10^{-29}
$1.1288 \times 10^{+1}$	1.8563×10^{-27}	1.5569×10^{-27}	5.4364×10^{-28}	7.1470×10^{-29}
$1.2743 \times 10^{+1}$	1.2482×10^{-27}	1.0705×10^{-27}	4.2975×10^{-28}	1.1442×10^{-28}
$1.4384 \times 10^{+1}$	1.0167×10^{-27}	9.0054×10^{-28}	4.6201×10^{-28}	2.4934×10^{-28}
$1.6238 \times 10^{+1}$	1.0930×10^{-27}	1.0120×10^{-27}	6.9940×10^{-28}	5.9960×10^{-28}
$1.8330 \times 10^{+1}$	1.5552×10^{-27}	1.5000×10^{-27}	1.2952×10^{-27}	1.3756×10^{-27}
$2.0691 \times 10^{+1}$	2.5731×10^{-27}	2.5413×10^{-27}	2.4477×10^{-27}	2.7229×10^{-27}
$2.3357 \times 10^{+1}$	4.2750×10^{-27}	4.2624×10^{-27}	4.2581×10^{-27}	4.6470×10^{-27}
$2.6367 \times 10^{+1}$	6.7595×10^{-27}	6.7588×10^{-27}	6.8082×10^{-27}	7.2990×10^{-27}
$2.9764 \times 10^{+1}$	1.0216×10^{-26}	1.0221×10^{-26}	1.0301×10^{-26}	1.0913×10^{-26}
$3.3598 \times 10^{+1}$	1.4733×10^{-26}	1.4740×10^{-26}	1.4828×10^{-26}	1.5478×10^{-26}
$3.7927 \times 10^{+1}$	2.0198×10^{-26}	2.0204×10^{-26}	2.0279×10^{-26}	2.0871×10^{-26}
$4.2813 \times 10^{+1}$	2.6427×10^{-26}	2.6430×10^{-26}	2.6483×10^{-26}	2.6949×10^{-26}

Table 2 Continued

Temperature	$1.0000 \times 10^{+13}$	$1.0000 \times 10^{+14}$	$1.0000 \times 10^{+15}$	$1.0000 \times 10^{+16}$
$4.8329 \times 10^{+1}$	3.3080×10^{-26}	3.3081×10^{-26}	3.3108×10^{-26}	3.3380×10^{-26}
$5.4556 \times 10^{+1}$	3.9719×10^{-26}	3.9718×10^{-26}	3.9718×10^{-26}	3.9727×10^{-26}
$6.1585 \times 10^{+1}$	4.5840×10^{-26}	4.5836×10^{-26}	4.5803×10^{-26}	4.5467×10^{-26}
$6.9519 \times 10^{+1}$	5.0981×10^{-26}	5.0973×10^{-26}	5.0891×10^{-26}	5.0068×10^{-26}
$7.8476 \times 10^{+1}$	5.4688×10^{-26}	5.4672×10^{-26}	5.4511×10^{-26}	5.2971×10^{-26}
$8.8587 \times 10^{+1}$	5.6317×10^{-26}	5.6289×10^{-26}	5.6006×10^{-26}	5.3452×10^{-26}
$1.0000 \times 10^{+2}$	5.4643×10^{-26}	5.4600×10^{-26}	5.4169×10^{-26}	5.0497×10^{-26}
$1.1288 \times 10^{+2}$	4.8054×10^{-26}	4.8000×10^{-26}	4.7473×10^{-26}	4.3205×10^{-26}
$1.2743 \times 10^{+2}$	3.7056×10^{-26}	3.7006×10^{-26}	3.6520×10^{-26}	3.2713×10^{-26}
$1.4384 \times 10^{+2}$	2.5207×10^{-26}	2.5172×10^{-26}	2.4837×10^{-26}	2.2228×10^{-26}
$1.6238 \times 10^{+2}$	1.6067×10^{-26}	1.6047×10^{-26}	1.5856×10^{-26}	1.4340×10^{-26}
$1.8330 \times 10^{+2}$	1.0253×10^{-26}	1.0243×10^{-26}	1.0140×10^{-26}	9.3032×10^{-27}
$2.0691 \times 10^{+2}$	6.8151×10^{-27}	6.8094×10^{-27}	6.7531×10^{-27}	6.2811×10^{-27}
$2.3357 \times 10^{+2}$	4.8041×10^{-27}	4.8008×10^{-27}	4.7682×10^{-27}	4.4880×10^{-27}
$2.6367 \times 10^{+2}$	3.6303×10^{-27}	3.6283×10^{-27}	3.6080×10^{-27}	3.4300×10^{-27}
$2.9764 \times 10^{+2}$	2.9709×10^{-27}	2.9695×10^{-27}	2.9559×10^{-27}	2.8344×10^{-27}
$3.3598 \times 10^{+2}$	2.6325×10^{-27}	2.6315×10^{-27}	2.6217×10^{-27}	2.5330×10^{-27}
$3.7927 \times 10^{+2}$	2.5051×10^{-27}	2.5044×10^{-27}	2.4969×10^{-27}	2.4291×10^{-27}
$4.2813 \times 10^{+2}$	2.5290×10^{-27}	2.5284×10^{-27}	2.5226×10^{-27}	2.4688×10^{-27}
$4.8329 \times 10^{+2}$	2.6670×10^{-27}	2.6665×10^{-27}	2.6618×10^{-27}	2.6184×10^{-27}
$5.4556 \times 10^{+2}$	2.8839×10^{-27}	2.8835×10^{-27}	2.8797×10^{-27}	2.8447×10^{-27}
$6.1585 \times 10^{+2}$	3.1444×10^{-27}	3.1441×10^{-27}	3.1411×10^{-27}	3.1134×10^{-27}
$6.9519 \times 10^{+2}$	3.4117×10^{-27}	3.4114×10^{-27}	3.4092×10^{-27}	3.3881×10^{-27}
$7.8476 \times 10^{+2}$	3.6363×10^{-27}	3.6362×10^{-27}	3.6345×10^{-27}	3.6192×10^{-27}
$8.8587 \times 10^{+2}$	3.7577×10^{-27}	3.7576×10^{-27}	3.7565×10^{-27}	3.7463×10^{-27}
$1.0000 \times 10^{+3}$	3.7292×10^{-27}	3.7291×10^{-27}	3.7285×10^{-27}	3.7223×10^{-27}
$1.1288 \times 10^{+3}$	3.5534×10^{-27}	3.5534×10^{-27}	3.5530×10^{-27}	3.5494×10^{-27}
$1.2743 \times 10^{+3}$	3.2556×10^{-27}	3.2555×10^{-27}	3.2553×10^{-27}	3.2533×10^{-27}
$1.4384 \times 10^{+3}$	2.8992×10^{-27}	2.8992×10^{-27}	2.8991×10^{-27}	2.8981×10^{-27}
$1.6238 \times 10^{+3}$	2.5406×10^{-27}	2.5406×10^{-27}	2.5406×10^{-27}	2.5400×10^{-27}
$1.8330 \times 10^{+3}$	2.2180×10^{-27}	2.2180×10^{-27}	2.2179×10^{-27}	2.2177×10^{-27}
$2.0691 \times 10^{+3}$	1.9487×10^{-27}	1.9487×10^{-27}	1.9487×10^{-27}	1.9486×10^{-27}
$2.3357 \times 10^{+3}$	1.7295×10^{-27}	1.7295×10^{-27}	1.7295×10^{-27}	1.7294×10^{-27}

Table 2 Continued

Temperature	$1.0000 \times 10^{+13}$	$1.0000 \times 10^{+14}$	$1.0000 \times 10^{+15}$	$1.0000 \times 10^{+16}$
$2.6367 \times 10^{+3}$	1.5520×10^{-27}	1.5520×10^{-27}	1.5520×10^{-27}	1.5520×10^{-27}
$2.9764 \times 10^{+3}$	1.4103×10^{-27}	1.4103×10^{-27}	1.4103×10^{-27}	1.4103×10^{-27}
$3.3598 \times 10^{+3}$	1.2979×10^{-27}	1.2979×10^{-27}	1.2979×10^{-27}	1.2979×10^{-27}
$3.7927 \times 10^{+3}$	1.2071×10^{-27}	1.2071×10^{-27}	1.2071×10^{-27}	1.2071×10^{-27}
$4.2813 \times 10^{+3}$	1.1340×10^{-27}	1.1340×10^{-27}	1.1340×10^{-27}	1.1340×10^{-27}
$4.8329 \times 10^{+3}$	1.0755×10^{-27}	1.0755×10^{-27}	1.0755×10^{-27}	1.0755×10^{-27}
$5.4556 \times 10^{+3}$	1.0291×10^{-27}	1.0291×10^{-27}	1.0291×10^{-27}	1.0291×10^{-27}
$6.1585 \times 10^{+3}$	9.9219×10^{-28}	9.9219×10^{-28}	9.9219×10^{-28}	9.9219×10^{-28}
$6.9519 \times 10^{+3}$	9.6312×10^{-28}	9.6312×10^{-28}	9.6312×10^{-28}	9.6312×10^{-28}
$7.8476 \times 10^{+3}$	9.4101×10^{-28}	9.4101×10^{-28}	9.4101×10^{-28}	9.4101×10^{-28}
$8.8587 \times 10^{+3}$	9.2418×10^{-28}	9.2418×10^{-28}	9.2418×10^{-28}	9.2418×10^{-28}
$1.0000 \times 10^{+4}$	9.1170×10^{-28}	9.1170×10^{-28}	9.1170×10^{-28}	9.1170×10^{-28}
$1.1288 \times 10^{+4}$	9.0466×10^{-28}	9.0466×10^{-28}	9.0466×10^{-28}	9.0466×10^{-28}
$1.2743 \times 10^{+4}$	9.0079×10^{-28}	9.0079×10^{-28}	9.0079×10^{-28}	9.0079×10^{-28}
$1.4384 \times 10^{+4}$	9.0022×10^{-28}	9.0022×10^{-28}	9.0022×10^{-28}	9.0022×10^{-28}
$1.6238 \times 10^{+4}$	9.0252×10^{-28}	9.0252×10^{-28}	9.0252×10^{-28}	9.0252×10^{-28}
$1.8330 \times 10^{+4}$	9.0781×10^{-28}	9.0781×10^{-28}	9.0781×10^{-28}	9.0781×10^{-28}
$2.0691 \times 10^{+4}$	9.1573×10^{-28}	9.1573×10^{-28}	9.1573×10^{-28}	9.1573×10^{-28}
$2.3357 \times 10^{+4}$	9.2623×10^{-28}	9.2623×10^{-28}	9.2623×10^{-28}	9.2622×10^{-28}
$2.6367 \times 10^{+4}$	9.3931×10^{-28}	9.3931×10^{-28}	9.3931×10^{-28}	9.3931×10^{-28}
$2.9764 \times 10^{+4}$	9.5481×10^{-28}	9.5481×10^{-28}	9.5481×10^{-28}	9.5481×10^{-28}
$3.3598 \times 10^{+4}$	9.7281×10^{-28}	9.7281×10^{-28}	9.7281×10^{-28}	9.7281×10^{-28}
$3.7927 \times 10^{+4}$	9.9333×10^{-28}	9.9333×10^{-28}	9.9333×10^{-28}	9.9333×10^{-28}
$4.2813 \times 10^{+4}$	1.0164×10^{-27}	1.0164×10^{-27}	1.0164×10^{-27}	1.0164×10^{-27}
$4.8329 \times 10^{+4}$	1.0421×10^{-27}	1.0421×10^{-27}	1.0421×10^{-27}	1.0421×10^{-27}
$5.4556 \times 10^{+4}$	1.0706×10^{-27}	1.0706×10^{-27}	1.0706×10^{-27}	1.0706×10^{-27}
$6.1585 \times 10^{+4}$	1.1020×10^{-27}	1.1020×10^{-27}	1.1020×10^{-27}	1.1020×10^{-27}
$6.9519 \times 10^{+4}$	1.1363×10^{-27}	1.1363×10^{-27}	1.1363×10^{-27}	1.1363×10^{-27}
$7.8476 \times 10^{+4}$	1.1738×10^{-27}	1.1738×10^{-27}	1.1738×10^{-27}	1.1738×10^{-27}
$8.8587 \times 10^{+4}$	1.2146×10^{-27}	1.2146×10^{-27}	1.2146×10^{-27}	1.2146×10^{-27}
$1.0000 \times 10^{+5}$	1.2590×10^{-27}	1.2590×10^{-27}	1.2590×10^{-27}	1.2590×10^{-27}

Table 3. Radiated power for argon

	Electron Density			
Temperature	$1.0000 \times 10^{+13}$	$1.0000 \times 10^{+14}$	$1.0000 \times 10^{+15}$	$1.0000 \times 10^{+16}$
$1.0000 \times 10^{+0}$	2.5335×10^{-31}	2.5255×10^{-31}	2.5078×10^{-31}	2.4005×10^{-31}
$1.1288 \times 10^{+0}$	1.0702×10^{-30}	1.0659×10^{-30}	1.0586×10^{-30}	1.0031×10^{-30}
$1.2743 \times 10^{+0}$	3.5614×10^{-30}	3.5283×10^{-30}	3.4909×10^{-30}	3.1654×10^{-30}
$1.4384 \times 10^{+0}$	1.2360×10^{-29}	1.2321×10^{-29}	1.2203×10^{-29}	1.0592×10^{-29}
$1.6238 \times 10^{+0}$	4.4852×10^{-29}	4.4806×10^{-29}	4.4340×10^{-29}	3.8598×10^{-29}
$1.8330 \times 10^{+0}$	1.4555×10^{-28}	1.4344×10^{-28}	1.3691×10^{-28}	1.1947×10^{-28}
$2.0691 \times 10^{+0}$	4.0014×10^{-28}	3.6828×10^{-28}	3.0391×10^{-28}	2.5552×10^{-28}
$2.3357 \times 10^{+0}$	8.8593×10^{-28}	6.9627×10^{-28}	4.9516×10^{-28}	4.1292×10^{-28}
$2.6367 \times 10^{+0}$	1.5775×10^{-27}	1.1317×10^{-27}	8.7594×10^{-28}	7.7792×10^{-28}
$2.9764 \times 10^{+0}$	2.5855×10^{-27}	2.0007×10^{-27}	1.7730×10^{-27}	1.6604×10^{-27}
$3.3598 \times 10^{+0}$	4.3562×10^{-27}	3.7617×10^{-27}	3.6123×10^{-27}	3.5129×10^{-27}
$3.7927 \times 10^{+0}$	7.4916×10^{-27}	6.9655×10^{-27}	7.0107×10^{-27}	6.8402×10^{-27}
$4.2813 \times 10^{+0}$	1.2681×10^{-26}	1.2296×10^{-26}	1.2600×10^{-26}	1.1951×10^{-26}
$4.8329 \times 10^{+0}$	2.0630×10^{-26}	2.0413×10^{-26}	2.0697×10^{-26}	1.9269×10^{-26}
$5.4556 \times 10^{+0}$	3.1848×10^{-26}	3.1653×10^{-26}	3.1558×10^{-26}	2.9256×10^{-26}
$6.1585 \times 10^{+0}$	4.6421×10^{-26}	4.6060×10^{-26}	4.5525×10^{-26}	4.2063×10^{-26}
$6.9519 \times 10^{+0}$	6.4205×10^{-26}	6.3667×10^{-26}	6.2744×10^{-26}	5.7733×10^{-26}
$7.8476 \times 10^{+0}$	8.4972×10^{-26}	8.4346×10^{-26}	8.2957×10^{-26}	7.6394×10^{-26}
$8.8587 \times 10^{+0}$	1.0829×10^{-25}	1.0765×10^{-25}	1.0583×10^{-25}	9.7522×10^{-26}
$1.0000 \times 10^{+1}$	1.3343×10^{-25}	1.3295×10^{-25}	1.3110×10^{-25}	1.1924×10^{-25}
$1.1288 \times 10^{+1}$	1.6050×10^{-25}	1.6006×10^{-25}	1.5806×10^{-25}	1.3912×10^{-25}
$1.2743 \times 10^{+1}$	1.8788×10^{-25}	1.8745×10^{-25}	1.8460×10^{-25}	1.5458×10^{-25}
$1.4384 \times 10^{+1}$	2.1337×10^{-25}	2.1282×10^{-25}	2.0806×10^{-25}	1.6321×10^{-25}
$1.6238 \times 10^{+1}$	2.3411×10^{-25}	2.3328×10^{-25}	2.2547×10^{-25}	1.6331×10^{-25}
$1.8330 \times 10^{+1}$	2.4560×10^{-25}	2.4432×10^{-25}	2.3201×10^{-25}	1.5215×10^{-25}
$2.0691 \times 10^{+1}$	2.3852×10^{-25}	2.3657×10^{-25}	2.1851×10^{-25}	1.2608×10^{-25}
$2.3357 \times 10^{+1}$	1.9701×10^{-25}	1.9460×10^{-25}	1.7348×10^{-25}	8.9176×10^{-26}
$2.6367 \times 10^{+1}$	1.2765×10^{-25}	1.2581×10^{-25}	1.1035×10^{-25}	5.5987×10^{-26}
$2.9764 \times 10^{+1}$	7.0593×10^{-26}	6.9706×10^{-26}	6.2242×10^{-26}	3.4326×10^{-26}
$3.3598 \times 10^{+1}$	3.9733×10^{-26}	3.9367×10^{-26}	3.6190×10^{-26}	2.2185×10^{-26}
$3.7927 \times 10^{+1}$	2.4926×10^{-26}	2.4766×10^{-26}	2.3310×10^{-26}	1.5660×10^{-26}
$4.2813 \times 10^{+1}$	1.7548×10^{-26}	1.7469×10^{-26}	1.6721×10^{-26}	1.2151×10^{-26}

Table 3 Continued

Temperature	$1.0000 \times 10^{+13}$	$1.0000 \times 10^{+14}$	$1.0000 \times 10^{+15}$	$1.0000 \times 10^{+16}$
$4.8329 \times 10^{+1}$	1.3753×10^{-26}	1.3710×10^{-26}	1.3287×10^{-26}	1.0382×10^{-26}
$5.4556 \times 10^{+1}$	1.1989×10^{-26}	1.1964×10^{-26}	1.1712×10^{-26}	9.8261×10^{-27}
$6.1585 \times 10^{+1}$	1.1703×10^{-26}	1.1688×10^{-26}	1.1536×10^{-26}	1.0330×10^{-26}
$6.9519 \times 10^{+1}$	1.2707×10^{-26}	1.2699×10^{-26}	1.2612×10^{-26}	1.1895×10^{-26}
$7.8476 \times 10^{+1}$	1.4952×10^{-26}	1.4948×10^{-26}	1.4904×10^{-26}	1.4528×10^{-26}
$8.8587 \times 10^{+1}$	1.8150×10^{-26}	1.8148×10^{-26}	1.8129×10^{-26}	1.7956×10^{-26}
$1.0000 \times 10^{+2}$	2.1408×10^{-26}	2.1408×10^{-26}	2.1399×10^{-26}	2.1307×10^{-26}
$1.1288 \times 10^{+2}$	2.3693×10^{-26}	2.3692×10^{-26}	2.3687×10^{-26}	2.3617×10^{-26}
$1.2743 \times 10^{+2}$	2.5736×10^{-26}	2.5736×10^{-26}	2.5733×10^{-26}	2.5688×10^{-26}
$1.4384 \times 10^{+2}$	2.9448×10^{-26}	2.9447×10^{-26}	2.9445×10^{-26}	2.9423×10^{-26}
$1.6238 \times 10^{+2}$	3.4675×10^{-26}	3.4674×10^{-26}	3.4668×10^{-26}	3.4606×10^{-26}
$1.8330 \times 10^{+2}$	3.9542×10^{-26}	3.9540×10^{-26}	3.9522×10^{-26}	3.9349×10^{-26}
$2.0691 \times 10^{+2}$	4.2381×10^{-26}	4.2377×10^{-26}	4.2341×10^{-26}	4.1994×10^{-26}
$2.3357 \times 10^{+2}$	4.1802×10^{-26}	4.1796×10^{-26}	4.1737×10^{-26}	4.1185×10^{-26}
$2.6367 \times 10^{+2}$	3.6923×10^{-26}	3.6915×10^{-26}	3.6843×10^{-26}	3.6163×10^{-26}
$2.9764 \times 10^{+2}$	2.9011×10^{-26}	2.9004×10^{-26}	2.8934×10^{-26}	2.8274×10^{-26}
$3.3598 \times 10^{+2}$	2.0792×10^{-26}	2.0787×10^{-26}	2.0734×10^{-26}	2.0244×10^{-26}
$3.7927 \times 10^{+2}$	1.4412×10^{-26}	1.4408×10^{-26}	1.4375×10^{-26}	1.4063×10^{-26}
$4.2813 \times 10^{+2}$	1.0189×10^{-26}	1.0187×10^{-26}	1.0167×10^{-26}	9.9781×10^{-27}
$4.8329 \times 10^{+2}$	7.5670×10^{-27}	7.5658×10^{-27}	7.5535×10^{-27}	7.4374×10^{-27}
$5.4556 \times 10^{+2}$	5.9903×10^{-27}	5.9895×10^{-27}	5.9816×10^{-27}	5.9067×10^{-27}
$6.1585 \times 10^{+2}$	5.0610×10^{-27}	5.0605×10^{-27}	5.0552×10^{-27}	5.0041×10^{-27}
$6.9519 \times 10^{+2}$	4.5272×10^{-27}	4.5268×10^{-27}	4.5230×10^{-27}	4.4868×10^{-27}
$7.8476 \times 10^{+2}$	4.2695×10^{-27}	4.2693×10^{-27}	4.2665×10^{-27}	4.2395×10^{-27}
$8.8587 \times 10^{+2}$	4.1899×10^{-27}	4.1897×10^{-27}	4.1876×10^{-27}	4.1673×10^{-27}
$1.0000 \times 10^{+3}$	4.2270×10^{-27}	4.2268×10^{-27}	4.2252×10^{-27}	4.2099×10^{-27}
$1.1288 \times 10^{+3}$	4.3534×10^{-27}	4.3532×10^{-27}	4.3520×10^{-27}	4.3403×10^{-27}
$1.2743 \times 10^{+3}$	4.5246×10^{-27}	4.5245×10^{-27}	4.5236×10^{-27}	4.5148×10^{-27}
$1.4384 \times 10^{+3}$	4.6974×10^{-27}	4.6973×10^{-27}	4.6967×10^{-27}	4.6903×10^{-27}
$1.6238 \times 10^{+3}$	4.8336×10^{-27}	4.8336×10^{-27}	4.8331×10^{-27}	4.8287×10^{-27}
$1.8330 \times 10^{+3}$	4.8992×10^{-27}	4.8992×10^{-27}	4.8989×10^{-27}	4.8960×10^{-27}
$2.0691 \times 10^{+3}$	4.8563×10^{-27}	4.8563×10^{-27}	4.8561×10^{-27}	4.8543×10^{-27}
$2.3357 \times 10^{+3}$	4.6968×10^{-27}	4.6968×10^{-27}	4.6967×10^{-27}	4.6956×10^{-27}

Table 3 Continued

Temperature	$1.0000 \times 10^{+13}$	$1.0000 \times 10^{+14}$	$1.0000 \times 10^{+15}$	$1.0000 \times 10^{+16}$
$2.6367 \times 10^{+3}$	4.4414×10^{-27}	4.4414×10^{-27}	4.4413×10^{-27}	4.4407×10^{-27}
$2.9764 \times 10^{+3}$	4.1205×10^{-27}	4.1205×10^{-27}	4.1205×10^{-27}	4.1202×10^{-27}
$3.3598 \times 10^{+3}$	3.7841×10^{-27}	3.7841×10^{-27}	3.7841×10^{-27}	3.7839×10^{-27}
$3.7927 \times 10^{+3}$	3.4574×10^{-27}	3.4574×10^{-27}	3.4574×10^{-27}	3.4573×10^{-27}
$4.2813 \times 10^{+3}$	3.1727×10^{-27}	3.1727×10^{-27}	3.1727×10^{-27}	3.1727×10^{-27}
$4.8329 \times 10^{+3}$	2.9214×10^{-27}	2.9214×10^{-27}	2.9214×10^{-27}	2.9214×10^{-27}
$5.4556 \times 10^{+3}$	2.7117×10^{-27}	2.7117×10^{-27}	2.7117×10^{-27}	2.7117×10^{-27}
$6.1585 \times 10^{+3}$	2.5364×10^{-27}	2.5364×10^{-27}	2.5364×10^{-27}	2.5364×10^{-27}
$6.9519 \times 10^{+3}$	2.3915×10^{-27}	2.3915×10^{-27}	2.3915×10^{-27}	2.3915×10^{-27}
$7.8476 \times 10^{+3}$	2.2741×10^{-27}	2.2741×10^{-27}	2.2741×10^{-27}	2.2741×10^{-27}
$8.8587 \times 10^{+3}$	2.1797×10^{-27}	2.1797×10^{-27}	2.1797×10^{-27}	2.1797×10^{-27}
$1.0000 \times 10^{+4}$	2.1041×10^{-27}	2.1041×10^{-27}	2.1041×10^{-27}	2.1040×10^{-27}
$1.1288 \times 10^{+4}$	2.0449×10^{-27}	2.0449×10^{-27}	2.0449×10^{-27}	2.0449×10^{-27}
$1.2743 \times 10^{+4}$	1.9991×10^{-27}	1.9991×10^{-27}	1.9991×10^{-27}	1.9991×10^{-27}
$1.4384 \times 10^{+4}$	1.9651×10^{-27}	1.9651×10^{-27}	1.9651×10^{-27}	1.9651×10^{-27}
$1.6238 \times 10^{+4}$	1.9410×10^{-27}	1.9410×10^{-27}	1.9410×10^{-27}	1.9410×10^{-27}
$1.8330 \times 10^{+4}$	1.9253×10^{-27}	1.9253×10^{-27}	1.9253×10^{-27}	1.9253×10^{-27}
$2.0691 \times 10^{+4}$	1.9176×10^{-27}	1.9176×10^{-27}	1.9176×10^{-27}	1.9176×10^{-27}
$2.3357 \times 10^{+4}$	1.9170×10^{-27}	1.9170×10^{-27}	1.9170×10^{-27}	1.9170×10^{-27}
$2.6367 \times 10^{+4}$	1.9223×10^{-27}	1.9223×10^{-27}	1.9223×10^{-27}	1.9223×10^{-27}
$2.9764 \times 10^{+4}$	1.9336×10^{-27}	1.9336×10^{-27}	1.9336×10^{-27}	1.9336×10^{-27}
$3.3598 \times 10^{+4}$	1.9508×10^{-27}	1.9508×10^{-27}	1.9508×10^{-27}	1.9508×10^{-27}
$3.7927 \times 10^{+4}$	1.9731×10^{-27}	1.9731×10^{-27}	1.9731×10^{-27}	1.9731×10^{-27}
$4.2813 \times 10^{+4}$	2.0007×10^{-27}	2.0007×10^{-27}	2.0007×10^{-27}	2.0007×10^{-27}
$4.8329 \times 10^{+4}$	2.0335×10^{-27}	2.0335×10^{-27}	2.0335×10^{-27}	2.0335×10^{-27}
$5.4556 \times 10^{+4}$	2.0715×10^{-27}	2.0715×10^{-27}	2.0715×10^{-27}	2.0715×10^{-27}
$6.1585 \times 10^{+4}$	2.1148×10^{-27}	2.1148×10^{-27}	2.1148×10^{-27}	2.1148×10^{-27}
$6.9519 \times 10^{+4}$	2.1635×10^{-27}	2.1635×10^{-27}	2.1635×10^{-27}	2.1635×10^{-27}
$7.8476 \times 10^{+4}$	2.2177×10^{-27}	2.2177×10^{-27}	2.2177×10^{-27}	2.2177×10^{-27}
$8.8587 \times 10^{+4}$	2.2777×10^{-27}	2.2777×10^{-27}	2.2777×10^{-27}	2.2777×10^{-27}
$1.0000 \times 10^{+5}$	2.3437×10^{-27}	2.3437×10^{-27}	2.3437×10^{-27}	2.3437×10^{-27}

Table 4. Radiated power for titanium

	Electron Density			
Temperature	$1.0000 \times 10^{+13}$	$1.0000 \times 10^{+14}$	$1.0000 \times 10^{+15}$	$1.0000 \times 10^{+16}$
$1.0000 \times 10^{+0}$	1.6937×10^{-26}	8.1684×10^{-27}	2.3642×10^{-27}	5.7245×10^{-28}
$1.1288 \times 10^{+0}$	9.6861×10^{-27}	3.7720×10^{-27}	1.1993×10^{-27}	4.8270×10^{-28}
$1.2743 \times 10^{+0}$	4.8999×10^{-27}	2.0814×10^{-27}	8.7434×10^{-28}	3.2812×10^{-28}
$1.4384 \times 10^{+0}$	3.4306×10^{-27}	2.0806×10^{-27}	1.1922×10^{-27}	3.4040×10^{-28}
$1.6238 \times 10^{+0}$	3.7926×10^{-27}	3.0378×10^{-27}	2.0044×10^{-27}	5.3167×10^{-28}
$1.8330 \times 10^{+0}$	5.2739×10^{-27}	4.7285×10^{-27}	3.1984×10^{-27}	8.6635×10^{-28}
$2.0691 \times 10^{+0}$	7.5029×10^{-27}	6.8915×10^{-27}	4.0977×10^{-27}	1.0956×10^{-27}
$2.3357 \times 10^{+0}$	9.7638×10^{-27}	8.5939×10^{-27}	3.6825×10^{-27}	9.4378×10^{-28}
$2.6367 \times 10^{+0}$	1.0534×10^{-26}	8.4349×10^{-27}	2.9518×10^{-27}	8.7818×10^{-28}
$2.9764 \times 10^{+0}$	9.3481×10^{-27}	7.1961×10^{-27}	3.1760×10^{-27}	1.2053×10^{-27}
$3.3598 \times 10^{+0}$	8.4495×10^{-27}	7.0436×10^{-27}	4.4527×10^{-27}	1.8682×10^{-27}
$3.7927 \times 10^{+0}$	9.3364×10^{-27}	8.5364×10^{-27}	6.5307×10^{-27}	2.4533×10^{-27}
$4.2813 \times 10^{+0}$	1.1589×10^{-26}	1.1062×10^{-26}	8.7351×10^{-27}	2.4856×10^{-27}
$4.8329 \times 10^{+0}$	1.3898×10^{-26}	1.3397×10^{-26}	9.9725×10^{-27}	2.4130×10^{-27}
$5.4556 \times 10^{+0}$	1.5031×10^{-26}	1.4454×10^{-26}	1.0065×10^{-26}	2.9475×10^{-27}
$6.1585 \times 10^{+0}$	1.5277×10^{-26}	1.4684×10^{-26}	1.0286×10^{-26}	4.5416×10^{-27}
$6.9519 \times 10^{+0}$	1.6221×10^{-26}	1.5705×10^{-26}	1.1990×10^{-26}	7.6402×10^{-27}
$7.8476 \times 10^{+0}$	1.9298×10^{-26}	1.8894×10^{-26}	1.6017×10^{-26}	1.2776×10^{-26}
$8.8587 \times 10^{+0}$	2.5369×10^{-26}	2.5070×10^{-26}	2.2931×10^{-26}	2.0522×10^{-26}
$1.0000 \times 10^{+1}$	3.4964×10^{-26}	3.4752×10^{-26}	3.3197×10^{-26}	3.1389×10^{-26}
$1.1288 \times 10^{+1}$	4.8416×10^{-26}	4.8267×10^{-26}	4.7149×10^{-26}	4.5689×10^{-26}
$1.2743 \times 10^{+1}$	6.5831×10^{-26}	6.5727×10^{-26}	6.4912×10^{-26}	6.3399×10^{-26}
$1.4384 \times 10^{+1}$	8.7042×10^{-26}	8.6964×10^{-26}	8.6297×10^{-26}	8.4166×10^{-26}
$1.6238 \times 10^{+1}$	1.1150×10^{-25}	1.1142×10^{-25}	1.1070×10^{-25}	1.0735×10^{-25}
$1.8330 \times 10^{+1}$	1.3803×10^{-25}	1.3792×10^{-25}	1.3694×10^{-25}	1.3187×10^{-25}
$2.0691 \times 10^{+1}$	1.6522×10^{-25}	1.6507×10^{-25}	1.6368×10^{-25}	1.5644×10^{-25}
$2.3357 \times 10^{+1}$	1.9095×10^{-25}	1.9076×10^{-25}	1.8900×10^{-25}	1.7988×10^{-25}
$2.6367 \times 10^{+1}$	2.1352×10^{-25}	2.1332×10^{-25}	2.1144×10^{-25}	2.0133×10^{-25}
$2.9764 \times 10^{+1}$	2.3218×10^{-25}	2.3198×10^{-25}	2.3024×10^{-25}	2.1983×10^{-25}
$3.3598 \times 10^{+1}$	2.4643×10^{-25}	2.4627×10^{-25}	2.4472×10^{-25}	2.3408×10^{-25}
$3.7927 \times 10^{+1}$	2.5567×10^{-25}	2.5551×10^{-25}	2.5408×10^{-25}	2.4266×10^{-25}
$4.2813 \times 10^{+1}$	2.5860×10^{-25}	2.5845×10^{-25}	2.5699×10^{-25}	2.4405×10^{-25}

Table 4 Continued

Temperature	$1.0000 \times 10^{+13}$	$1.0000 \times 10^{+14}$	$1.0000 \times 10^{+15}$	$1.0000 \times 10^{+16}$
$4.8329 \times 10^{+1}$	2.5449×10^{-25}	2.5432×10^{-25}	2.5265×10^{-25}	2.3704×10^{-25}
$5.4556 \times 10^{+1}$	2.3977×10^{-25}	2.3955×10^{-25}	2.3734×10^{-25}	2.1670×10^{-25}
$6.1585 \times 10^{+1}$	2.0401×10^{-25}	2.0372×10^{-25}	2.0084×10^{-25}	1.7570×10^{-25}
$6.9519 \times 10^{+1}$	1.4778×10^{-25}	1.4751×10^{-25}	1.4488×10^{-25}	1.2373×10^{-25}
$7.8476 \times 10^{+1}$	9.6863×10^{-26}	9.6698×10^{-26}	9.5092×10^{-26}	8.2535×10^{-26}
$8.8587 \times 10^{+1}$	6.4707×10^{-26}	6.4622×10^{-26}	6.3791×10^{-26}	5.7198×10^{-26}
$1.0000 \times 10^{+2}$	4.6466×10^{-26}	4.6422×10^{-26}	4.5992×10^{-26}	4.2467×10^{-26}
$1.1288 \times 10^{+2}$	3.6194×10^{-26}	3.6170×10^{-26}	3.5929×10^{-26}	3.3899×10^{-26}
$1.2743 \times 10^{+2}$	3.0349×10^{-26}	3.0335×10^{-26}	3.0195×10^{-26}	2.8976×10^{-26}
$1.4384 \times 10^{+2}$	2.7346×10^{-26}	2.7337×10^{-26}	2.7254×10^{-26}	2.6510×10^{-26}
$1.6238 \times 10^{+2}$	2.6417×10^{-26}	2.6412×10^{-26}	2.6363×10^{-26}	2.5919×10^{-26}
$1.8330 \times 10^{+2}$	2.7187×10^{-26}	2.7184×10^{-26}	2.7157×10^{-26}	2.6911×10^{-26}
$2.0691 \times 10^{+2}$	2.9419×10^{-26}	2.9418×10^{-26}	2.9405×10^{-26}	2.9282×10^{-26}
$2.3357 \times 10^{+2}$	3.2739×10^{-26}	3.2738×10^{-26}	3.2733×10^{-26}	3.2678×10^{-26}
$2.6367 \times 10^{+2}$	3.6505×10^{-26}	3.6505×10^{-26}	3.6502×10^{-26}	3.6475×10^{-26}
$2.9764 \times 10^{+2}$	3.9919×10^{-26}	3.9919×10^{-26}	3.9916×10^{-26}	3.9890×10^{-26}
$3.3598 \times 10^{+2}$	4.2241×10^{-26}	4.2241×10^{-26}	4.2237×10^{-26}	4.2196×10^{-26}
$3.7927 \times 10^{+2}$	4.2992×10^{-26}	4.2991×10^{-26}	4.2984×10^{-26}	4.2914×10^{-26}
$4.2813 \times 10^{+2}$	4.1598×10^{-26}	4.1597×10^{-26}	4.1585×10^{-26}	4.1471×10^{-26}
$4.8329 \times 10^{+2}$	3.7518×10^{-26}	3.7516×10^{-26}	3.7500×10^{-26}	3.7342×10^{-26}
$5.4556 \times 10^{+2}$	3.1072×10^{-26}	3.1070×10^{-26}	3.1052×10^{-26}	3.0879×10^{-26}
$6.1585 \times 10^{+2}$	2.3840×10^{-26}	2.3839×10^{-26}	2.3823×10^{-26}	2.3676×10^{-26}
$6.9519 \times 10^{+2}$	1.7690×10^{-26}	1.7688×10^{-26}	1.7678×10^{-26}	1.7571×10^{-26}
$7.8476 \times 10^{+2}$	1.3202×10^{-26}	1.3201×10^{-26}	1.3194×10^{-26}	1.3125×10^{-26}
$8.8587 \times 10^{+2}$	1.0268×10^{-26}	1.0267×10^{-26}	1.0263×10^{-26}	1.0218×10^{-26}
$1.0000 \times 10^{+3}$	8.3689×10^{-27}	8.3686×10^{-27}	8.3656×10^{-27}	8.3362×10^{-27}
$1.1288 \times 10^{+3}$	7.1750×10^{-27}	7.1748×10^{-27}	7.1728×10^{-27}	7.1528×10^{-27}
$1.2743 \times 10^{+3}$	6.4616×10^{-27}	6.4614×10^{-27}	6.4600×10^{-27}	6.4460×10^{-27}
$1.4384 \times 10^{+3}$	6.0607×10^{-27}	6.0606×10^{-27}	6.0596×10^{-27}	6.0496×10^{-27}
$1.6238 \times 10^{+3}$	5.8869×10^{-27}	5.8868×10^{-27}	5.8861×10^{-27}	5.8788×10^{-27}
$1.8330 \times 10^{+3}$	5.8706×10^{-27}	5.8705×10^{-27}	5.8700×10^{-27}	5.8647×10^{-27}
$2.0691 \times 10^{+3}$	5.9837×10^{-27}	5.9836×10^{-27}	5.9832×10^{-27}	5.9794×10^{-27}
$2.3357 \times 10^{+3}$	6.1753×10^{-27}	6.1753×10^{-27}	6.1750×10^{-27}	6.1724×10^{-27}

Table 4 Continued

Temperature	$1.0000 \times 10^{+13}$	$1.0000 \times 10^{+14}$	$1.0000 \times 10^{+15}$	$1.0000 \times 10^{+16}$
$2.6367 \times 10^{+3}$	6.4067×10^{-27}	6.4067×10^{-27}	6.4065×10^{-27}	6.4047×10^{-27}
$2.9764 \times 10^{+3}$	6.6344×10^{-27}	6.6344×10^{-27}	6.6343×10^{-27}	6.6331×10^{-27}
$3.3598 \times 10^{+3}$	6.8014×10^{-27}	6.8014×10^{-27}	6.8013×10^{-27}	6.8005×10^{-27}
$3.7927 \times 10^{+3}$	6.8742×10^{-27}	6.8742×10^{-27}	6.8742×10^{-27}	6.8737×10^{-27}
$4.2813 \times 10^{+3}$	6.8064×10^{-27}	6.8064×10^{-27}	6.8064×10^{-27}	6.8061×10^{-27}
$4.8329 \times 10^{+3}$	6.6235×10^{-27}	6.6235×10^{-27}	6.6235×10^{-27}	6.6233×10^{-27}
$5.4556 \times 10^{+3}$	6.3453×10^{-27}	6.3453×10^{-27}	6.3453×10^{-27}	6.3452×10^{-27}
$6.1585 \times 10^{+3}$	6.0047×10^{-27}	6.0047×10^{-27}	6.0047×10^{-27}	6.0046×10^{-27}
$6.9519 \times 10^{+3}$	5.6443×10^{-27}	5.6443×10^{-27}	5.6443×10^{-27}	5.6443×10^{-27}
$7.8476 \times 10^{+3}$	5.2925×10^{-27}	5.2925×10^{-27}	5.2925×10^{-27}	5.2925×10^{-27}
$8.8587 \times 10^{+3}$	4.9714×10^{-27}	4.9714×10^{-27}	4.9714×10^{-27}	4.9714×10^{-27}
$1.0000 \times 10^{+4}$	4.6847×10^{-27}	4.6847×10^{-27}	4.6847×10^{-27}	4.6847×10^{-27}
$1.1288 \times 10^{+4}$	4.4373×10^{-27}	4.4373×10^{-27}	4.4373×10^{-27}	4.4373×10^{-27}
$1.2743 \times 10^{+4}$	4.2303×10^{-27}	4.2303×10^{-27}	4.2303×10^{-27}	4.2303×10^{-27}
$1.4384 \times 10^{+4}$	4.0596×10^{-27}	4.0596×10^{-27}	4.0596×10^{-27}	4.0596×10^{-27}
$1.6238 \times 10^{+4}$	3.9212×10^{-27}	3.9212×10^{-27}	3.9212×10^{-27}	3.9212×10^{-27}
$1.8330 \times 10^{+4}$	3.8109×10^{-27}	3.8109×10^{-27}	3.8109×10^{-27}	3.8109×10^{-27}
$2.0691 \times 10^{+4}$	3.7253×10^{-27}	3.7253×10^{-27}	3.7253×10^{-27}	3.7253×10^{-27}
$2.3357 \times 10^{+4}$	3.6617×10^{-27}	3.6617×10^{-27}	3.6617×10^{-27}	3.6617×10^{-27}
$2.6367 \times 10^{+4}$	3.6160×10^{-27}	3.6160×10^{-27}	3.6160×10^{-27}	3.6160×10^{-27}
$2.9764 \times 10^{+4}$	3.5881×10^{-27}	3.5881×10^{-27}	3.5881×10^{-27}	3.5881×10^{-27}
$3.3598 \times 10^{+4}$	3.5749×10^{-27}	3.5749×10^{-27}	3.5749×10^{-27}	3.5749×10^{-27}
$3.7927 \times 10^{+4}$	3.5740×10^{-27}	3.5740×10^{-27}	3.5740×10^{-27}	3.5740×10^{-27}
$4.2813 \times 10^{+4}$	3.5854×10^{-27}	3.5854×10^{-27}	3.5854×10^{-27}	3.5854×10^{-27}
$4.8329 \times 10^{+4}$	3.6082×10^{-27}	3.6082×10^{-27}	3.6082×10^{-27}	3.6082×10^{-27}
$5.4556 \times 10^{+4}$	3.6418×10^{-27}	3.6418×10^{-27}	3.6418×10^{-27}	3.6418×10^{-27}
$6.1585 \times 10^{+4}$	3.6491×10^{-27}	3.6491×10^{-27}	3.6491×10^{-27}	3.6491×10^{-27}
$6.9519 \times 10^{+4}$	3.7398×10^{-27}	3.7398×10^{-27}	3.7398×10^{-27}	3.7398×10^{-27}
$7.8476 \times 10^{+4}$	3.8036×10^{-27}	3.8036×10^{-27}	3.8036×10^{-27}	3.8036×10^{-27}
$8.8587 \times 10^{+4}$	3.8778×10^{-27}	3.8778×10^{-27}	3.8778×10^{-27}	3.8778×10^{-27}
$1.0000 \times 10^{+5}$	3.9620×10^{-27}	3.9620×10^{-27}	3.9620×10^{-27}	3.9620×10^{-27}

Table 5. Radiated power for iron

	Electron Density			
Temperature	$1.0000 \times 10^{+13}$	$1.0000 \times 10^{+14}$	$1.0000 \times 10^{+15}$	$1.0000 \times 10^{+16}$
$1.0000 \times 10^{+0}$	8.9290×10^{-27}	7.4728×10^{-27}	3.0782×10^{-27}	5.0259×10^{-28}
$1.1288 \times 10^{+0}$	1.3949×10^{-26}	1.0219×10^{-26}	3.4528×10^{-27}	7.5322×10^{-28}
$1.2743 \times 10^{+0}$	1.7586×10^{-26}	8.7972×10^{-27}	2.1043×10^{-27}	7.1129×10^{-28}
$1.4384 \times 10^{+0}$	1.4986×10^{-26}	5.0613×10^{-27}	1.1906×10^{-27}	4.6384×10^{-28}
$1.6238 \times 10^{+0}$	9.3437×10^{-27}	3.2191×10^{-27}	1.2499×10^{-27}	4.4885×10^{-28}
$1.8330 \times 10^{+0}$	6.4016×10^{-27}	3.3547×10^{-27}	2.1034×10^{-27}	7.5237×10^{-28}
$2.0691 \times 10^{+0}$	6.4502×10^{-27}	4.9171×10^{-27}	3.6812×10^{-27}	1.3433×10^{-27}
$2.3357 \times 10^{+0}$	8.4546×10^{-27}	7.5249×10^{-27}	5.3311×10^{-27}	1.7088×10^{-27}
$2.6367 \times 10^{+0}$	1.1180×10^{-26}	1.0134×10^{-26}	5.2890×10^{-27}	1.3882×10^{-27}
$2.9764 \times 10^{+0}$	1.2330×10^{-26}	1.0498×10^{-26}	4.0528×10^{-27}	1.3310×10^{-27}
$3.3598 \times 10^{+0}$	1.0633×10^{-26}	8.5913×10^{-27}	3.7384×10^{-27}	1.8975×10^{-27}
$3.7927 \times 10^{+0}$	8.7562×10^{-27}	7.3838×10^{-27}	4.6173×10^{-27}	2.7928×10^{-27}
$4.2813 \times 10^{+0}$	8.5552×10^{-27}	7.8106×10^{-27}	6.1554×10^{-27}	3.1783×10^{-27}
$4.8329 \times 10^{+0}$	9.2999×10^{-27}	8.8726×10^{-27}	7.2949×10^{-27}	2.8663×10^{-27}
$5.4556 \times 10^{+0}$	9.3727×10^{-27}	9.0377×10^{-27}	7.0977×10^{-27}	2.8202×10^{-27}
$6.1585 \times 10^{+0}$	8.4754×10^{-27}	8.1889×10^{-27}	6.4320×10^{-27}	3.3777×10^{-27}
$6.9519 \times 10^{+0}$	7.9494×10^{-27}	7.7399×10^{-27}	6.5080×10^{-27}	4.3104×10^{-27}
$7.8476 \times 10^{+0}$	8.4403×10^{-27}	8.2925×10^{-27}	7.4236×10^{-27}	5.2795×10^{-27}
$8.8587 \times 10^{+0}$	9.6965×10^{-27}	9.5796×10^{-27}	8.8256×10^{-27}	6.3442×10^{-27}
$1.0000 \times 10^{+1}$	1.1500×10^{-26}	1.1395×10^{-26}	1.0645×10^{-26}	8.0898×10^{-27}
$1.1288 \times 10^{+1}$	1.4136×10^{-26}	1.4043×10^{-26}	1.3344×10^{-26}	1.1083×10^{-26}
$1.2743 \times 10^{+1}$	1.8209×10^{-26}	1.8134×10^{-26}	1.7556×10^{-26}	1.5696×10^{-26}
$1.4384 \times 10^{+1}$	2.4288×10^{-26}	2.4234×10^{-26}	2.3806×10^{-26}	2.2330×10^{-26}
$1.6238 \times 10^{+1}$	3.2931×10^{-26}	3.2896×10^{-26}	3.2611×10^{-26}	3.1529×10^{-26}
$1.8330 \times 10^{+1}$	4.4694×10^{-26}	4.4674×10^{-26}	4.4507×10^{-26}	4.3845×10^{-26}
$2.0691 \times 10^{+1}$	5.9976×10^{-26}	5.9967×10^{-26}	5.9891×10^{-26}	5.9651×10^{-26}
$2.3357 \times 10^{+1}$	7.8966×10^{-26}	7.8964×10^{-26}	7.8952×10^{-26}	7.9076×10^{-26}
$2.6367 \times 10^{+1}$	1.0154×10^{-25}	1.0155×10^{-25}	1.0157×10^{-25}	1.0192×10^{-25}
$2.9764 \times 10^{+1}$	1.2721×10^{-25}	1.2721×10^{-25}	1.2724×10^{-25}	1.2763×10^{-25}
$3.3598 \times 10^{+1}$	1.5498×10^{-25}	1.5498×10^{-25}	1.5499×10^{-25}	1.5523×10^{-25}
$3.7927 \times 10^{+1}$	1.8365×10^{-25}	1.8365×10^{-25}	1.8363×10^{-25}	1.8350×10^{-25}
$4.2813 \times 10^{+1}$	2.1157×10^{-25}	2.1157×10^{-25}	2.1150×10^{-25}	2.1075×10^{-25}

Table 5 Continued

Temperature	$1.0000 \times 10^{+13}$	$1.0000 \times 10^{+14}$	$1.0000 \times 10^{+15}$	$1.0000 \times 10^{+16}$
$4.8329 \times 10^{+1}$	2.3710×10^{-25}	2.3709×10^{-25}	2.3695×10^{-25}	2.3528×10^{-25}
$5.4556 \times 10^{+1}$	2.5829×10^{-25}	2.5827×10^{-25}	2.5802×10^{-25}	2.5508×10^{-25}
$6.1585 \times 10^{+1}$	2.7268×10^{-25}	2.7264×10^{-25}	2.7225×10^{-25}	2.6794×10^{-25}
$6.9519 \times 10^{+1}$	2.7807×10^{-25}	2.7802×10^{-25}	2.7752×10^{-25}	2.7225×10^{-25}
$7.8476 \times 10^{+1}$	2.7372×10^{-25}	2.7367×10^{-25}	2.7315×10^{-25}	2.6798×10^{-25}
$8.8587 \times 10^{+1}$	2.6217×10^{-25}	2.6212×10^{-25}	2.6167×10^{-25}	2.5724×10^{-25}
$1.0000 \times 10^{+2}$	2.4385×10^{-25}	2.4381×10^{-25}	2.4346×10^{-25}	2.3995×10^{-25}
$1.1288 \times 10^{+2}$	2.2302×10^{-25}	2.2298×10^{-25}	2.2258×10^{-25}	2.1856×10^{-25}
$1.2743 \times 10^{+2}$	1.9221×10^{-25}	1.9217×10^{-25}	1.9167×10^{-25}	1.8681×10^{-25}
$1.4384 \times 10^{+2}$	1.5196×10^{-25}	1.5191×10^{-25}	1.5140×10^{-25}	1.4645×10^{-25}
$1.6238 \times 10^{+2}$	1.1299×10^{-25}	1.1295×10^{-25}	1.1255×10^{-25}	1.0871×10^{-25}
$1.8330 \times 10^{+2}$	8.4278×10^{-26}	8.4251×10^{-26}	8.3982×10^{-26}	8.1449×10^{-26}
$2.0691 \times 10^{+2}$	6.5507×10^{-26}	6.5490×10^{-26}	6.5321×10^{-26}	6.3731×10^{-26}
$2.3357 \times 10^{+2}$	5.3700×10^{-26}	5.3689×10^{-26}	5.3584×10^{-26}	5.2586×10^{-26}
$2.6367 \times 10^{+2}$	4.6428×10^{-26}	4.6421×10^{-26}	4.6355×10^{-26}	4.5725×10^{-26}
$2.9764 \times 10^{+2}$	4.2020×10^{-26}	4.2015×10^{-26}	4.1975×10^{-26}	4.1587×10^{-26}
$3.3598 \times 10^{+2}$	4.0008×10^{-26}	4.0006×10^{-26}	3.9981×10^{-26}	3.9745×10^{-26}
$3.7927 \times 10^{+2}$	3.9475×10^{-26}	3.9474×10^{-26}	3.9460×10^{-26}	3.9328×10^{-26}
$4.2813 \times 10^{+2}$	4.0161×10^{-26}	4.0161×10^{-26}	4.0154×10^{-26}	4.0087×10^{-26}
$4.8329 \times 10^{+2}$	4.1590×10^{-26}	4.1589×10^{-26}	4.1586×10^{-26}	4.1552×10^{-26}
$5.4556 \times 10^{+2}$	4.2939×10^{-26}	4.2938×10^{-26}	4.2936×10^{-26}	4.2915×10^{-26}
$6.1585 \times 10^{+2}$	4.3267×10^{-26}	4.3267×10^{-26}	4.3265×10^{-26}	4.3242×10^{-26}
$6.9519 \times 10^{+2}$	4.1930×10^{-26}	4.1930×10^{-26}	4.1927×10^{-26}	4.1896×10^{-26}
$7.8476 \times 10^{+2}$	3.8693×10^{-26}	3.8693×10^{-26}	3.8688×10^{-26}	3.8648×10^{-26}
$8.8587 \times 10^{+2}$	3.3730×10^{-26}	3.3729×10^{-26}	3.3725×10^{-26}	3.3677×10^{-26}
$1.0000 \times 10^{+3}$	2.7673×10^{-26}	2.7672×10^{-26}	2.7667×10^{-26}	2.7621×10^{-26}
$1.1288 \times 10^{+3}$	2.1859×10^{-26}	2.1859×10^{-26}	2.1855×10^{-26}	2.1817×10^{-26}
$1.2743 \times 10^{+3}$	1.7130×10^{-26}	1.7129×10^{-26}	1.7126×10^{-26}	1.7099×10^{-26}
$1.4384 \times 10^{+3}$	1.3651×10^{-26}	1.3651×10^{-26}	1.3649×10^{-26}	1.3630×10^{-26}
$1.6238 \times 10^{+3}$	1.1216×10^{-26}	1.1216×10^{-26}	1.1215×10^{-26}	1.1202×10^{-26}
$1.8330 \times 10^{+3}$	9.6136×10^{-27}	9.6135×10^{-27}	9.6127×10^{-27}	9.6041×10^{-27}
$2.0691 \times 10^{+3}$	8.5405×10^{-27}	8.5404×10^{-27}	8.5398×10^{-27}	8.5339×10^{-27}
$2.3357 \times 10^{+3}$	7.8435×10^{-27}	7.8434×10^{-27}	7.8430×10^{-27}	7.8389×10^{-27}

Table 5 Continued

Temperature	$1.0000 \times 10^{+13}$	$1.0000 \times 10^{+14}$	$1.0000 \times 10^{+15}$	$1.0000 \times 10^{+16}$
$2.6367 \times 10^{+3}$	7.3968×10^{-27}	7.3967×10^{-27}	7.3964×10^{-27}	7.3936×10^{-27}
$2.9764 \times 10^{+3}$	7.1443×10^{-27}	7.1443×10^{-27}	7.1441×10^{-27}	7.1420×10^{-27}
$3.3598 \times 10^{+3}$	7.0103×10^{-27}	7.0103×10^{-27}	7.0102×10^{-27}	7.0088×10^{-27}
$3.7927 \times 10^{+3}$	6.9695×10^{-27}	6.9695×10^{-27}	6.9694×10^{-27}	6.9685×10^{-27}
$4.2813 \times 10^{+3}$	6.9787×10^{-27}	6.9787×10^{-27}	6.9786×10^{-27}	6.9780×10^{-27}
$4.8329 \times 10^{+3}$	7.0110×10^{-27}	7.0110×10^{-27}	7.0109×10^{-27}	7.0105×10^{-27}
$5.4556 \times 10^{+3}$	7.0513×10^{-27}	7.0513×10^{-27}	7.0513×10^{-27}	7.0511×10^{-27}
$6.1585 \times 10^{+3}$	7.0513×10^{-27}	7.0513×10^{-27}	7.0513×10^{-27}	7.0512×10^{-27}
$6.9519 \times 10^{+3}$	7.0295×10^{-27}	7.0295×10^{-27}	7.0295×10^{-27}	7.0294×10^{-27}
$7.8476 \times 10^{+3}$	6.9688×10^{-27}	6.9688×10^{-27}	6.9688×10^{-27}	6.9687×10^{-27}
$8.8587 \times 10^{+3}$	6.8675×10^{-27}	6.8675×10^{-27}	6.8675×10^{-27}	6.8674×10^{-27}
$1.0000 \times 10^{+4}$	6.7359×10^{-27}	6.7359×10^{-27}	6.7359×10^{-27}	6.7359×10^{-27}
$1.1288 \times 10^{+4}$	6.5887×10^{-27}	6.5887×10^{-27}	6.5887×10^{-27}	6.5887×10^{-27}
$1.2743 \times 10^{+4}$	6.4360×10^{-27}	6.4360×10^{-27}	6.4360×10^{-27}	6.4360×10^{-27}
$1.4384 \times 10^{+4}$	6.2841×10^{-27}	6.2841×10^{-27}	6.2841×10^{-27}	6.2841×10^{-27}
$1.6238 \times 10^{+4}$	6.1454×10^{-27}	6.1454×10^{-27}	6.1454×10^{-27}	6.1454×10^{-27}
$1.8330 \times 10^{+4}$	6.0229×10^{-27}	6.0229×10^{-27}	6.0229×10^{-27}	6.0229×10^{-27}
$2.0691 \times 10^{+4}$	5.9202×10^{-27}	5.9202×10^{-27}	5.9202×10^{-27}	5.9202×10^{-27}
$2.3357 \times 10^{+4}$	5.8383×10^{-27}	5.8383×10^{-27}	5.8383×10^{-27}	5.8383×10^{-27}
$2.6367 \times 10^{+4}$	5.7754×10^{-27}	5.7754×10^{-27}	5.7754×10^{-27}	5.7754×10^{-27}
$2.9764 \times 10^{+4}$	5.7323×10^{-27}	5.7323×10^{-27}	5.7323×10^{-27}	5.7323×10^{-27}
$3.3598 \times 10^{+4}$	5.7078×10^{-27}	5.7078×10^{-27}	5.7078×10^{-27}	5.7078×10^{-27}
$3.7927 \times 10^{+4}$	5.6992×10^{-27}	5.6992×10^{-27}	5.6992×10^{-27}	5.6992×10^{-27}
$4.2813 \times 10^{+4}$	5.7076×10^{-27}	5.7076×10^{-27}	5.7076×10^{-27}	5.7076×10^{-27}
$4.8329 \times 10^{+4}$	5.7320×10^{-27}	5.7320×10^{-27}	5.7320×10^{-27}	5.7320×10^{-27}
$5.4556 \times 10^{+4}$	5.7698×10^{-27}	5.7698×10^{-27}	5.7698×10^{-27}	5.7698×10^{-27}
$6.1585 \times 10^{+4}$	5.8221×10^{-27}	5.8221×10^{-27}	5.8221×10^{-27}	5.8221×10^{-27}
$6.9519 \times 10^{+4}$	5.8883×10^{-27}	5.8883×10^{-27}	5.8883×10^{-27}	5.8883×10^{-27}
$7.8476 \times 10^{+4}$	5.9688×10^{-27}	5.9688×10^{-27}	5.9688×10^{-27}	5.9688×10^{-27}
$8.8587 \times 10^{+4}$	6.0631×10^{-27}	6.0631×10^{-27}	6.0631×10^{-27}	6.0631×10^{-27}
$1.0000 \times 10^{+5}$	6.1713×10^{-27}	6.1713×10^{-27}	6.1713×10^{-27}	6.1713×10^{-27}

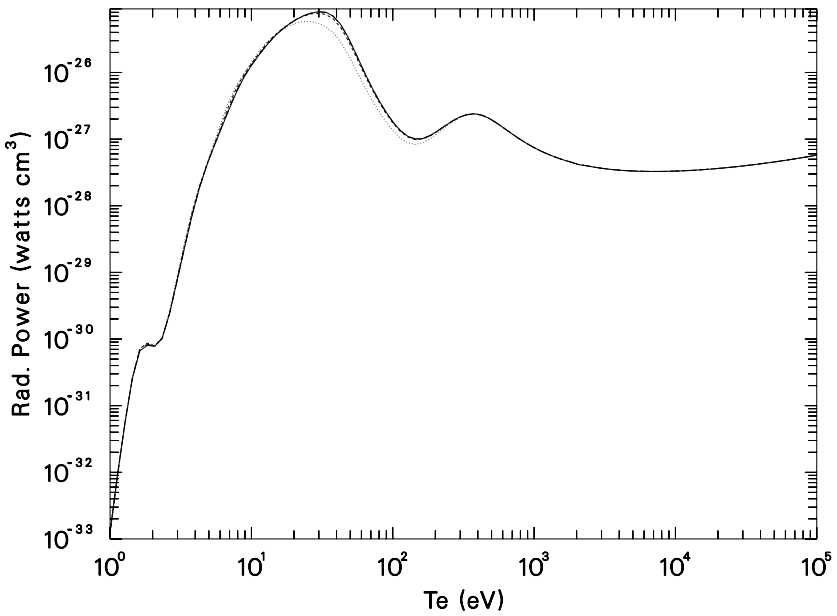

FIG. 1. Radiated power versus electron temperature for neon at electron densities of 10^{13} (solid line), 10^{14} (long dashes), 10^{15} (short dashes), and 10^{16} (dotted line) cm^{-3}.

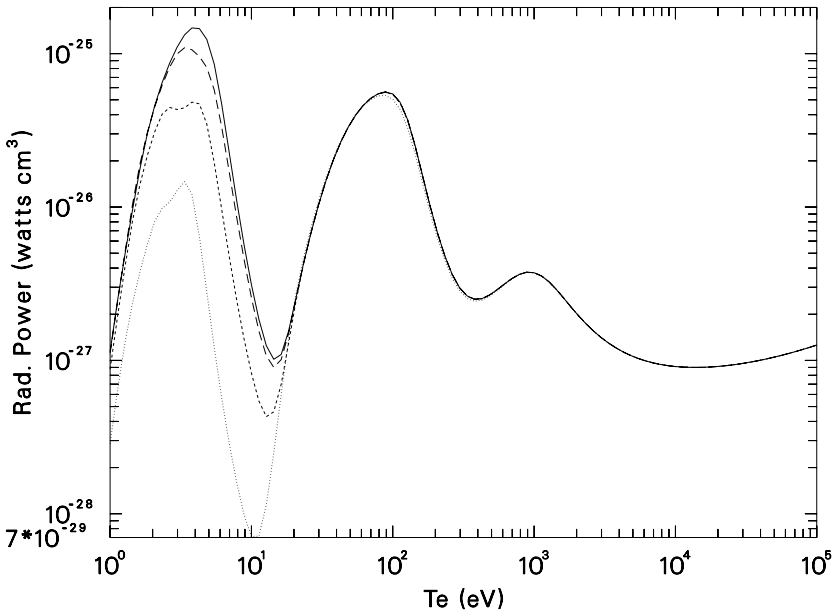

FIG. 2. Radiated power versus electron temperature for silicon at electron densities of 10^{13} (solid line), 10^{14} (long dashes), 10^{15} (short dashes), and 10^{16} (dotted line) cm^{-3}.

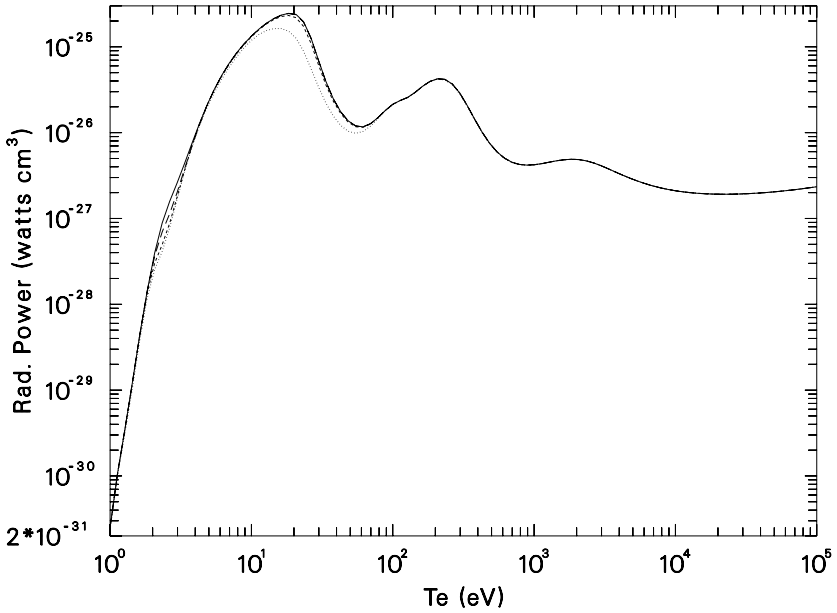

FIG. 3. Radiated power versus electron temperature for argon at electron densities of 10^{13} (solid line), 10^{14} (long dashes), 10^{15} (short dashes), and 10^{16} (dotted line) cm^{-3}.

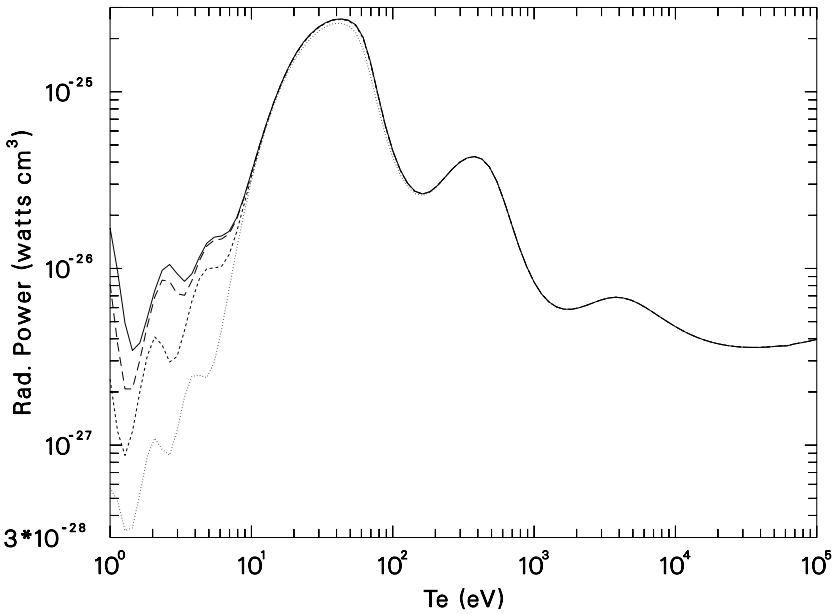

FIG. 4. Radiated power versus electron temperature for titanium at electron densities of 10^{13} (solid line), 10^{14} (long dashes), 10^{15} (short dashes), and 10^{16} (dotted line) cm^{-3}.

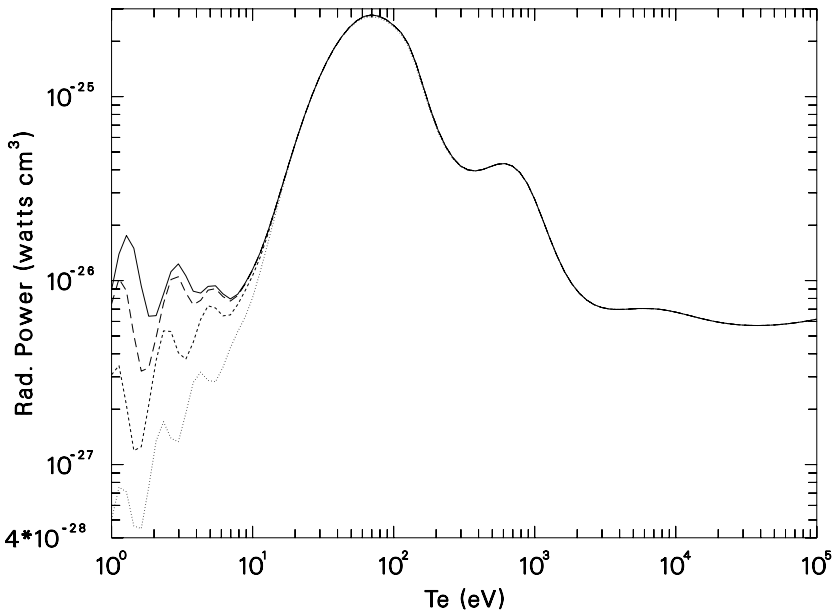

FIG. 5. Radiated power versus electron temperature for iron at electron densities of 10^{13} (solid line), 10^{14} (long dashes), 10^{15} (short dashes), and 10^{16} (dotted line) cm^{-3}.

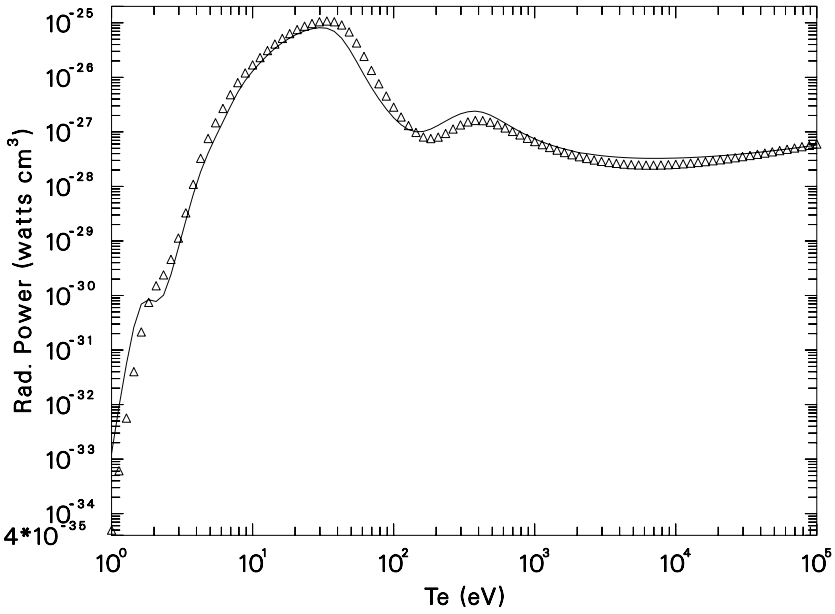

FIG. 6. Comparison of radiated power calculated with present method (solid line) with results from ADPAK (triangles) for neon at electron density of 10^{14}.

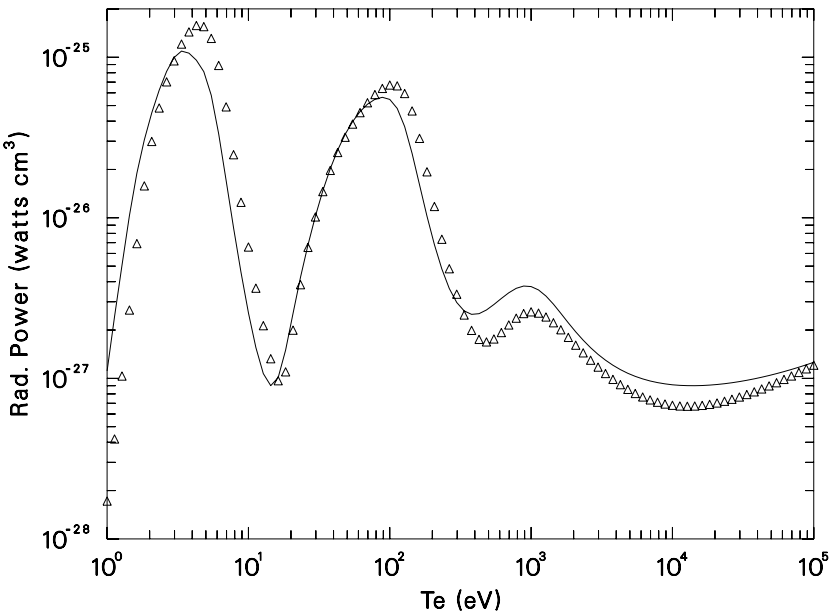

FIG. 7. Comparison of radiated power calculated with present method (solid line) with results from ADPAK (triangles) for silicon at electron density of 10^{14}.

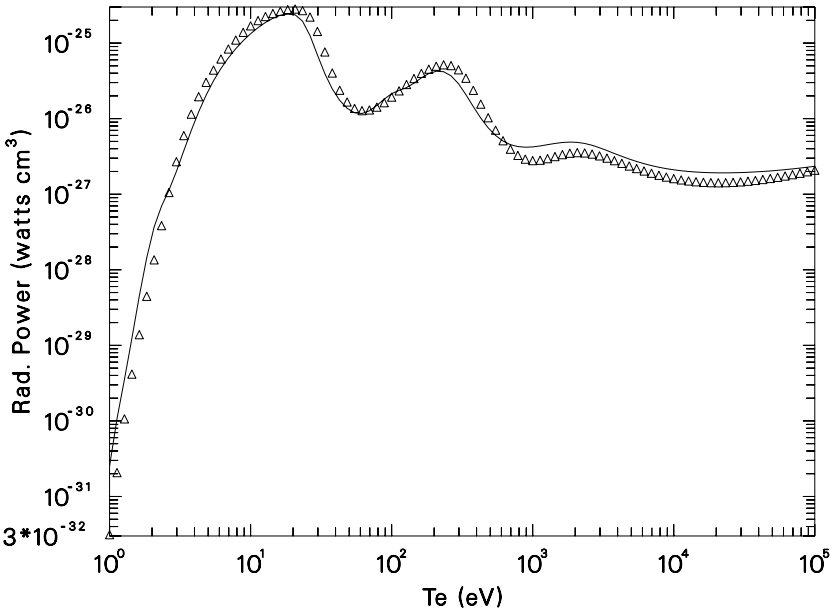

FIG. 8. Comparison of radiated power calculated with present method (solid line) with results from ADPAK (triangles) for argon at electron density of 10^{14}.

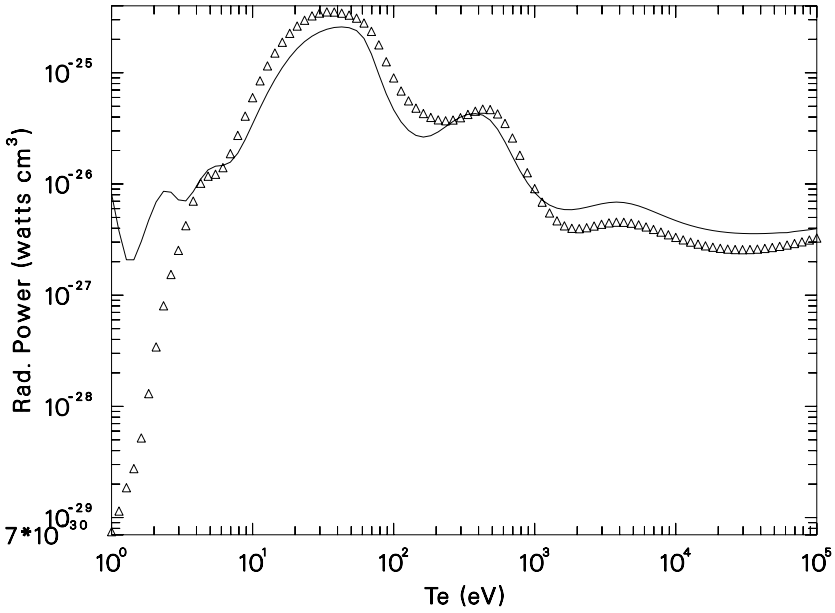

FIG. 9. Comparison of radiated power calculated with present method (solid line) with results from ADPAK (triangles) for titanium at electron density of 10^{14}.

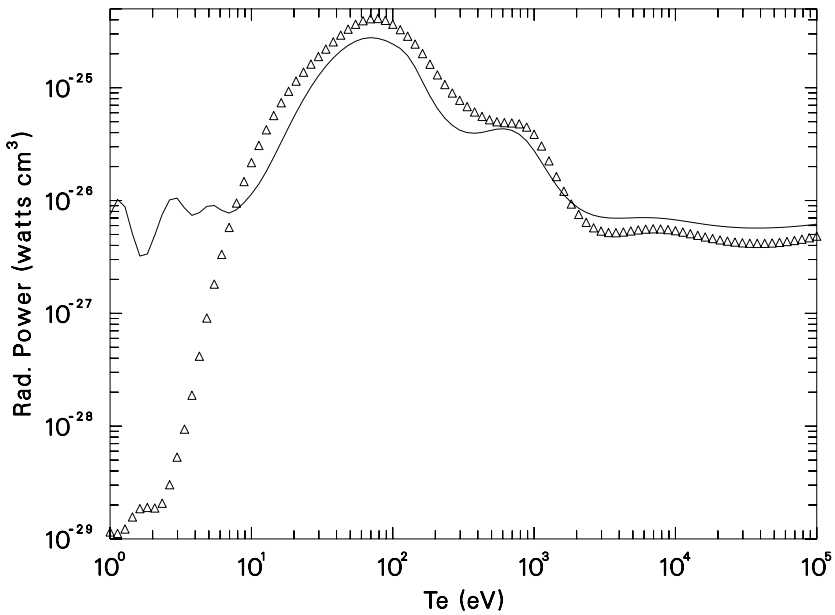

FIG. 10. Comparison of radiated power calculated with present method (solid line) with results from ADPAK (triangles) for iron at electron density of 10^{14}.

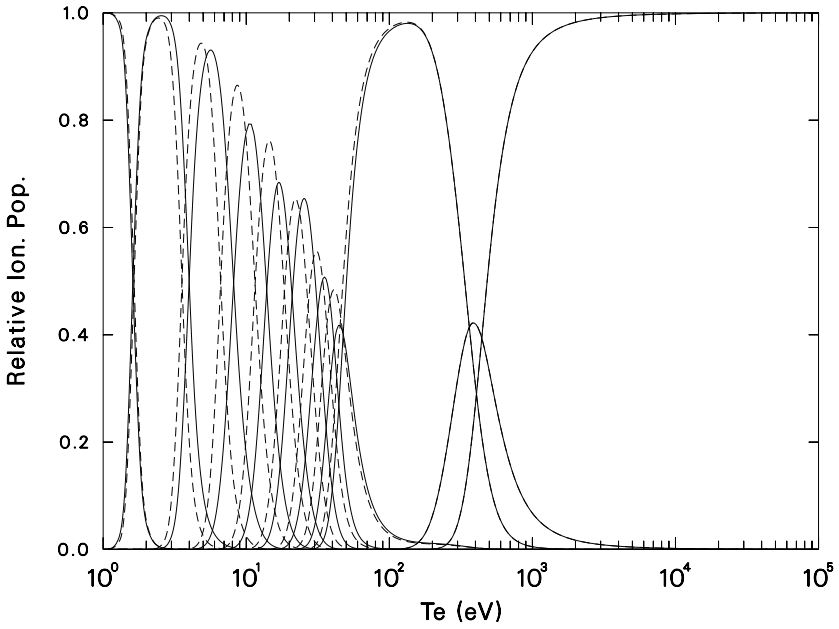

FIG. 11. Relative ionization stage populations for neon as a function of electron temperature for electron densities of 10^{13} (solid lines) and 10^{16} (dashed lines). (solid line) with results from ADPAK (triangles) for argon at electron density of 10^{14}.

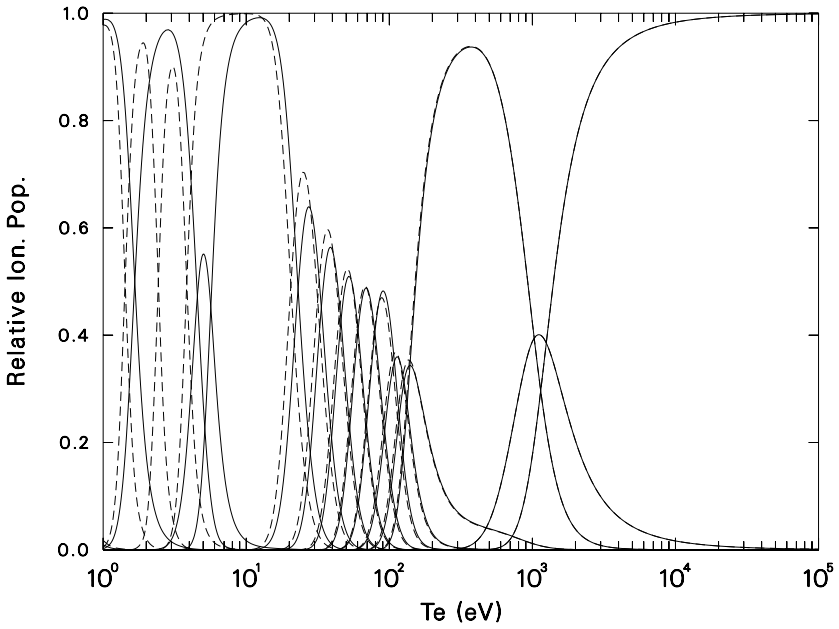

FIG. 12. Relative ionization stage populations for silicon as a function of electron temperature for electron densities of 10^{13} (solid lines) and 10^{16} (dashed lines).

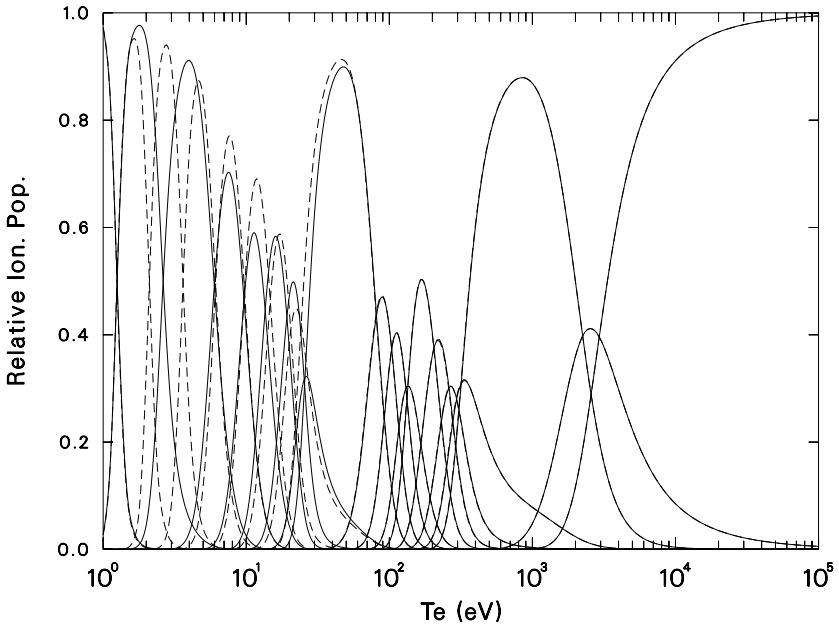

FIG. 13. Relative ionization stage populations for argon as a function of electron temperature for electron densities of 10^{13} (solid lines) and 10^{16} (dashed lines). (solid line) with results from ADPAK (triangles) for argon at electron density of 10^{14}.

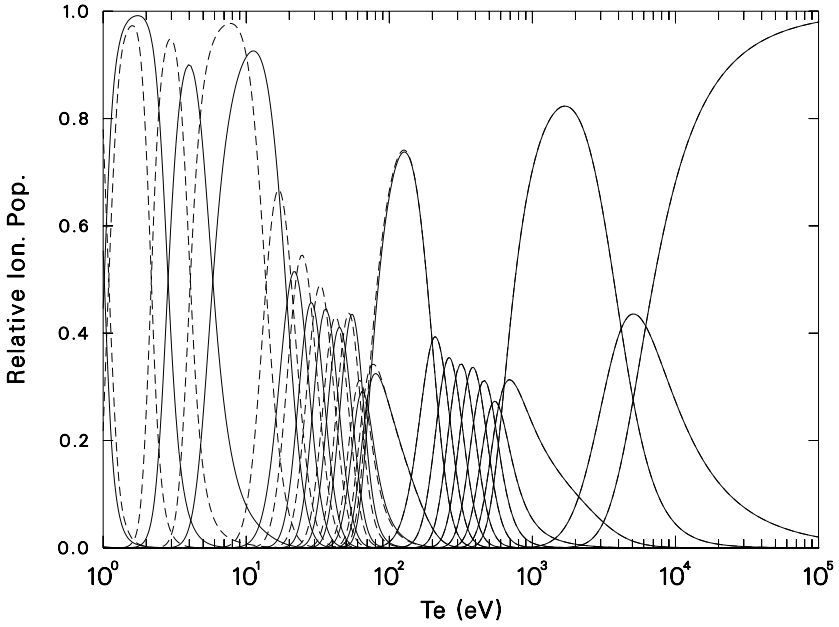

FIG. 14. Relative ionization stage populations for titanium as a function of electron temperature for electron densities of 10^{13} (solid lines) and 10^{16} (dashed lines).

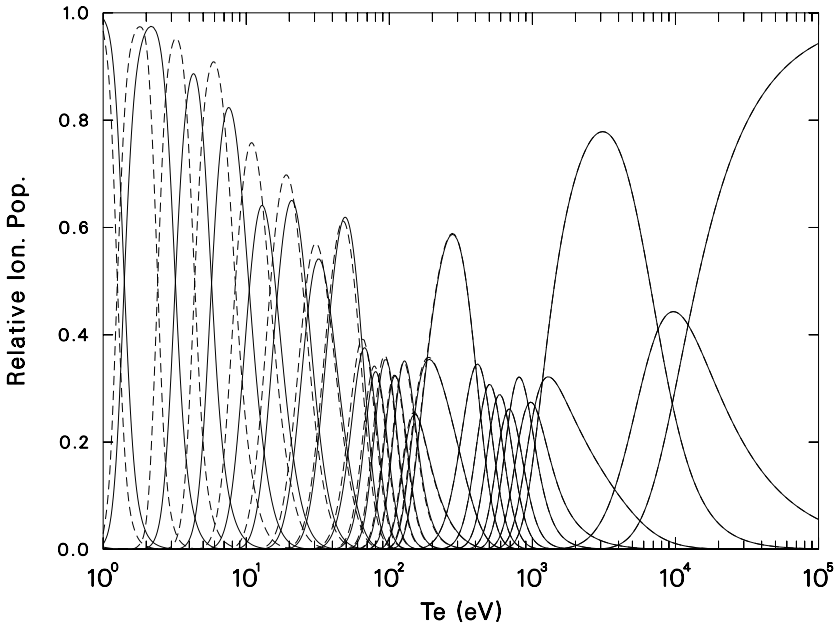

FIG. 15. Relative ionization stage populations for iron as a function of electron temperature for electron densities of 10^{13} (solid lines) and 10^{16} (dashed lines).

In figures 6–10 we show comparisons between our present calculations (the solid lines) and calculations from the ADPAK code [4, 5] (triangles) at an electron density of 10^{14}. We note that the ADPAK code uses a coronal model and thus has nearly no electron density dependence. One sees from figure 6-10 that the ADPAK calculations follow our detailed calculations quite closely for the lighter elements. However, for titanium and iron, especially at low temperatures, the differences become significant.

Finally, in figures 11-15 we give ionization stage populations for each element. In each figure we give the populations for the bounding electron densities of 10^{13} (solid line) and 10^{16} (dashed line cm^{-3}. In each case we note that the higher densities tend to reach higher ionization states at lower temperatures compared to the lower density calculations. At temperatures over 100 eV the density effect is insignificant, which is consistent with the radiated power calculations.

4. Summary

We have calculated radiated power loss over a wide range of electron temperature and density for neon, silicon, argon, titanium, and iron using the model we have found to be most reliable from previous work. The results of these calculations have been presented in tabular and graphical form. These calculations should be of use in plasma modeling calculations for magnetic fusion plasmas.

This work was supported under the auspices of the United States Department of Energy.

REFERENCES

[1] R. E. H. Clark and J. Abdallah, Jr., previous paper in this journal.
[2] D. Post, J. Abdallah, R. E. H. Clark, and N. Putvinskaya, Phys. Plasmas, **2**, 2328, (1995).
[3] J. Abdallah, Jr., R. E. H. Clark, D. P. Kilcrease, G. Csanak, and C. J. Fontes, Proceedings of the 10^{th} APS Topical Conference on Atomic Processes in Plasmas, AIP Proceedings, **381**, 131, (1996).
[4] R. Hulse, Nucl. Technol. Fusion, **3**, 259, (1983).
[5] D. E. Post, R. V. Jensen, C. B. Tarter, W. H. Grasberger, and W. A. Lokke, At. Nuc. Data Tables, **20**, 397, (1977).
[6] J. Abdallah, Jr., R. E. H. Clark, and R. D. Cowan, Los Alamos Manual No. LA-11436-M I, 1988
[7] R. D. Cowan, *Theory of Atomic Spectra*, (University of California Press, Berkely, 1981).
[8] R. E. H. Clark, J. Abdallah, Jr., G. Csanak, J. B. Mann, and R. D. Cowan, Los Alamos Manual No. LA-11436-M II, 1988
[9] J. B. Mann, At. Data Nuc. Data Tables, **29**, 407, (1983).
[10] J. Abdallah, Jr. and R. E. H. Clark, Los Alamos Manual No. LA-11926, (1990).

Effective rates for calculation of steady state and time dependent plasmas

R.E.H. Clark[1], J. Abdallah, Jr.[2], C.J. Fontes[3] Los Alamos National Laboratory
Los Alamos, New Mexico,
United States of America

Abstract. We have applied the atomic physics and plasma modeling codes developed at the Los Alamos National Laboratory to plasmas of neon, silicon, argon, titanium, and iron. For each plasma we have calculated effective ionization and recombination rate coefficients using two different approximations. These effective rate coefficients can be used to solve the steady state and time dependent plasma problem. We compare the results of plasma modeling from the two different methods and compare to a complete solution using the full set of coupled rate equations for both steady state and time dependent plasmas.

1. Introduction

In the previous two papers [1, 2] (Paper I and Paper II) we developed the method to be used in calculating radiated power from plasmas which are not in local thermodynamic equilibrium (nonLTE plasmas) and applied the method to calculate radiated power loss from plasmas of neon, silicon, argon, titanium, and iron for a range of electron temperature and density. The radiated power from plasma impurities is of considerable importance in magnetic fusion energy (MFE) devices [3]. The calculations were carried out using the atomic physics codes developed at the Los Alamos National Laboratory [4]. All calculations of radiated power were for plasmas in a steady state condition. In this paper we introduce the method of using effective ionization and recombination rate coefficients to determine the ionization balance for a plasma both for the steady state and for time dependent plasmas. We compare calculated radiated power and ionization balance from several methods and make a recommendation for a set of effective rate coefficients for plasmas of neon, silicon, argon, titanium, and iron.

In the next section we present a summary of the theoretical methods used in the calculation of the effective rates. In section 3 we apply the methods to plasmas in steady state. In section 4 we extend the method to time dependent plasmas and compare to full calculations using the entire set of coupled rate equations. Finally we summarize the results obtained here.

2. Theoretical methods

In Paper I [1] we compared several atomic physics models. Our recommendation was to use Model D for plasma simulations. We have used that model for all plasma models

[1] email address: rehc@lanl.gov
[2] email address: abd@lanl.gov
[3] email address: cjf@lanl.gov

presented in this paper. In Model D a large number of atomic configurations are included for each stage of ionization. There are approximately 1000 distinct configurations included for each ion stage. This causes the modeling of a plasma to be fairly time consuming computationally, but should give the best possible results.

Our goal is to use the atomic physics models in the plasma simulation code [5], FINE, to calculate effective ionization and recombination rate coefficients. We will obtain these rate coefficients for each ionization stage. Then the solution for a plasma at arbitrary temperatures and density will require only N effective rate coefficients for ionization and N for recombination, where N is the number of ionization stages. This will greatly reduce the amount of computational time for solution of the problem, provided that adequate effective rate coefficients can be found.

The steady state situation of a plasma occurs when the state populations are no longer changing with time. In the time dependent situation the populations evolve with time according to the relation

$$\frac{dN_i}{dt} = R^I_{i-1}N_{i-1} - R^I_i N_i - R^R_{i-1}N_i + R^R_i N_{i+1} \tag{1}$$

where N_i is the population of ionization stage i, R^I_i is the effective ionization rate from ionization stage i, and R^R_i is the effective recombination rate from ionization stage i+1 to ionization stage i. We note that this recombination rate is actually calculated from the ionization stage i+1, but we label it with the ionization stage i in order to have effective rates both into and out of each given ionization stage from 1 to N, N being the number of ionization stages. Thus we do not give any effective rates for the fully stripped ionization stage, although that stage does recombine into the hydrogenic stage. We note that this notation means that the effective recombination rate coefficient is multiplied by the population of the next higher ionization stage to arrive at a recombination rate. The steady state solution requires that

$$\frac{dN_i}{dt} = 0 \tag{2}$$

for each ionization stage. It is easily shown that this implies that the relation

$$\frac{N_i}{N_{i-1}} = \frac{R^R_i}{R^I_i} \tag{3}$$

must hold for adjacent ionization stages. If effective ionization and recombination rate coefficients are available, this relationship along with the requirement that the sum of the ionization stage populations must equal the total number of ions is sufficient to determine all of the populations of the ionization stages.

We examine two methods of producing the effective rate coefficients. The first method, which we designate SSD, solves the steady state problem explicitly tracking all configurations of each ionization stage, including all doubly excited states and including all

autoionizations (AI) and di-electronic recombinations (DR). At steady state, the effective ionization rate coefficient is obtained by adding up all the possible ionization processes; the effective recombination rate coefficient is obtained by summing all the recombination processes. We thus obtain an effective rate coefficient for ionization and for recombination for each stage of ionization.

The second method, which we call SSX, is similar except that we use a branching ratio treatment of the autoionization and di-electronic parts of the process. This method has been discussed in detail elsewhere [6]. In this method we do not explicitly follow each doubly excited state; we determine the relative probability for autoionization as opposed to radiative stabilization for each doubly excited state. This reduces the magnitude of both the ionization and recombination effective rate coefficient and thus slows down the time scale required to reach steady state. We note that the SSX treatment will not be valid at very high densities, because it will not have a perfect balance between AI and DR. Thus at very high densities the SSX method will not go to the local thermodynamic equilibrium (LTE) solution. However, at the densities of interest in MFE plasmas, it should be quite accurate. We will test the level of accuracy in the next section.

For both the SSD and SSX methods we also obtain an effective radiated power per stage of ionization. This is the sum of all radiative processes from a given ionization stage divided by the relative population of that ionization stage. This quantity is used later to reconstruct the total radiated power by multiplying by the calculated ionization stage populations.

We note that there are numerical difficulties in arriving at effective rate coefficients for all stages of ionization at a given temperature. This arises from the fact that for complex systems with many ionization stages, only a few stages will have significant population at steady state for a given temperature. The other ionization stages will have very small populations. This causes numerical problems in arriving at a realistic summing up of ionization and recombination rates from ionization stages where the populations are affected by numerical roundoff errors. In such cases the relationship of equation 3 may not be satisfied. This can cause problems in using the effective rate coefficients to reconstruct the solution to the plasma. We have tried several methods to address this problem. The most satisfactory uses the relative ionization stage population, defined by

$$P_i = \frac{N_i}{\Sigma N_j}. \tag{4}$$

When the relation

$$P_i > \epsilon \tag{5}$$

holds we use the effective rate coefficients calculated from our modeling code. When this relation does not hold we use the following method to extend the effective rate coefficients. We first extrapolate the relative ionization stage populations and the effective ionization rate coefficients to all temperatures above which equation 5 does not hold. We do this by using a linear extrapolation on the log of the quantities. However, care must be taken

in the extrapolation to avoid unphysical situations. In practice we have found it works best to find an average slope of the log of each quantity over all ionization stages and use this average slope to extend the populations and ionization rate coefficients. We then use equation 3 with the extrapolated populations and ionization rate coefficients to derive effective recombination rate coefficients. This insures that the steady state rate coefficients will satisfy equation 3. A check on the stability of the extrapolation procedure is to vary the value of ϵ in equation 5 and compare calculated results for ionization balance and radiated power from the resulting extrapolated quantities. We have varied the value of ϵ from .001 to 10^{-9} with no significant difference in calculated quantities. For all results presented here we have used the value of 10^{-5} for ϵ. We follow an analogous procedure for temperatures below which equation 5 does not hold, except that we extrapolate the effective recombination rate coefficient and use the extrapolated population and equation 3 to arrive at an effective ionization rate coefficient for the lower temperatures. This insures that the dominant coefficient (ionization at high temperatures and recombination at low temperatures) is the extrapolated quantity and the other effective rate coefficient is derived from the dominant one.

The method outlined above has been used to construct tables of effective rate coefficients for ionization and recombination, ionization stage populations, and effective radiated power per ionization stage. From these quantities we can reconstruct the ionization stage populations and the total radiated power. The total radiated power is found by the relationship

$$I_{tot} = \Sigma I_i P_i \tag{6}$$

where I_{tot} is the total radiated power and I_i is the effective radiated power from ionization stage i. The P_i is the population of ionization stage i, given by equation 4.

3. Steady State

The steady state solution takes place when the populations of all ion stages become constant with time, so that equation 2 holds. In this section we will compare the solution of the steady state problem using the SSD and SSX methods. We then compare results from various methods used to interpolate on electron temperature and density.

We first compare the full steady state solution for total radiated power using the SSD and SSX methods. Figure 1 shows a comparison of the two methods for silicon; figure 2 shows the comparison for iron. In both figures the solid lines represent results from SSX and the circles represent the SSD results. The same four electron densities used in Paper II [2] are used here, electron densities of 10^{13}, 10^{14}, 10^{15}, and 10^{16} cm^{-3}. It is clear from the figures that the SSD and SSX methods are in essentially exact agreement for these electron densities. We note that we have choices in how to interpolate between tabulated electron temperatures and densities. The hope is that the tabulated points are close enough so that interpolated results will be insensitive to the method of interpolation. We thus use very simple interpolation schemes. We will examine two different interpolation schemes,

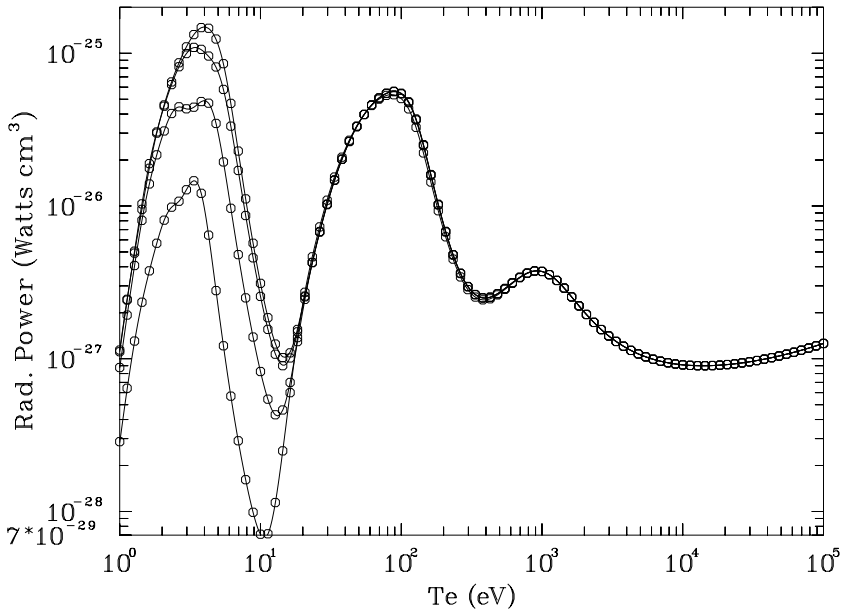

FIG. 1. Comparison of steady state radiated power for silicon using SSD (solid lines) and SSX methods (circles) for electron densities of 10^{13}, 10^{14}, 10^{15}, and 10^{16} cm^{-3}.

a linear interpolation on the log of all quantities and a straight linear interpolation on all quantities.

We first look at the linear on log interpolation. In this case it turns out that we do not need the effective rate coefficients at all. We arrive at the solution by interpolating on the ionization stage populations and use equation 6 to obtain the total radiated power. It can be shown that this will give equivalent results to interpolating on the effective rate coefficients, using the interpolated rate coefficients in equation 3 to find the ionization stage populations and then using equation 6 to obtain the total radiated power. This is a consequence of interpolating on the log of all quantities. If we are using a linear fit to the logs of the electron temperature and density then the effective rate coefficients are of the form

$$\ln R = a \ln T + b \tag{7}$$

and from equation 3 one sees that the log of the ionization stage populations will wind up being linear in the ln T also. Thus the linear on log interpolation on population is equivalent to linear on log interpolation of the effective rate coefficients. This provides a useful check on the self-consistency of the effective rate coefficients and the populations.

We have used the method outlined in the previous section to extrapolate the effective rate coefficients to all temperatures. We then interpolate on the rate coefficients and use equation 3 to obtain all of the ionization stage populations. Then equation 6 is used to obtain total radiated power. We also interpolate on the ionization populations directly and use equation 6 to obtain the total radiated power. We then compare the two methods at an electron density of 3x10^{15} cm^{-3}, intermediate between tabulated

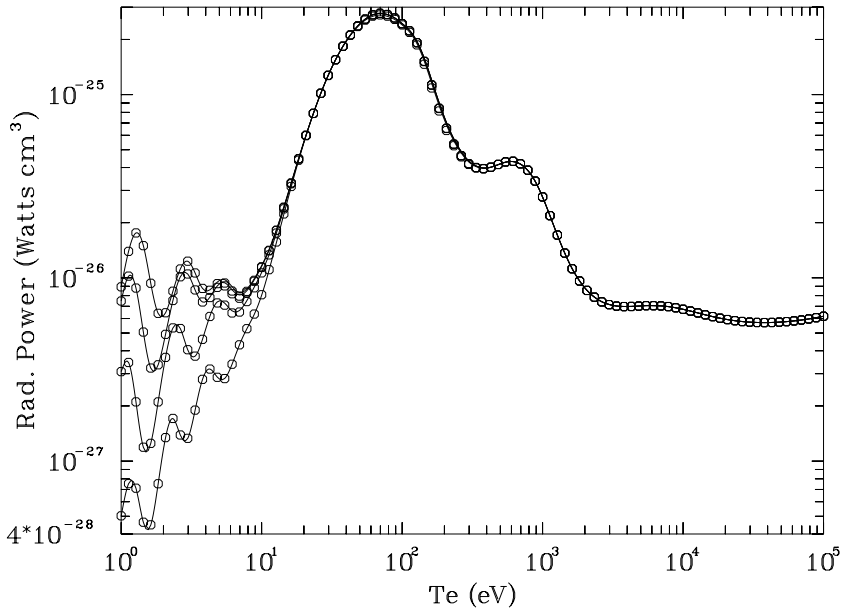

FIG. 2. Same as figure 1, but for iron.

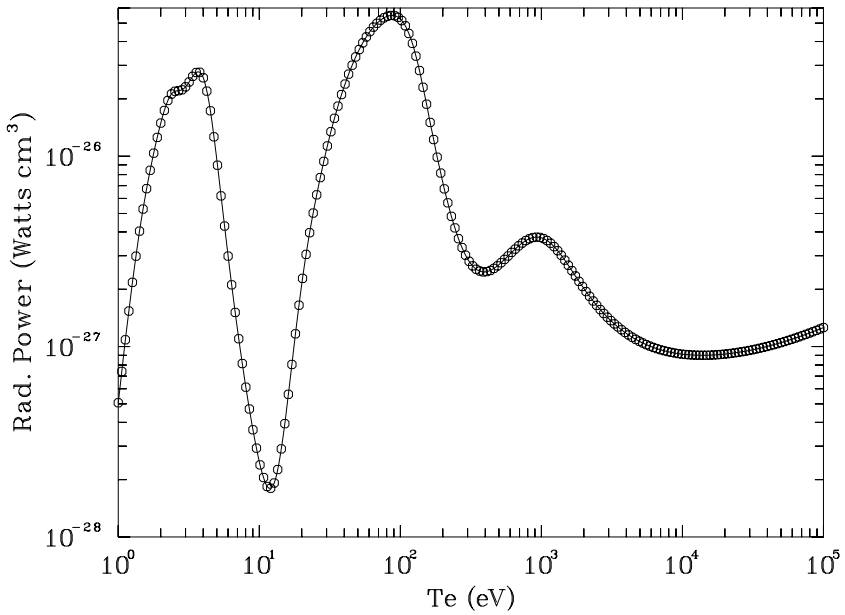

FIG. 3. Comparison of radiated power loss calculated by interpolating on populations (solid line) and interpolating on rate coefficients and solving for the populations (circles) for silicon at electron density of 3x10^{15} cm^{-3}.

densities, for silicon and for iron, two elements that exhibit relatively large variation of radiated power with electron density. The results are shown in figure 3 for silicon and figure 4 for iron. In both figures the solid line represents interpolating on ionization stage populations and the circles represents interpolation on the effective rates. We see that the radiated power from the two methods are the same. In figures 5 and 6 we show the same two cases but now the circles represent the results obtained from the full modeling code. Figures 5 and 6 show how well the interpolated results agree with the full calculation for

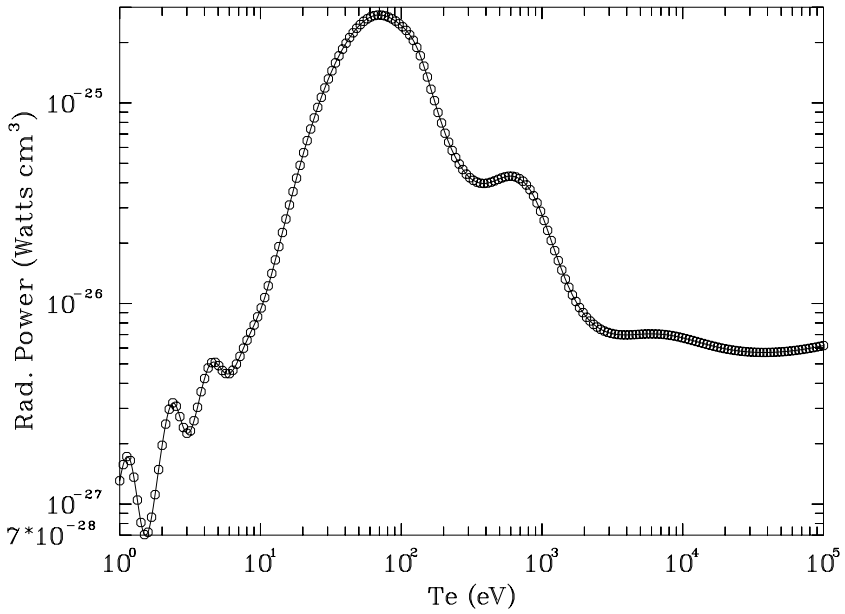

FIG. 4. Same as figure 3, but for iron.

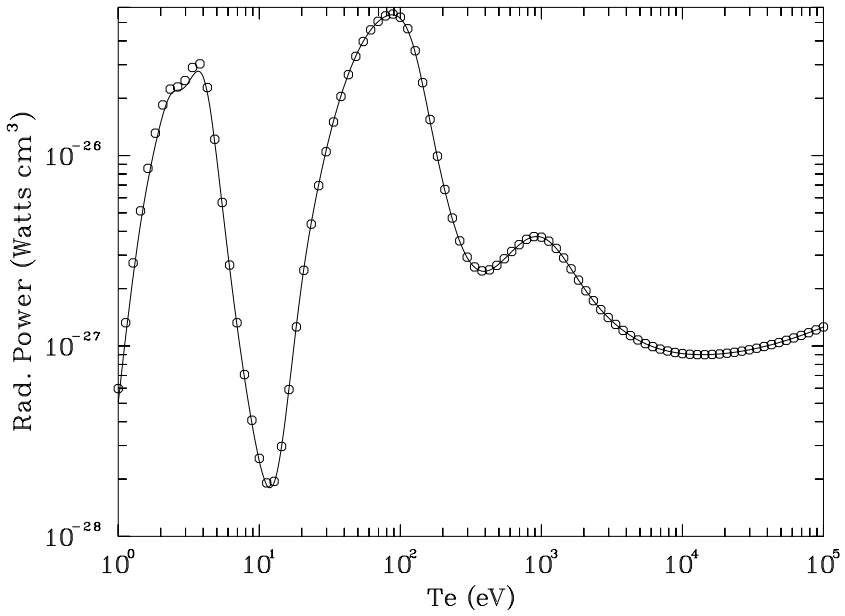

FIG. 5. Same as figure 3, but with the addition of results from full calculation (circles).

an intermediate electron density. We note that the full calculation requires several orders of magnitude more computational time to produce.

We next consider the possibility of a straight linear interpolation on ionization stage population and on effective rates coefficients. In this case the two interpolation schemes are easily seen to not be equivalent. In figures 7 and 8 we compare the interpolation on population (solid line), interpolation on effective rate (dashed line) and the full calculation (circles) for silicon and iron respectively. We see that neither straight linear interpolation method does a particularly good job reproducing the full calculation.

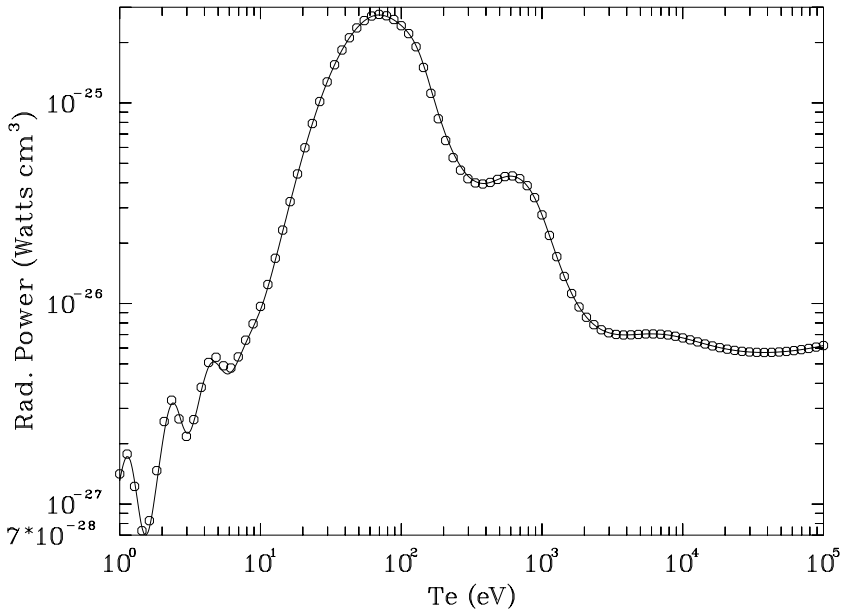

FIG. 6. Same as figure 5, but for iron.

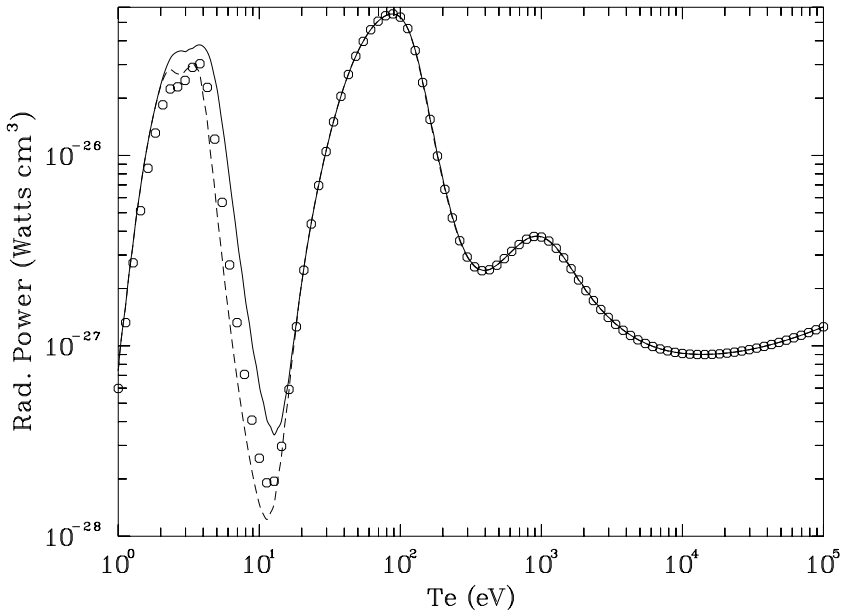

FIG. 7. Comparison of radiated power using linear fit to populations (solid line), linear fit to effective rate coefficients (dashed line), and full calculation (circles) for silicon at electron density of 3×10^{15}.

Finally we test a linear on log interpolation of the total radiated power. In this case we do not use the ionization stage populations, nor the effective rate coefficients, nor the radiated power per ion stage. We simply interpolate on the total radiated power. In figures 9 and 10 we show results for silicon and iron again at electron density of 3x10^{15} cm^{-3}. In both figures the solid line represents the interpolated total radiated power and the circles represent the full calculation. While the results are not quite as good as the linear on log interpolation of the populations, they are much superior to the straight linear

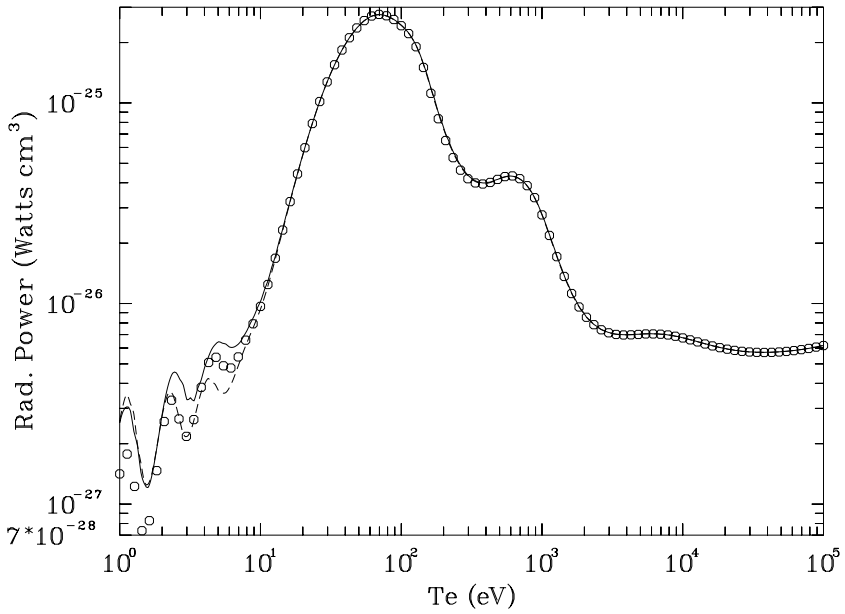

FIG. 8. Same as figure 7, but for iron.

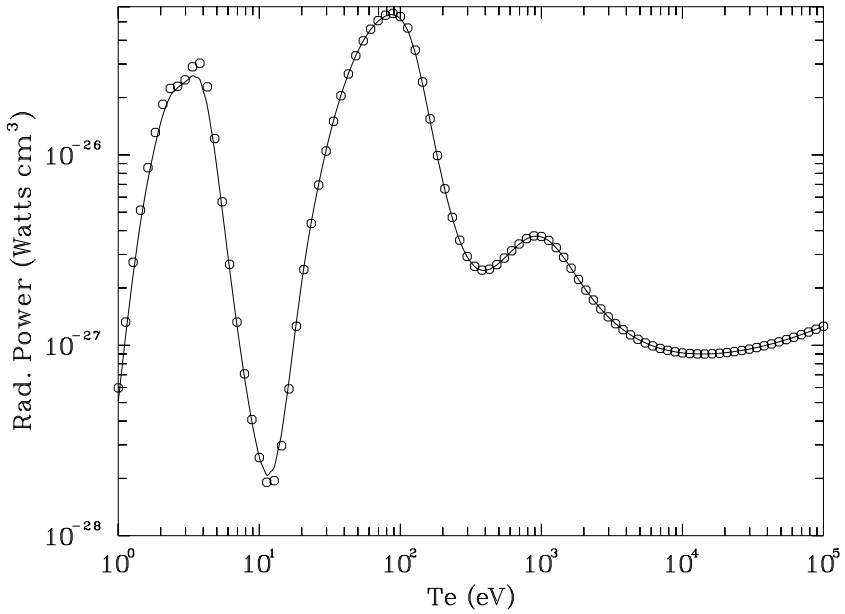

FIG. 9. Comparison of interpolation on total radiated power (solid line) and full calculation (circles) for silicon at electron density of 3×10^{15}.

interpolation of the populations or effective rate coefficients. Of course, this method does not yield the ionization stage population information at all.

In summary, for steady state calculations a simple linear on log fit to ionization stage populations can be used to reconstruct the total radiated power of a plasma. If ionization stage population information is not needed the total radiated power can be obtained by a simple linear on log interpolation from the tabulated total radiated power.

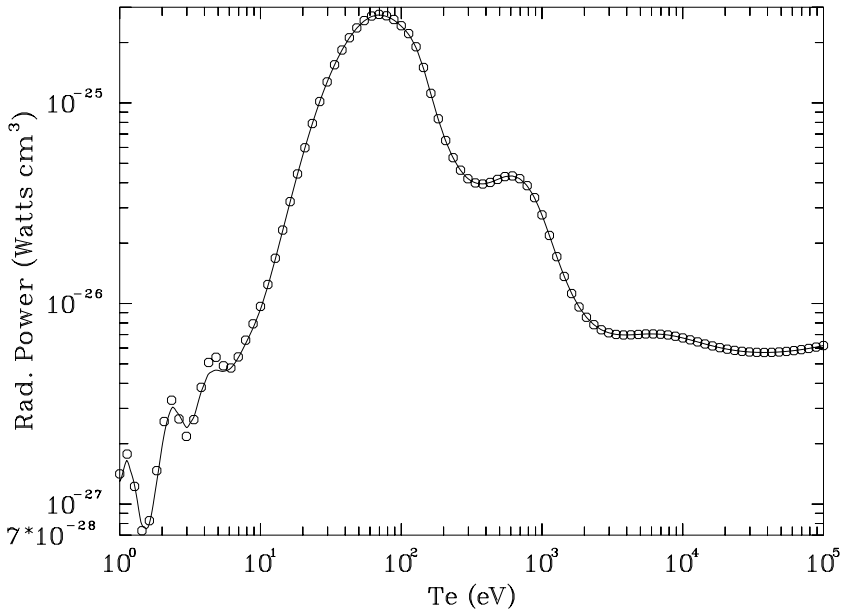

FIG. 10. Same as figure 9, but for iron.

4. Time Dependent Models

We now turn to the time dependent problem, in which the set of coupled rate equations represented by equation 1 must be solved. We again note that we need only solve one equation for each ionization stage instead of approximately 1000 per ionization stage. Thus it is possible to obtain time dependent solutions to a plasma in many orders of magnitude less computational time than it takes for a full calculation using the FINE code. In this section we will compare time dependent results from the SSD and SSX methods with full calculations from the FINE code for both radiated power and for ionization stage populations. We will then arrive at a recommended method for solution of the time dependent problem.

We begin with a brief summary of obtaining results using the SSD and SSX methods. In each case effective rate coefficients are available as described in section 2. We again note that the main difference in the two methods is in the treatment of autoionization. The SSD method follows doubly excited levels explicitly, while the SSX method uses branching ratios. Both methods derive the effective rates and radiated power per ion from a steady state solution. This fact will be important in understanding the time dependent solution using the effective rates compared to the full solution from the FINE code. The effective rate coefficients are used to solve the coupled rate equations represented by equation 1 to yield the ionization stage populations as a function of time. These populations are used in equation 6 to produce the total radiated power as a function of time. The two methods should arrive at the same long time solution and that solution should be the same as the steady state solution found in the previous section. This is another check on the self-consistency of the effective rate coefficients.

We first compare the SSX, SSD, and full solution from the FINE code on silicon at an electron temperature of 3eV and electron density of 10^{13} cm^{-3}. In figure 11 we show the radiated power calculated from the SSX method (solid line), the SSD method (dashed

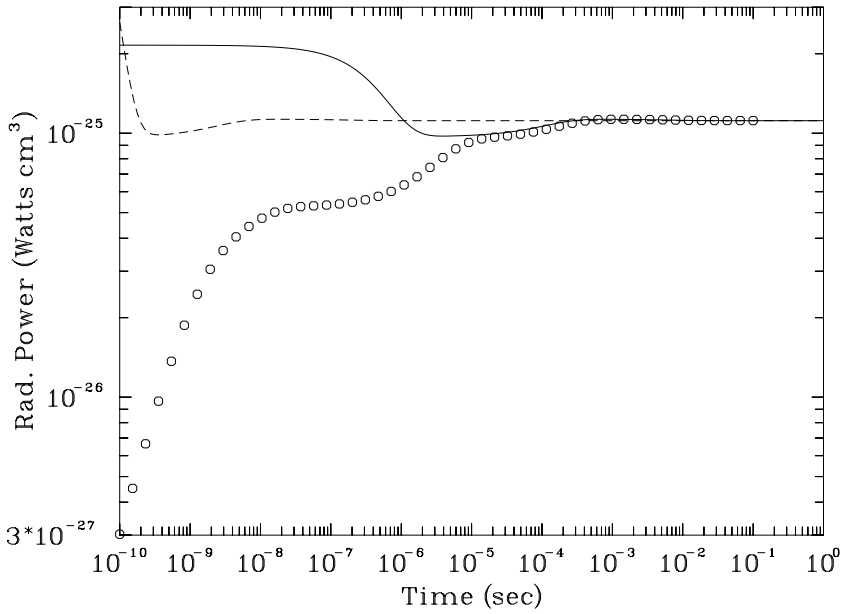

FIG. 11. Time dependent calculation of radiated power from SSX (solid line), SSD (dashed line), and full calculation (circles) for silicon at electron temperature of 3eV and electron density of 10^{13} cm^{-3}.

line), and the full calculation from FINE (circles). We started the calculations with all the population in the first ionization stage, neutral silicon. We then followed the solution as a function of time through one second.

We note that all three methods arrive at the same steady state solution, but on different paths. At very early times both the SSD and SSX methods calculate a much higher radiated power than the full calculation. This is due to the steady state radiated power per ion being much higher than the time evolving radiated power per ion. It takes some time for the plasma to evolve to the point where it radiates in the steady state mode.

We next note that the SSD method arrives at the steady state solution at a very early time. As we noted in section 2, the SSX method uses branching ratios for the autoionization and thus has lower effective rate coefficients. This should cause the SSX method to reach steady state more slowly than the SSD method. We see from figure 11 that this is the case. In fact, the SSX method approaches the FINE solution at a time around 10^{-5} seconds, which is roughly 1% of the time required to reach steady state. Thus, although on the expanded log scale it appears that the SSX and full FINE calculations do not agree very well, they are in essential agreement for 99% of the time required to reach steady state.

In figure 12 we show comparisons for the relative ionization stage populations for the same case. The plot symbols are the same as in figure 11. We again note that the SSD method arrives at steady state much earlier than the SSX or FINE calculations. We also see that the calculated populations from SSX are in fair agreement with the FINE calculation.

We now show similar comparisons for silicon at a electron temperature of 10eV and electron density of 10^{13} cm^{-3}. The radiated power comparison is shown in figure 13 and the relative ionization stage populations are shown in figure 14. The plot symbols are the

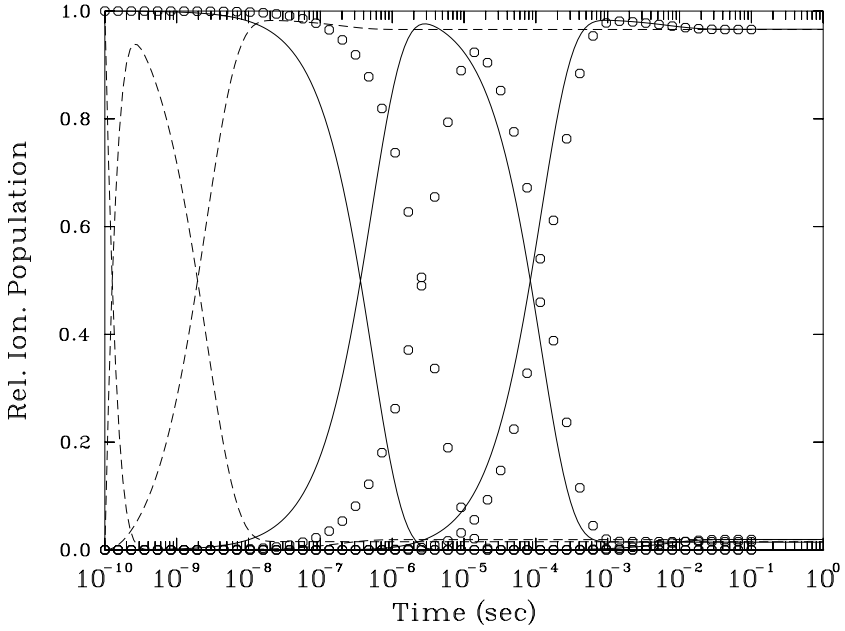

FIG. 12. Time dependent calculation of ion populations from SSX (solid line), SSD (dashed line), and full calculation (circles) for silicon at electron temperature of 3eV and electron density of 10^{13} cm^{-3}.

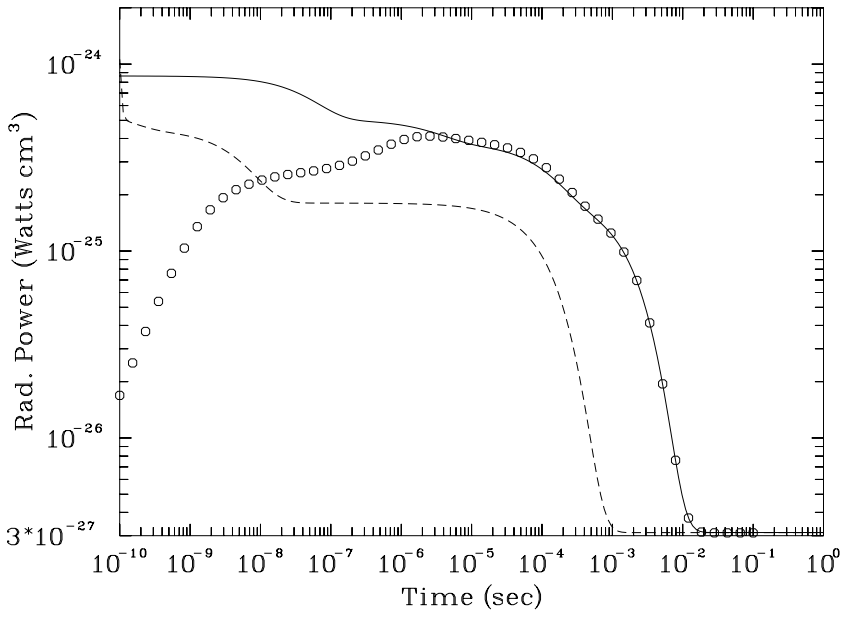

FIG. 13. Same as figure 11, but for iron.

same as in figures 11 and 12. Here we see that the SSD method is not as far off as it was at the lower temperature, but still reaches the steady state solution an order of magnitude too early.

We see that in this case the SSX method is in agreement with the full calculation over 99.9% of the time needed to reach steady state. We note that the calculations with the FINE code on these test cases took on the order of 100 hours on a Silicon Graphics Origin

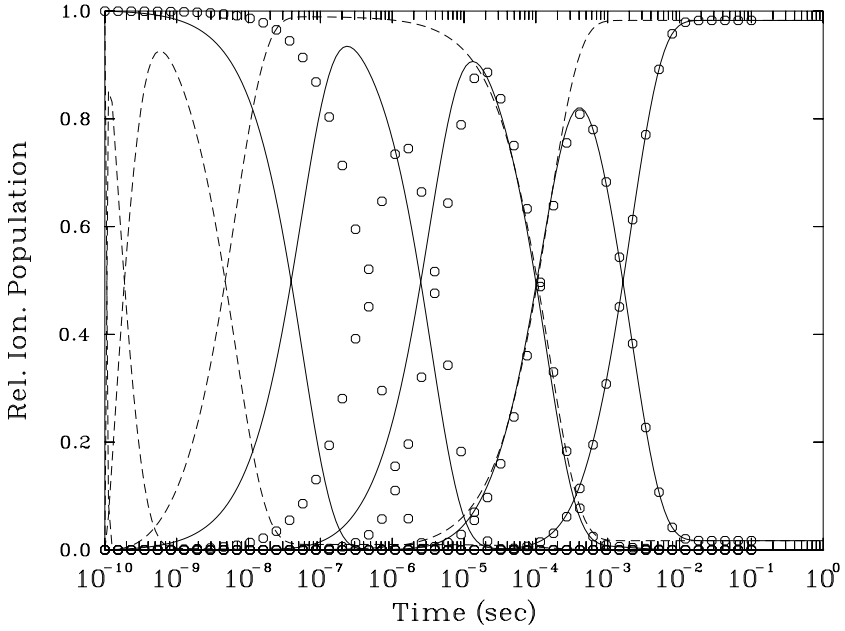

FIG. 14. Same as figure 12, but for iron.

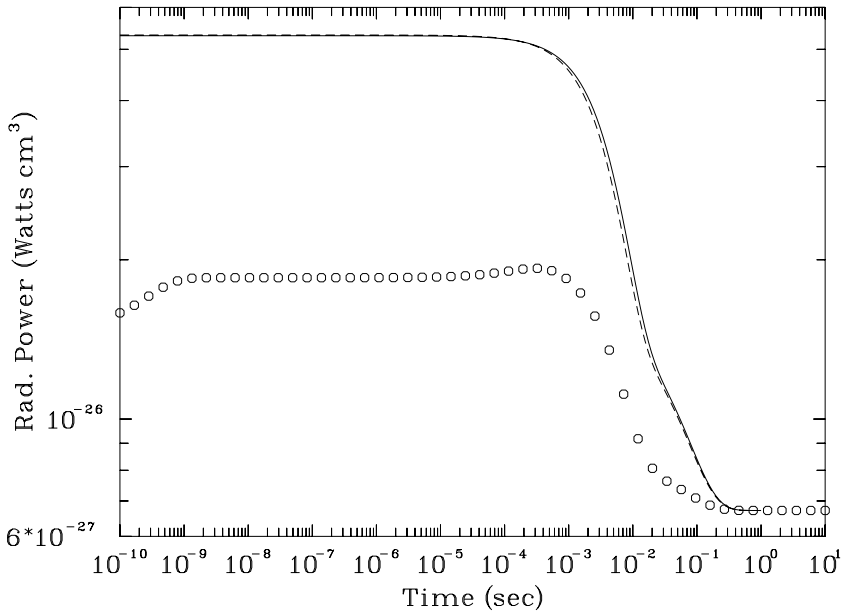

FIG. 15. Time dependent calculation of radiated power from SSX (solid line), SSD (dashed line), and full calculation (circles) for iron at electron temperature of 10000eV and electron density of 10^{13} cm^{-3}.

200 computer while the SSD and SSX calculations took on the order of a second. While we would like to do more extensive comparisons on full calculations it is clearly very time consuming to do so. However, we are able to run some additional comparisons at very high temperature where the simplest ionization stages are populated, namely the hydrogenic through lithium-like stages. These ionization stages do not have the large amount of complexity encountered in the near neutral silicon stages. We found we can run a FINE

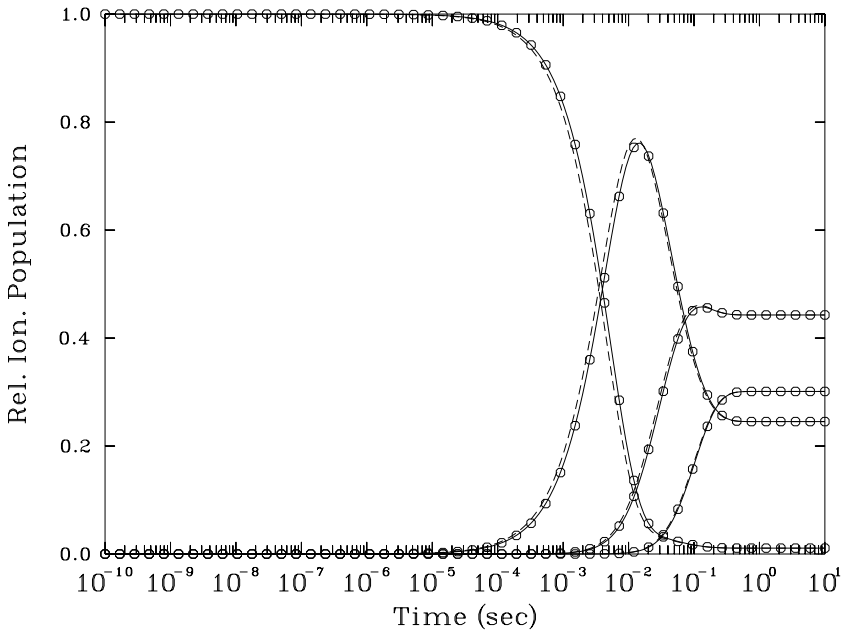

FIG. 16. Time dependent calculation of ion populations from SSX (solid line), SSD (dashed line), and full calculation (circles) for iron at electron temperature of 10000eV and electron density of 10^{13} cm^{-3}.

calculation in a few minutes on such cases. Thus we now look at some comparisons on high temperature iron.

We first look at the case of iron at electron temperature of 10000eV and electron density of 10^{13} cm^{-3}. In figure 15 we show the calculated radiated power from SSD, SSX, and the full FINE calculation. The plot symbols are the same as in figure 11. Here we note that the SSD and SSX methods are in agreement with each other. Also, the time scale for the SSD and SSX methods seem to be about the same as for the FINE method, but at times earlier than very near steady state the SSD and SSX methods predict much more radiated power. We will return to this point shortly.

Figure 16 shows the relative ionization stage populations for the same case. The plot symbols are the same. Here we see that all three methods agree very well on the time scale for the populations.

To show the effect of density we ran calculations at electron temperature of 10000eV and electron density of 10^{16} cm^{-3}. In figure 17 we show comparisons of the SSX method with the FINE calculation at both densities. The solid line represents the SSX method and the circles represent the FINE calculation at electron density of 10^{13} cm^{-3} while the dashed line represents the SSX method and the triangles represent the FINE calculation at electron density of 10^{16} cm^{-3}. We note that at both densities the two methods have similar time scales, but as noted above, the SSX method gives a higher radiated power at the earlier times.

In Paper II we noted that at high temperatures there was almost no density dependence on the radiated power. We see from figure 17 that the steady state radiated power from

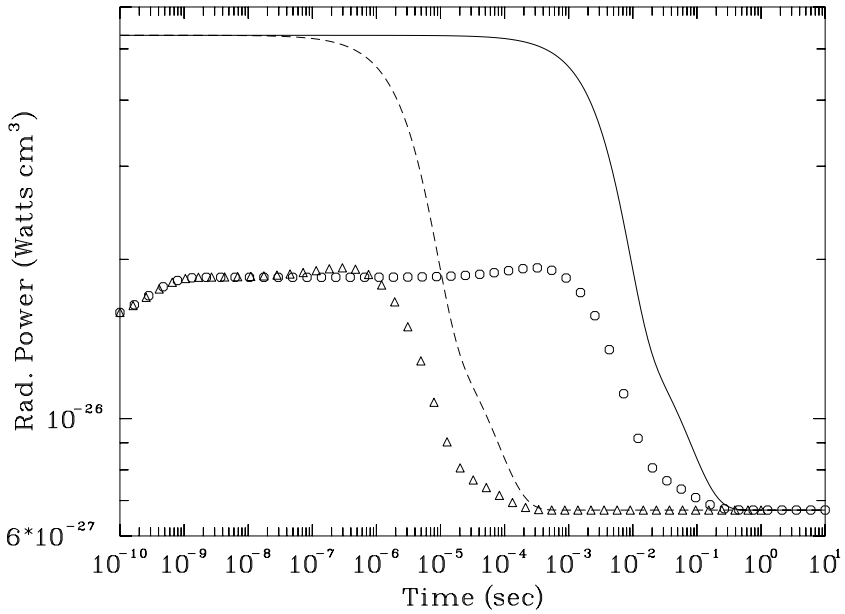

FIG. 17. Time dependent calculation of radiated power from SSX and full calculation at electron temperature of 10000eV and electron densities of 10^{13} and 10^{16} cm^{-3} (solid line, circles, dashed line, and triangles).

these two different densities are the same. However, the density does have a large effect on the time scale required to reach steady state, as would be expected since the rate for a process depends on the product of the number of particles and the rate coefficient. Thus the higher density case reaches steady state three orders of magnitude faster than the lower density.

We did an investigation into the high radiated power predicted by the SSX and SSD methods at early times. In figure 18 we show an analysis of one ionization stage, Fe XXIV, the lithium-like stage at electron temperature of 10000eV and electron density of 10^{13} cm^{-3}. In the time dependent calculations on iron, we started the calculations with all population in the lithium like stage. Figure 18 shows the effective radiated power of this ion stage as a function of time under three approximations. The solid line is the effective radiated power per ion from the FINE calculation. Recall that this effective power is multiplied by the relative ionization stage population to arrive at the contribution to the total radiated power. We now recall from figure 16 that this ion stage is the only one significantly populated until a time of around 10^{-4} second, so that the radiated power from this ionization stage should be the total radiated power up until this time. This is confirmed by comparing figure 18 with figure 15. The total radiated power is in agreement with the radiated power from this one ionization stage until this time. At this time ionization stage XXIV begins to be ionized to produce ionization stage XXV. It is also at this time that the solid line on figure 18 begins to increase until it reaches a steady state at a time of around .1 second. The reason for this rise is the radiated power due to recombinations from ionization stage XXV to XXIV. This is verified by the long dashed curve on figure 18. This curve is the radiated power excluding contributions from recombinations, calculated by the FINE code. We note that it follows the solid curve up until the time the solid curve begins to rise, showing that the rise is due to the radiation

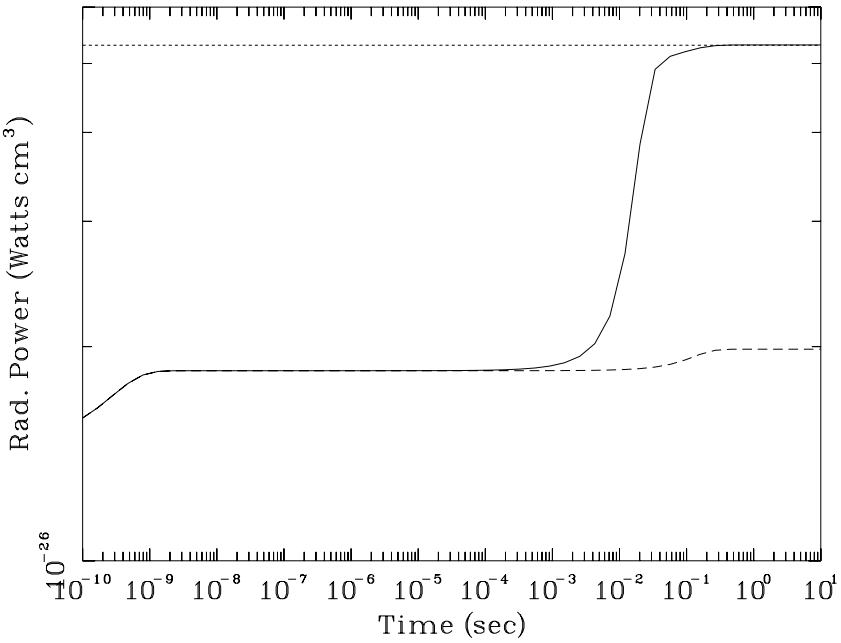

FIG. 18. Time dependent calculation radiated power from ionization stage XXIV only using full calculation (solid line), steady state solution (short dashes), and excluding bound free processes (long dashes).

from recombinations. The long dashed curve continues at the lower value. The short dashed curve on figure 18 is the effective radiated power from ionization stage XXIV used by both the SSD and SSX methods. Note that it merges with the FINE calculation at the late times. Thus we see that the high radiated power predicted by the SSD and SSX methods is due to the fact that various atomic processes take varying amounts of time to occur. The effective rate method cannot account for these time dependent processes, but can give useful estimates of the time scale to reach steady state, and in most cases can give good estimates of the radiated power over much of the time scale.

Finally, we show that the lower ionization stages do not affect the time scale for iron at the electron temperature of 10000eV and electron density of 10^{13} cm^{-3}. In figure 19 we compare two SSX calculations, one using only the ionization stages XXIV through XXVII (dashed line), the other using all ionization stages of iron (solid line). We note that the time to reach steady state is the same in each case. The lower ionization stages are ionized away very quickly and the long time scale is fixed only by the high lying ionization stages.

5. Summary and conclusion

We have presented methods for using effective rate coefficients to obtain ionization stage populations and radiated power for plasmas in both steady state and time dependent mode. For the steady state mode it is probably sufficient to do log based interpolations on total radiated power if ionization stage populations are not needed. If populations are needed, then it is sufficient to interpolate on ionization stage populations and effective radiated power per ionization stage to obtain the total radiated power.

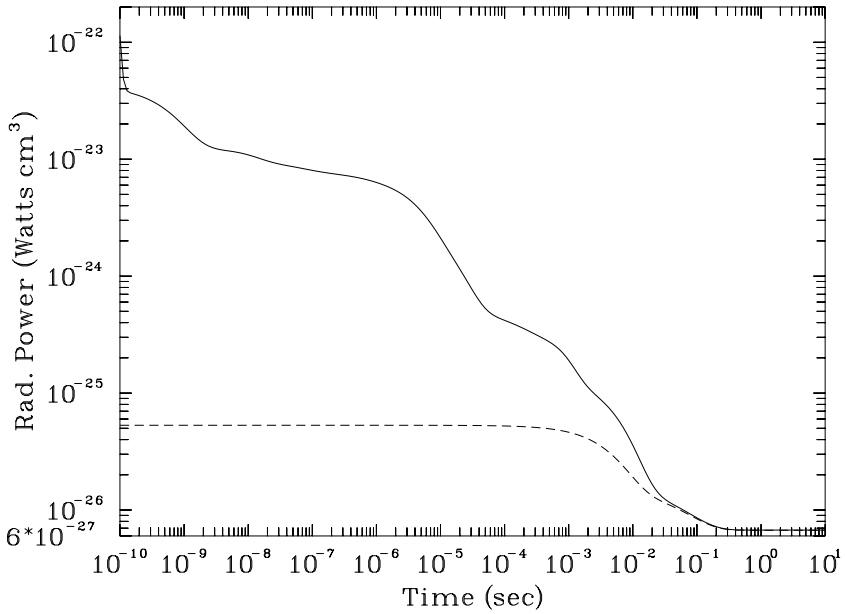

FIG. 19. Time dependent calculation of radiated power using last four ionization stages (dashed line) compared to using all ionization stages (solid line) from effective rate model SSX.

For time dependent problems, the coupled rate equations must be solved with the appropriate effective rate coefficients. We find that the SSX method appears to work well in predicting the time scale for reaching steady state and makes realistic predictions of total radiated power as a function of time, especially at times near the steady state time scale.

Because of the large volume of data for effective rate coefficients and radiated power per ion, and ionization stage populations, no attempt was made to produce tables of these quantities. These data are all available through the ALADDIN system maintained by the Atomic and Molecular Data Unit of the International Atomic Energy Agency. The information can be found on the Internet at the address http://www-amdis.iaea.org with links to the ALADDIN system.

This work was supported under the auspices of the United States Department of Energy.

REFERENCES

[1] R. E. H. Clark and J. Abdallah, Jr., previous paper in this journal.
[2] J. Abdallah, Jr. and R. E. H. Clark, previous paper in this journal.
[3] D. Post, J. Abdallah, R. E. H. Clark, and N. Putvinskaya, Phys. Plasmas, **2**, 2328, (1995).
[4] J. Abdallah, Jr., R. E. H. Clark, D. P. Kilcrease, G. Csanak, and C. J. Fontes, Proceedings of the 10^{th} APS Topical Conference on Atomic Processes in Plasmas, AIP Proceedings, **381**, 131, (1996).
[5] J. Abdallah, Jr. and R. E. H. Clark, Los Alamos Manual No. LA-11926, (1990).
[6] J. Abdallah, Jr. and R. E. H. Clark, J. Phys. B, **27**, 3589, (1994).

Contents of previous volumes of Atomic and Plasma–Material Interaction Data for Fusion

Volume 1 (1991)

Volume 2 (1992)

Volume 3 (1992)

Volume 4 (1993)

Volume 5 (1994)

Volume 6 (1995)

Volume 7/A (1998)

Volume 7/B (1998)

Volume 8 (2001)

Volume 9 (2001)

Volume 10 (2002)